NASA TECHNICAL MEMORANDUM

NASA TM X-3017

NASA TM X-3017

EFFECT OF SCREEN-INDUCED TOTAL-PRESSURE DISTORTION ON AXIAL-FLOW COMPRESSOR STABILITY

by James E. Calogeras, Roy L. Jobnsen, and Paul L. Burstadt

Lewis Research Center
Cleveland, Obio 44135

NATIONAL AERONAUTICS AND SPACE ADMINISTRATION • WASHINGTON, D. C. • MAY 1974

1. Report No. NASA TM X-3017	2. Government Accession No.	3. Recipient's Catalog No.
4. Title and Subtitle EFFECT OF SCREEN-INDUCED TOTAL-PRESSURE DISTORTION ON AXIAL-FLOW COMPRESSOR STABILITY		5. Report Date MAY 1974 6. Performing Organization Code
7. Author(s) James E. Calogeras, Roy L. Johnsen, and Paul L. Burstadt		8. Performing Organization Report No. E-7792 10. Work Unit No. 501-24
9. Performing Organization Name and Address Lewis Research Center National Aeronautics and Space Administration Cleveland, Ohio 44135		11. Contract or Grant No. 13. Type of Report and Period Covered Technical Memorandum
12. Sponsoring Agency Name and Address National Aeronautics and Space Administration Washington, D.C. 20546		14. Sponsoring Agency Code

15. Supplementary Notes

16. Abstract

An experimental investigation was made to determine the effects of screen-induced total-pressure distortions on two J85-GE-13 turbojet engines. Results were compared to those from a previous program run with a third engine. All compressors were found to be sensitive to a critical angle of circumferential distortion equal to 60°, and they all adhered closely to the parallel compressor model. It was found that the sensitivity of compressor exit pressure to virtually any type of distortion pattern could be determined by defining stall lines for undistorted, hub radial distorted, and tip radial distorted inflows. The effect of multiple sectors of circumferential distortion was defined.

17. Key Words (Suggested by Author(s))	18. Distribution Statement
Distortion; Compressor stability; Stall margin; Parallel compressor; Distortion index; Circumferential distortion; Radial distortion	Unclassified - unlimited Category 01

19. Security Classif. (of this report)	20. Security Classif. (of this page)	21. No. of Pages	22. Price*
Unclassified	Unclassified	79	$4.00

* For sale by the National Technical Information Service, Springfield, Virginia 22151

EFFECT OF SCREEN-INDUCED TOTAL-PRESSURE DISTORTION ON AXIAL-FLOW COMPRESSOR STABILITY

by James E. Calogeras, Roy L. Johnsen, and Paul L. Burstadt

Lewis Research Center

SUMMARY

An experimental investigation was made to determine the effects of screen-induced total-pressure distortions on two J85-GE-13 turbojet engines. The results were compared to those from a similar test program run in 1969 on a third engine. All the compressors were found to be sensitive to a critical angle of circumferential distortion equal to 60°. Although the compressors reacted differently to total-pressure defects located in the hub and tip regions, they all adhered closely to the parallel compressor model. Furthermore, it was determined that the sensitivity of each compressor to virtually any type of distortion pattern could be defined by simply obtaining stall lines for an undistorted, a single hub radial distorted, and a single tip radial distorted inflow. The effect of multiple sectors of circumferential distortion was defined.

INTRODUCTION

In recent years much of the research done at the NASA Lewis Research Center in the area of inlet-engine compatibility has been accomplished with the use of a J85-GE-13 turbojet engine. In particular, an investigation was conducted in the Lewis 10- by 10-Foot Supersonic Wind Tunnel to measure time-variant distortions produced in a supersonic inlet just prior to the stall of the J85 compressor (ref. 1). An extensive test program was run in the Propulsion Systems Laboratory Altitude Chamber of the Lewis Center to determine the effect of steady-state total-pressure distortion on the same J85-GE-13 turbojet engine (ref. 2). In this latter test, screens were placed upstream of the compressor face to effect total-pressure distortion, and results were used to develop a distortion index which in turn could be applied to the data recorded in the wind tunnel investigation.

As is sometimes the case, the analysis of data obtained in the wind tunnel and altitude chamber programs raised further questions as to the compatibility of an inlet with the J85 turbojet. For example, a question arose as to the applicability of a distortion index derived from one J85-GE-13 compressor to results obtained with other J85 compressors. And the need for more data of the multiple-per-revolution circumferential distortion type also became apparent.

This report presents the results of an experimental investigation undertaken to answer some of these questions. Steady-state inlet total-pressure distortions were produced by placing screens approximately one engine diameter upstream of the compressor face of two J85-GE-13 turbojet engines. This program included several multiple-per-revolution circumferential distortion patterns, as well as several patterns with combined radial and circumferential distortions. In addition, an attempt was made to simulate, with screens, two of the peak instantaneous distortion patterns recorded in the wind tunnel program and compare their effects on the stability of the J85 compressor. This investigation was conducted in the Propulsion Systems Laboratory Altitude Chamber of the NASA Lewis Research Center.

APPARATUS AND PROCEDURE

Installation

The installation of the J85-GE-13 turbojet engine in the Propulsion Systems Laboratory Altitude Chamber is shown in figure 1. A photograph of the engine installation is presented in figure 1(a). Figure 1(b) is a schematic drawing detailing the more pertinent measuring stations. A direct-connect installation was used, with the engine mounted on a thrust stand within the chamber and the engine inlet duct passing through a labyrinth seal in the forward bulkhead. The airflow measuring station had been calibrated in a previous test program. The flow coefficient was found to be repeatable to within ± 0.3 percent.

The General Electric J85-GE-13 is an afterburning turbojet engine possessing a high thrust-weight ratio. The engine consists of an eight-stage axial-flow compressor coupled directly to a two-stage turbine. It incorporates controlled compressor interstage bleed and variable inlet guide vanes, a through-flow annular combustor, and an afterburner (not used in this test) with a variable-area primary exhaust nozzle. The engine inlet diameter is 40.9 cm.

The variable inlet guide vanes are mechanically linked to the compressor interstage bleed valves so that when the inlet guide vanes are fully closed, the bleed valves are fully open. Normally, compressor interstage bleed was scheduled linearly from full

open at a corrected engine rotor speed equal to 80 percent of rated speed to full closed at a corrected speed of 94 percent. For all testing during this investigation, interstage bleed was rescheduled to provide linear variation at corrected engine speeds between 76 and 90 percent. This schedule corresponds to the maximum allowable bleed closure for safe engine operation and was required to obtain many of the stalls at corrected speeds below 94 percent of rated speed.

The compressor was stalled by slowly closing the exhaust nozzle. To avoid exceeding the temperature limit of the turbine during this procedure, the first-stage turbine nozzle was made smaller in area than the standard unit. At any point on the compressor map, then, the turbine was matched to the compressor at a lower turbine inlet temperature.

Two engines other than the one reported in references 1 and 2 were used during the course of this investigation. For testing of the first four screen patterns (table I), engine A was fitted with a turbine nozzle approximately 14 percent smaller in area than the standard unit. For mapping the undistorted stall line, as well as for use with screen patterns 5 to 33, engines A and B were fitted with a turbine nozzle approximately 26 percent smaller than the standard unit.

In this investigation, the exhaust nozzle was manually controlled. During certain portions of the test program, however, an exhaust nozzle area less than the minimum obtainable with the standard nozzle was required. To obtain these smaller areas, six airflow blockage plates were installed inside the nozzle leaves.

The screen patterns used in this investigation are listed in table I. (Symbols are defined in appendix A.) The mesh number associated with the screens indicates the number of wires in each linear inch of the square grid. A number 1 mesh grid structure was used to support the distortion screens. This grid structure had wire diameters of 0.203 cm and a porosity of 84.6 percent. It was located 42.80 cm, about one compressor face diameter, upstream of the inlet guide vanes. At military rated speed, the support grid produced a total-pressure difference $(P_{max} - P_{min})_2$ of about 4 percent of the compressor face average total pressure. Finally, the engine bullet-nose was extended to an axial position just upstream of the screen location. The bullet-nose extension and screen pattern 6 are shown in figures 1(c) and (d).

Instrumentation

Details of the steady-state pressure and temperature instrumentation used in the data analysis are presented in figure 2. The compressor face instrumentation was located 8.89 cm upstream of the inlet guide vanes. This left an axial distance of 33.91 cm, or slightly less than one compressor face diameter, between the distortion screens and

the compressor face instrumentation. The five total-pressure probes of each compressor face rake were area weighted radially, and each probe represented a 60° circumferential sector. During analysis, an adjustment in the data corresponding to one or more probes on a compressor face rake was made whenever the boundary of a screen pattern did not coincide with a circumferential position midway between rakes. For these cases, weighting of the probes on either side of the screen boundary was done by assuming a square-wave pressure distribution of extent equal to the physical extent of the screen.

Test Procedure

Atmospheric air was supplied to the inlet duct and was throttled to obtain a nominal Reynolds number index ReI of 0.70 at the compressor face. This value corresponded to the ReI associated with the inlet-engine compatibility tests referred to in the INTRODUCTION. The altitude chamber pressure P_0 was maintained at 31.0266 kN/m^2. This was just low enough to ensure exhaust nozzle operation at critical flow for all engine operating conditions in the range of interest.

After the desired simulated flight conditions were stabilized, main burner lightoff was made at idle throttle setting from a windmill rotor speed of about 60 percent of rated speed. The required rotor speed was then established at the minimum obtainable compressor pressure ratio. At the idle throttle setting, the minimum speed with the nozzle wide open was about 94 percent of rated speed. For speeds below about 94 percent the exhaust nozzle area was reduced while the idle throttle setting was maintained. For speeds above 94 percent, the throttle was advanced with the exhaust nozzle full open.

Each compressor stall point was approached along a line of constant corrected engine rotor speed. Incremental reductions of exhaust nozzle area forced the compressor to operate at higher compressor pressure ratios. Engine rotor speed was maintained at a constant value by manually biasing the throttle. Steady-state data were taken at each increment of nozzle area. Turbine discharge total temperature was monitored at each steady-state point and also at the stall point. Curves were drawn of compressor pressure ratio as a function of turbine discharge temperature. These curves were extrapolated to the turbine discharge temperature reading at the point of stall to determine the corresponding compressor pressure ratio. Corrected airflow at the stall point was then determined by extrapolating the constant-speed characteristic to the compressor pressure ratio at stall. In several instances, compressor stall occurred after a steady-state reading but before any reduction of exhaust nozzle area was made. Such instances required no extrapolation. In no case did the turbine discharge temperature at stall

deviate from the immediately preceding steady-state reading by more than 27.8 kelvins.

U.S. customary units were used in the design of the test model and for the recording and computing of experimental data. These units were converted to the International System of Units (SI) for presentation in this report.

RESULTS AND DISCUSSION

Clean Inlet Results

Compressor performance with undistorted inflow is presented for engine B, engine A, and the 1969 engine in figures 3(a) to (c), respectively. The same support grid structure was used in all these clean inlet tests to effect a more valid comparison with the distorted-inflow test results. The cusp in the stall line fairings at 90-percent corrected engine speed was probably related to the modified bleed schedule (effected by the linkage of the inlet guide vanes and the interstage bleed valves) used in this investigation (see the section Installation). At this speed, the inlet guide vanes were just fully open and the interstage bleed valves just fully closed. This tended to increase the loading of the front stages of the compressor, thereby reducing its stability margin.

A comparison of figures 3(a) and (b) shows that with undistorted inflow, the compressor performance for engine A was almost identical to that of engine B. A further comparison of these results with the 1969 engine data (fig. 3(c)) shows that while the undistorted stall line is somewhat lower for the 1969 engine, the speed characteristics and the variation of compressor pressure ratio at stall with corrected airflow are almost identical to those of engines B and A. Subsequent figures will show that these similarities remain even with distorted inflows. Because of turbine temperature limitations, the 100-percent-corrected-speed stall point could not be obtained with engines B and A. But because of the similarity between these engines and the 1969 engine, an estimate of the stall line was made for engines B and A, above the 96-percent-corrected-speed region, that is considered slightly conservative. The stall line, the lines of constant corrected engine speed, and the standard engine normal operating line from engine B are shown in figures 3(b) and (c) and reproduced in subsequent figures for ease of reference.

Circumferential Distortion Patterns

The effect of 180° extent circumferential distortion on compressor performance is presented in figure 4. Figures 4(a) to (c) present data for the three engines used in both

screen programs, all with about the same screen porosity. As with undistorted inflow, the effects of this distortion on engines B and A were almost identical. The effect of about the same distortion on the 1969 engine was slightly more serious. This can be seen by comparing the undistorted stall line with the distorted stall line for the 1969 engine, against those same lines for engines B and A. The effect of a more intense distortion (lower porosity screen) on engine A is presented in figure 4(d). Because of the severity of this distortion, the engine could not be stabilized at corrected engine speeds above 87 percent.

The effect of 120° extent circumferential distortion on the compressor performance of engine A is presented in figures 5(a) and (b) for screen porosities of 50.6 and 26.4 percent, respectively. The stall line is about the same as that discussed for the 180° pattern with engine A, although in this case the engine was stabilized at corrected speeds above 87 percent with the 26.4-percent-porosity screen.

The effect of 60° extent circumferential distortion on the compressor performance of engine A and the 1969 engine is presented in figure 6. Here again, a comparison of these results with corresponding distortion patterns of greater extent shows very little effect of screen extent on compressor performance at stall. This same result was noted in the 1969 test program reported in reference 2.

The effect of 30° extent circumferential spoiling on compressor performance is presented in figures 7(a) and (b) for engine A and the 1969 engine, respectively. Although serious, the effect of a 30° spoiled sector was not as deleterious to compressor performance as was the effect of the 60° or greater spoiled sectors of the same screen porosity. This result too was noted in reference 2.

The effect of circumferential distortions using two diametrically opposed screens (two per revolution) of 50.6-percent porosity is presented in figures 8(a) to (c) for individual screen sectors of 90°, 45°, and 30° in circumferential extent, respectively. Compare the results of this figure with those of previous figures having comparable one-per-revolution distortion patterns of equivalent total circumferential extent (e.g., compare fig. 8(a) with fig. 4(a)). It becomes apparent that the degradation in compressor pressure ratio at stall caused by distorted inflow is less for cases of multiple spoiled sectors. This same result is indicated by the results presented in figure 9, a four-per-revolution circumferential distortion pattern of 50.6-percent-porosity screen. The reasons for this are discussed later in the section Distortion Correlations.

Pure and Partial Radial Distortion Patterns

The effect of hub radial distortion on compressor performance is presented in figure 10. As discussed in reference 2, the most obvious effect of this type of distortion

is a sizeable loss in the corrected airflow capacity and pressure ratio of the compressor that retains the same stall line. A comparison of figures 10(a) and (b) indicates there is no apparent difference between the sensitivity of engine B and that of the 1969 engine to this type of distortion. The screen pattern presented in figures 10(c) and (d) represents the most intense (lowest porosity screen) pure radial distortion tested in either of the two test programs. Unlike the less intense hub radial distortions, the loss in stall compressor pressure ratio more than compensates for the loss in corrected weight flow, particularly at the lower corrected speeds. As a result, stall margin is reduced. In the process of testing this pattern initially, engine A failed after obtaining the single high-corrected-speed stall point presented in figure 10(d).

The effect of partial hub radial distortion on compressor performance is presented in figure 11. Variations in both circumferential and radial extents are shown in the sketches accompanying figures 11(a) to (e). Figure 11(b) is a reference pattern from the 1969 test program which corresponds to the pattern shown in figure 11(a). A comparison of the two figures indicates about the same degradation in performance for both engines. A comparison of figures 11(a) and (c) shows little effect of radial extent. A comparison of figures 11(c) to (e) shows that the only improvement in compressor sensitivity to this type of distortion occurred as the circumferential extent was decreased from 120° to 60°. This same type of improvement in compressor performance occurred, for full-span circumferential distortions, as the circumferential extent was decreased from 60° to 30° (cf. figs. 6(a) and 7(a)). This result suggests that the compressor may respond in a somewhat different manner to distortions that leave room for spanwise flow redistribution.

Results recorded with a partial midspan radial distortion pattern are presented in figure 12. Very little loss in compressor pressure ratio at stall occurred. These results, coupled with the results of a full midspan radial distortion pattern reported in reference 2, indicate that a low-pressure region located in the vicinity of the mean blade chord has little effect on compressor performance.

The effect of partial tip radial distortion on compressor performance is presented in figure 13. Contrary to partial hub radial distortion, a comparison of figures 13(a) and (b) indicates that an increase in the radial extent of the spoiled sector contributed to a further degradation in the compressor pressure ratio at stall. But like the partial hub radial distortions, there was some improvement in compressor performance at stall as the circumferential extent was decreased from 120° to 60°. This improvement is indicated by a comparison of figures 13(b) and (d). The most interesting aspect of this figure can be seen by comparing figures 13(b) and (c). These figures show that, relative to each undistorted stall line, the 1969 engine was significantly more sensitive to partial tip radial distortions than was engine B at corrected speeds above 90 percent of rated speed. This aspect will be further discussed later in the section Distortion Correlations.

The effect of a four-per-revolution partial tip radial distortion on compressor performance is presented in figure 14. This pattern simulated a steady-state distortion produced in the two-dimensional mixed-compression inlet reported in reference 3. To produce this pattern, the inlet was operated at an unusual off-design condition. As seen in figure 14, the only effect of this distortion on compressor pressure ratio at stall occurred at the lowest speed tested.

Combined Radial and Circumferential Distortion Patterns

Results obtained with distortion patterns consisting of pure hub radial and partial tip radial components are presented in figure 15. This type of pattern frequently occurred at various instants of time during the inlet-engine compatibility tests reported in reference 1. The adverse effect of the hub radial distortion on the pumping characteristics of the compressor is evident in all three parts of this figure. The effect of the intensity of hub radial distortion on compressor performance is evident by comparing figures 15(a) and (b), while the effect of the extent of the tip radial sector can be seen by comparing figures 15(b) and (c).

The distortion pattern presented in figure 16 represents the simulation of another steady-state distortion pattern produced by the inlet reported in reference 3. Here, inlet operation was near design. Attempts to simulate the peak instantaneous distortion points at angular displacements α of 5° and 0° from reference 1 are presented in figures 17(a) and (b), respectively. The inlet-induced distortion contours are compared with the screen-induced contours in figure 18. It is worth mentioning that the screen simulation of the $\alpha = 5^{\circ}$ stall point (pattern 4) was the highest amplitude steady-state distortion recorded in either this program or the programs reported in references 1 and 2.

Distortion Correlations

The compressor total-pressure ratio at stall for undistorted inflow is presented in figure 19 as a function of corrected engine speed. In some of the compressor performance curves which follow (figs. 20, 27, and 28), this pressure ratio is used to normalize the distorted-inflow stall compressor pressure ratio at the same corrected engine speeds. In figure 19, the solid fairing corresponds to engine B data. However, because of the similarity between engines A and B (cf. figs. 3(a) and (b)), this same curve was used with the results of engine A. (The compressor pressure ratio at stall for the 1969 engine with undistorted inflow was about 3 percent less than that of engines A and B

over the entire speed range.)

In figure 20, stall compressor pressure ratio is plotted as a function of circumferential extent of spoiling. Figure 20(a) pertains to distortions consisting of a single spoiled sector, whereas figure 20(b) pertains to multiple-per-revolution distorted inflows. In each case, stall compressor pressure ratio fell rapidly as the spoiled angle was increased from 0° to about 60°, and then stabilized at a nearly constant minimum value from 60° to 180°. Hence, 60° is the critical angle of distortion for the J85-GE-13 compressor. That is, it is the minimum angle of spoiling to which the compressor will respond in a quasi-steady-state manner. These results confirm the findings of reference 2, which were concerned with the 1969 engine. Therefore, it may be concluded that 60° is the critical angle for any J85-GE-13 compressor.

There are several interesting aspects of figure 20 that are worth mentioning. One is that the compressor pressure ratio at stall can be improved if a single distorted sector of extent greater than the critical angle is divided into multiple sectors with extents less than the critical angle. This same finding was reported in reference 4. Furthermore, although it is less apparent in this figure, the stability margin of the compressor can be improved if, when presented with a one-per-revolution circumferential distortion of any extent, a second spoiled sector of equal extent and intensity is added to the inlet flow field. For example, compare the data points of the two- and four-per-revolution, 30° distorted-inflow stalls with those of the one-per-revolution, 30° distortion at nominal corrected speeds of 87 and 93 percent. The nominal 99-percent-speed condition does not illustrate this result as effectively because the one-per-revolution stall point was significantly lower in actual corrected speed than either the two- or four-per-revolution stall points (table I). Apparently, it is the worst individual sector of a multiple-per-revolution distortion pattern that limits the compressor discharge total pressure. Additional spoiled sectors of equal or less intensity merely decrease the average compressor face total pressure and thereby increase the resultant compressor pressure ratio at stall.

Another interesting aspect of this figure is evidence of the adherence of this compressor to the parallel compressor model described to some degree in references 4 and 5. According to this theory, the compressor discharge static pressure at stall is limited by that portion of the compressor with the lowest inflow total pressure. Hence, once the extent of a constant-intensity spoiled sector exceeds the critical angle, compressor discharge static pressure will remain constant with further increases of extent. But if it is assumed that compressor discharge static and total pressures are about equal (a good assumption in this case), the constant-pressure-ratio fairings of figure 20 would appear to contradict this model. However, the results presented in figure 21 explain this apparent contradiction. These results show that the compressor face total pressure downstream of the spoiled sector $P_{min,2}$ decreased with circumferential

extent, even though the screen porosity was constant. And at each corrected speed, the compressor discharge average total pressure $\overline{P}_3$ decreased at the same rate. The variation of $P_{min,2}$ with the extent of circumferential distortion is probably caused by engine-induced circumferential flow redistributions taking place upstream of the inlet guide vanes (cf. ref. 6). In any case, had $P_{min,2}$ been held constant in this test, the average compressor discharge pressure $\overline{P}_3$ would have remained constant, as prescribed by the parallel compressor model.

The adherence of the J85-GE-13 compressor to the parallel compressor model prompted the correlation of stall data shown in figures 22 to 25 (see also ref. 7). A total of 176 distorted-inflow stall points are presented in these figures. Since the compressor has already been shown to be sensitive to a critical spoiling angle of about 60°, the $\left(P'_{min,60^\circ}\right)_{2,r}$ used in these figures was defined as the lowest mean pressure in any 60° sector of a compressor flow annulus ring (see appendix B). By using this definition, any circumferential distortion pattern with individual sector extent less than the critical angle was treated as a distortion of extent equal to 60°.

In figure 22, the maximum localized compressor pressure ratio at stall is presented as a function of corrected engine speed (percent of rated speed) for distortion patterns consisting of single- and multiple-per-revolution pure circumferential distortions. Data from engines A and B and the 1969 engine are presented in figures 22(a) and (b), respectively. In accordance with the parallel compressor model, the parameter $\overline{P}_3 \Big/ \left(P_{min,60^\circ}\right)_{2,r}$ correlated quite well with the undistorted-inflow stall line. Corrected speed was used as the independent variable rather than corrected airflow simply because the data scatter was significantly less. In most cases, the ring in which $\left(P_{min,60^\circ}\right)_{2,r}$ was defined was that ring adjacent to the hub of the compressor. But for pure circumferential distortion, only very small differences occurred between the $\left(P_{min,60^\circ}\right)_{2,r}$ of the five rings comprising the compressor face area.

The maximum localized compressor pressure ratio at stall is presented in figure 23 for full and partial hub radial distortion patterns. Figures 23(a) and (b) correspond to engines A and B and the 1969 engine, respectively. Unlike the results obtained with pure circumferential distortions, these results show that the solid line faired through the data rises above the undistorted stall line at corrected speeds above 90 percent of rated engine speed. This result is probably caused by a radial flow redistribution taking place inside the compressor. But it is noteworthy that both the pure hub radial patterns and the partial hub radial patterns follow the same curve, and that the difference between this curve and the undistorted stall line is about the same for engines A and B

and the 1969 engine.

Maximum localized compressor pressure ratio at stall is presented in figure 24 for pure and partial tip radial distortion patterns. Figures 24(a) and (b) correspond to engine B and the 1969 engine, respectively. Like the results of hub radial distortions, these results show that the local stall compressor pressure ratio is higher than that given by the undistorted stall line. But unlike the hub radial case, these results show that the sensitivity of engine B to tip radial distortions is less than that of the 1969 engine.

The correlation parameter $\overline{P}_3 \Big/ \left(P_{\text{min, }60^\circ}\right)_{2,r}$ is shown in figure 25 for distortions consisting of combined radial and circumferential components. Again, figures 25(a) and (b) correspond to engines A and B and the 1969 engine, respectively. With the exception of pattern 15 in figure 25(a), these data correlated quite well with the undistorted-inflow stall line of each engine. This is not surprising in that there was very little difference between the $\left(P_{\text{min, }60^\circ}\right)_{2,r}$ measured at the hub and that measured at the tip in any of these cases except screen pattern 15. With that exception, there was little room for radial flow redistribution inside the compressor; so the net result appears quite similar to that of pure circumferential distortion.

The curves faired through the data points of figures 22 to 25 are summarized in figure 26. The significance of this figure is that a complete description of the sensitivity of the compressor to distortion dictates a separate description of both the hub and tip blade regions, as well as the compressor taken as a whole. Still, the sensitivity to distortion of the hub and tip regions can each be described with a single radial distortion pattern. And the full-span circumferential distortion sensitivity can be described simply by defining the undistorted stall line.

It is evident in figure 26 that, for the 1972 engines (engines A and B), the hub region was considerably more sensitive to distortion than the tip region. For the 1969 engine, the hub region was slightly more sensitive to distortion at corrected engine speeds below 93 percent of rated speed, and slightly less sensitive above this speed. Over the entire speed range, however, both the hub and tip sections of engines A and B compressors produced a higher compressor pressure ratio at stall than corresponding sections of the 1969 compressor. It is probably for this reason that the overall compressor pressure ratio at stall with both undistorted and full-span circumferentially distorted inflows is higher for engines A and B.

Loss in stall compressor pressure ratio is presented in figure 27 as a function of the weighted circumferential distortion index DPCWR defined in appendix B. Only those stall points recorded with engines A and B which had a circumferential distortion

component are shown in this figure (except for screen patterns 4 and 5). This distortion parameter was first developed with the 1969 engine and is reported in reference 2. Figure 27(a) corresponds to data recorded with full-span circumferential distortions; figure 27(b) refers to partial radial and combined distortion patterns. The curves faired through both these sets of points are second-order least-square fits of the data. The difference in these curves is a result of the difference in hub and tip sensitivity to distortion, as opposed to the reaction of the compressor to full-span circumferential distortion.

The data from figures 27(a) and (b) are combined in figure 28. The solid curve represents a least-square fit of all these data. The dashed curve corresponds to the correlation developed in reference 2. It is interesting to note the similarity of these two curves below a distortion amplitude of about 0.08. Above this value, the curve fit routine is limited by the scarcity of data.

If figures 27(a) and (b) are referred to, it is apparent that the large degree of scatter in figure 28 is caused by the difference in the sensitivity of the compressor to partial radial distortion patterns as opposed to pure circumferential distortions. This difference was not as obvious in the 1969 test reported in reference 2. Even though the ordinate in figure 28 is an expanded scale of compressor performance, the degree of scatter limits the usefulness of this distortion parameter to primarily first-order proximities to compressor stall. In fact, in a program designed to implement the distortion index presented in figures 27 and 28 on an analog computer (cf. ref. 7), this scatter could account for many of the false indications of stall-inducing distortion that were encountered. To avoid the occurrence of stall, it may ultimately be necessary to use compressor-related stall proximity functions such as those shown in figures 22 to 26 in an active onboard control system.

SUMMARY OF RESULTS

An experimental investigation was made to determine the effects of steady-state total-pressure distortion on the J85-GE-13 turbojet engine. Two engines were used in this program, and results are compared to those from a similar test run in 1969 on a third engine. Steady-state distortions were produced by placing screens approximately one engine diameter upstream of the compressor face. Several complex screen patterns were studied in order to develop a distortion index common to all compressors of this type. The following results were obtained:

1. Both compressors were found to be sensitive to a critical angle of 60° of circumferential spoiling. This result was identical to that found with the 1969 engine (ref. 2). The critical angle is associated with a minimum blade residence time necessary to affect

the compressor in a quasi-steady-state manner.

2. The reaction of all the compressors to undistorted inflows and to full-span circumferentially distorted inflows was quite similar. There were, however, significant differences between compressors in the sensitivity of the hub and tip portions of the compressor to pressure defects located in these regions. Because of this, the use of a single distortion index based solely on compressor face pressures could have significant errors if applied to distortions of this type.

3. The J85-GE-13 compressor was found to adhere closely to the parallel compressor model. Because of this, all the stall points recorded in both this program and the 1969 program were tightly correlated with the maximum local compressor pressure ratio in the spoiled region. The compressor face pressure used in this ratio was defined as the lowest mean pressure in any 60° sector of the flow field. This definition accounts for the effect of critical angle on the compressor. The use of such a correlation in an onboard control loop designed to avoid stall would dictate the prior availability of data pertaining to the particular sensitivity of hub and tip regions to distortion, as well as the undistorted stall line. But these data could be obtained in a simple test using a single hub and a single tip radial distortion screen.

4. Results obtained with multiple-per-revolution circumferential distortions confirm that it is the worst individual sector of the pattern that limits compressor discharge total pressure. Additional spoiled sectors of equal or less intensity effectively increase the resultant compressor pressure ratio at stall by lowering the average compressor face pressure.

5. A partial midspan radial distortion pattern was found to have a negligible effect on compressor performance. Combining this finding with the results of a pure midspan radial distortion reported in reference 2 leads to the general conclusion that a pressure defect located in the vicinity of the mean blade chord has little effect on compressor performance. Such a defect might well be generated by certain inlet noise abatement devices.

Lewis Research Center,
National Aeronautics and Space Administration,
Cleveland, Ohio, January 30, 1974,
501-24.

APPENDIX A

SYMBOLS

A	area, m^2
A_{SP}	area of spoiled flow, m^2
A_2	compressor face annulus area, 0.1193 m^2
DPCWR	distortion index (appendix B)
DPR	distortion parameter (appendix B)
N	engine speed, rpm
N*	rated engine speed, 16 500 rpm
$(N/N^*\sqrt{\theta}) \times 100$	corrected engine speed, percent of rated
P	total pressure, N/m^2
$\left(P_{\text{min, }60^o}\right)_r$	lowest mean pressure of any 60^o sector of a compressor face equal-area annular ring, N/m^2 (appendix B)
ReI	Reynolds number index, $\delta_2/\varphi\sqrt{\theta_2}$
T	total temperature, K
W	engine airflow, kg/sec
W_{corr}	engine corrected airflow, $W\sqrt{\theta}/\delta$, kg/sec
α	angular displacement, deg
β	spoiled sector angle, deg
δ	local corrected total pressure, $P/101.325\ kN/m^2$
θ	local corrected total temperature, T/288.2 K
φ	$(399\ K)\theta^{3/2}/(T_2 + 110.8\ K)$
Subscripts:	
max	maximum
min	minimum
r	any of five equal-area annular rings comprising compressor face flow annulus (appendix B)
0	altitude chamber measuring station
1	inlet airflow measuring station

2 compressor face measuring station

3 compressor discharge measuring station

5 turbine discharge measuring station

8 nozzle throat station

Superscript:

$\bar{}$ average

APPENDIX B

DEFINITION OF DISTORTION INDEX

The weighted circumferential distortion parameter used in this report is defined as follows:

$$\text{DPCWR} \equiv \left[\left(1 - \frac{P_{\text{min, }60^\circ}}{\overline{P}}\right)_r \sqrt{\frac{\beta_r}{180}}\right]_2$$

The compressor face annular area was divided into five equal-area rings, with one probe of each total-pressure rake centrally located in each ring. The distortion index was then calculated in each of the rings, and the largest of these values is presented in table I and throughout this report.

For the two pure radial patterns run in this program, the value listed in table I under the heading "Distortion" is defined as the largest value of the following parameter calculated in each of the five rings:

$$\text{DPR} \equiv 1 - \frac{\overline{P}_{r,2}}{\overline{P}_2}$$

The term $P_{\text{min, }60^\circ}$ is defined as the lowest mean total pressure in any 60° sector of a compressor face flow annulus ring, that is,

$$\left(P_{\text{min, }60^\circ}\right)_{2,r} \equiv \frac{1}{60^\circ}\int_{\xi}^{\xi+60^\circ} P_{2,r}(\alpha)\, d\alpha \Bigg]_{\text{Minimum value over range } 0^\circ \le \xi \le 360^\circ}$$

where

60° critical angle of spoiling for compressor

α angular displacement

ξ dummy variable

An example of this definition for a square-wave pressure distribution with a 30^{o} spoiled sector is shown in the following sketch:

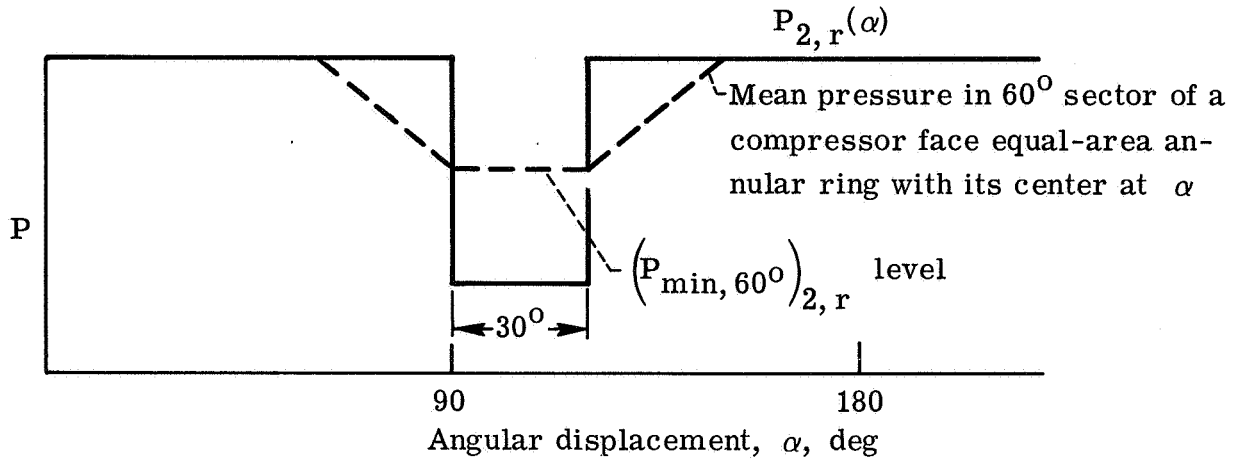

REFERENCES

1. Calogeras, James E.; Burstadt, Paul L.; and Coltrin, Robert E.: Instantaneous and Dynamic Analysis of Supersonic Inlet-Engine Compatibility. Paper 71-667, AIAA, June 1971.
2. Calogeras, James E.; Mehalic, Charles M.; and Burstadt, Paul L.: Experimental Investigation of the Effect of Screen Induced Total Pressure Distortion on Turbojet Stall Margin. NASA TM X-2239, 1971.
3. Baumbick, Robert J.; Neiner, George H.; and Cole, Gary L.: Experimental Dynamic Response of a Two-Dimensional, Mach 2.7, Mixed Compression Inlet. NASA TN D-6957, 1972.
4. Reid, C.: The Response of Axial Flow Compressors To Intake Flow Distortion. Paper 69-GT-29, ASME, March, 1969.
5. Pearson, H.; and McKenzie, A. B.: Wakes in Axial Compressors. Jour. Roy. Aeron. Soc., vol. 63, no. 583, July 1959, pp. 415-416.
6. Coltrin, Robert E.; and Choby, David A.: Steady-State Interactions from Mach 1.98 to 2.58 Between a Turbojet Engine and an Axisymmetric Inlet with 60-Percent Internal Area Contraction. NASA TM X-1780, 1969.
7. Costakis, William G.: Analog Computer Implementation of Four Instantaneous Distortion Indices. NASA TM X-2993, 1974.

TABLE I. - SCREEN PATTERNS

Pattern	Type	Mesh number	Wire diameter, cm	Porosity, percent of open area	Circumferential extent, deg	Spoiled-area ratio, A_{SP}/A_2	Corrected engine speed, $\frac{N \times 100}{N^* \sqrt{\theta}}$, percent of rated	Pressure ratio, $\left(\frac{P}{P_{\text{min, 60}^\circ}}\right)_{2,r} \sqrt{\overline{P}_1}$	Average inlet total pressure, $\overline{P}_1$, N/m^2	Pressure ratio, $\overline{P}_2/\overline{P}_1$	Distortion, $\left[\left(1 - \frac{P_{\text{min, 60}^\circ}}{\overline{P}}\right)_r \sqrt{\frac{\beta_r}{\pi}}\right]_2$	Engine	Remarks
1	Circumferential	9	0.137	26.4	180	0.500	86.7	0.795	86 571	0.883	0.0991	A	Stall point
2	Circumferential	9	0.137	26.4	120	0.333	86.5	0.838	81 045	0.929	0.0772	A	Stall point
							92.8	.776	87 610	.902	.1108	A	Stall point
							98.8	.724	94 839	.879	.1400	A	Stall point
3	Circumferential	9	0.137	26.4	60	0.167	86.4	0.878	69 620	0.961	0.0495	A	Stall point
							89.5	.857	69 394	.955	.0583	↓	↓
							92.8	.834	69 268	.947	.0681		
							95.8	.803	69 795	.937	.0823		
							98.9	.771	69 863	.927	.0973		
4	Instantaneous				~180		92.8	0.538	105 761	0.670	0.2015	B	Stall point (see RESULTS AND DISCUSSION
5	Instantaneous				~120		87.3	0.896	84 482	0.893	0.0478	A	T_5 limit - no stall
6	Circumferential	9	0.081	50.6	180	0.500	87.2	0.898	74 576	0.945	0.0428	A	Stall point
							92.8	.860	77 003	.924	.0596	A	↓
							98.5	.818	80 047	.899	.0803	A	
							87.2	.901	74 762	.946	.0386	B	
							93.2	.865	77 974	.921	.0579	B	
							98.5	.822	81 402	.896	.0769	B	↓
7	Circumferential	9	0.081	50.6	120	0.333	87.0	0.920	73 643	0.960	0.0342	A	Stall point
							92.9	.887	75 990	.944	.0485	A	Stall point
							98.2	.850	79 026	.927	.0667	A	Stall point
8	Circumferential	9	0.081	50.6	60	0.167	86.9	0.927	68 582	0.971	0.0270	A	Stall point
							93.0	.896	68 999	.960	.0375	A	Stall point
							98.1	.855	69 431	.946	.0548	A	Stall point
9	Circumferential	9	0.081	50.6	30	0.083	87.1	0.953	68 231	0.978	0.0144	A	Stall point
							93.0	.933	68 632	.968	.0208	A	Stall point
							98.1	.908	69 234	.957	.0284	A	Stall point
10	Hub radial	9	0.137	26.4	360	0.400	99.5	0.712	81 311	0.842	[a]0.1480	A	Stall point (engine failed)
							87.2	.833	74 722	.908	[a].0789	B	Stall point
							92.9	.786	76 966	.881	[a].1025	↓	↓
							96.1	.795	78 853	.863	[a].1215		
							98.8	.726	79 250	.850	[a].1408	↓	↓
11	Circumferential (2/rev)	9	0.081	50.6	2/90	0.500	87.0	0.909	73 372	0.948	0.0234	A	Stall point
							88.8	.900	76 486	.943	.0266	↓	↓
							92.4	.880	77 275	.931	.0321		
							98.0	.838	80 884	.906	.0463	↓	↓
12	Circumferential (2/rev)	9	0.081	50.6	2/45	0.250	86.9	0.938	74 212	0.967	0.0171	A	Stall point
							92.6	.917	76 943	.955	.0221	A	Stall point
							98.9	.871	81 819	.933	.0327	A	Stall point
13	Circumferential (2/rev)	9	0.081	50.6	2/30	0.167	87.3	0.955	73 742	0.972	0.0109	B	Stall point
							92.9	.937	76 222	.961	.0154	B	Stall point
							98.5	.907	79 552	.945	.0210	B	Stall point
14	Circumferential (4/rev)	9	0.081	50.6	4/30	0.333	86.9	0.943	73 153	0.962	0.0058	B	Stall point
							93.0	.929	76 892	.945	.0085	B	Stall point
							98.6	.887	81 554	.922	.0125	B	Stall point

	and circumferential (2/rev)	tip) $7\frac{1}{2}$ (circumferential)	.081	57.4	2/20	.089	92.7 98.8	.897 .844	73 804 79 057	.963 .945	.0204 .0340	B B	Stall point Stall point
16	Partial tip radial (4/rev)	9	0.081	50.6	4/30	0.133	86.9 92.9 98.7	0 942 .925 .894	70 957 71 030 72 307	0.974 .966 .949	0.0062 .0084 .0120	B B B	Stall point Stall point T_5 limit - no stall
17	Partial hub radial	9	0.104	39.7	120	0.113	86.9 92.9 98.6	0.908 .873 .832	69 433 69 469 69 920	0.974 .964 .954	0.0475 .0661 .0887	B B B	Stall point Stall point Stall point
18	Partial hub radial	9	0.104	39.7	120	0.067	86.9 92.9 98.4	0.905 .869 .824	70 294 71 452 72 973	0.970 .959 .946	0.0427 .0596 .0845	B B B	Stall point Stall point Stall point
19	Partial hub radial	9	0.104	39.7	60	0.057	86.8 92.8 98.5	0.909 .874 .830	68 209 68 793 68 603	0.976 .967 .956	0.0368 .0509 .0710	B B B	Stall point Stall point Stall point
21	Partial hub radial	9	0.104	39.7	30	0.028	86.7 92.5 97.7	0.947 .926 .903	68 885 68 943 69 163	0.979 .971 .962	0.0174 .0242 .0323	B B B	Stall point Stall point Stall point
23	Partial tip radial	9	0.104	39.7	120	0.133	86.9 92.9 98.5	0.902 .869 .822	71 020 72 542 74 568	0.969 .958 .943	0.0377 .0536 .0771	B B B	Stall point Stall point Stall point
24	Partial tip radial	9	0.104	39.7	120	0.067	87.2 92.9 98.3	0.917 .884 .854	68 806 ------ 68 874	0.977 ----- .956	0.0311 .0443 .0566	B B B	Stall point Data recording no good Stall point
25	Partial tip radial	9	0.104	39.7	60	0.067	87.0 92.9 98.7	0.911 ----- .831	69 505 69 763 69 633	0.976 .962 .953	0.0294 .0510 .0598	B B B	Stall point Stall point Stall point
29	Mid-span partial radial	9	0.104	39.7	120	0.087	86.6 92.6 97.8	0.914 .885 .840	74 081 76 794 80 766	0.973 .964 .948	0.0432 .0583 .0811	B B B	Stall point Stall point Stall point
30	Combined patterns 10 and 23	9 (Hub radial) 9 (Partial tip radial)	0.137 .104	26.4 39.7	360 120	0.400 .133	87.0 92.8 98.4	0.933 .911 .881	74 218 76 990 80 824	0.896 .861 .816	0.0620 .0850 .1195	B B B	Stall point Stall point Stall point
31	Hub radial	9	0.104	39.7	360	0.400	86.9 92.8 98.2	0.892 .857 .795	71 506 72 570 73 513	0.939 .922 .889	[a]0.0487 [a].0688 [a].1026	B B B	T_5 limit - no stall Stall point Stall point
32	Combined hub radial and partial tip radial	9 (Hub radial) 9 (Partial tip radial	0.104 .104	39.7 39.7	360 120	0.400 .200	87.0 92.8 98.7	0.871 .838 .756	77 808 80 864 90 435	0.910 .886 .830	0.0578 .0744 .1179	B B B	Stall point Stall point Stall point
33	Combined patterns 23 and 31	9 (Hub radial) 9 (Partial tip radial)	0.104 .104	39.7 39.7	360 120	0.400 .133	86.7 92.6 97.9	0.883 .845 .777	70 829 72 827 76 335	0.925 .900 .858	0.0516 .0704 .1077	B B B	Stall point Stall point Stall point

[a]DPR distortion definition (appendix B).

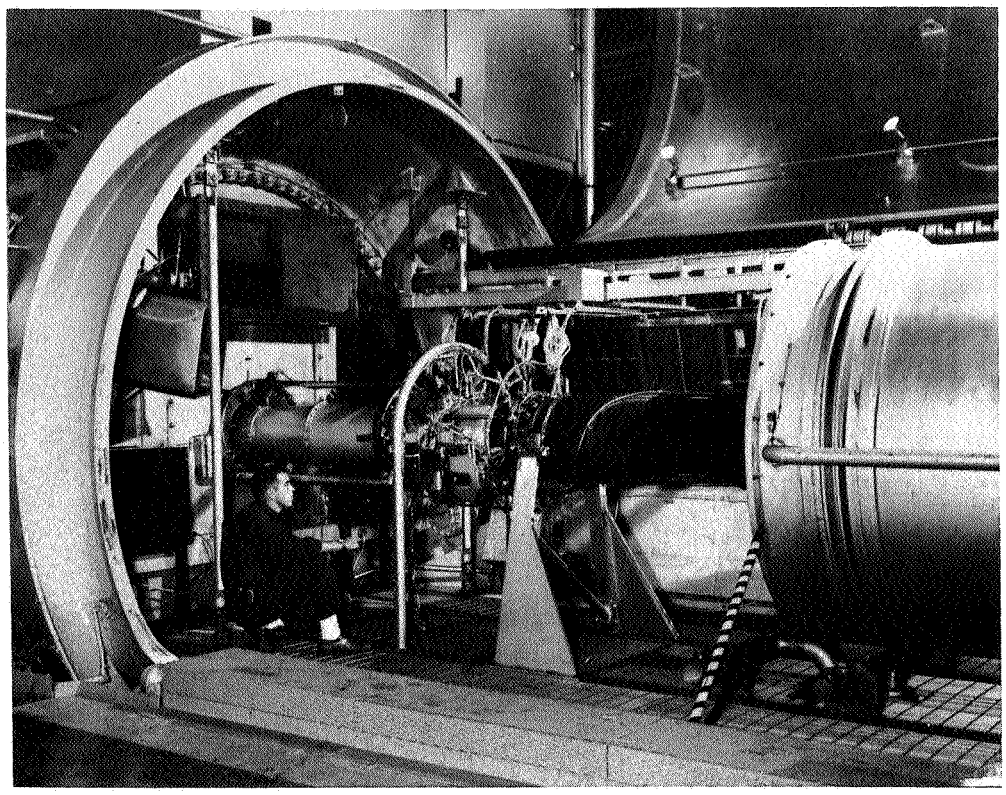

(a) Turbojet engine (J85-GE-13) installed in altitude chamber.

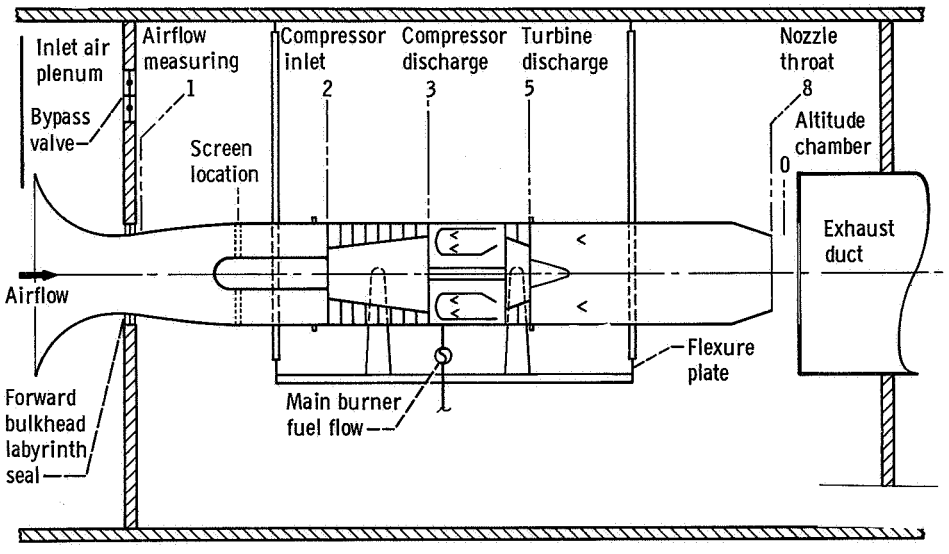

(b) Schematic showing measuring stations.

Figure 1. - Test installation.

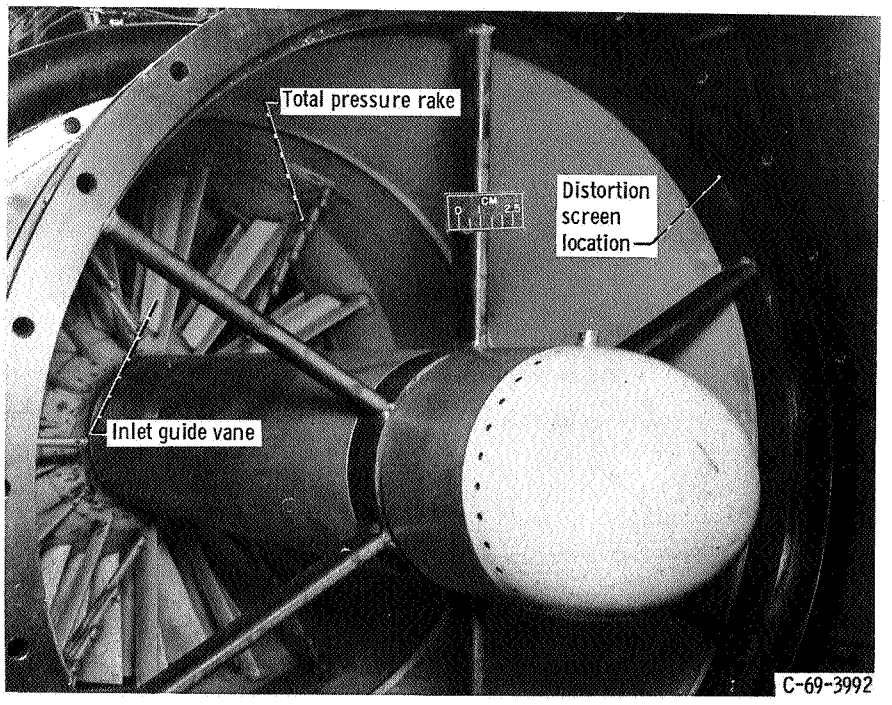

(c) Bullet-nose extension.

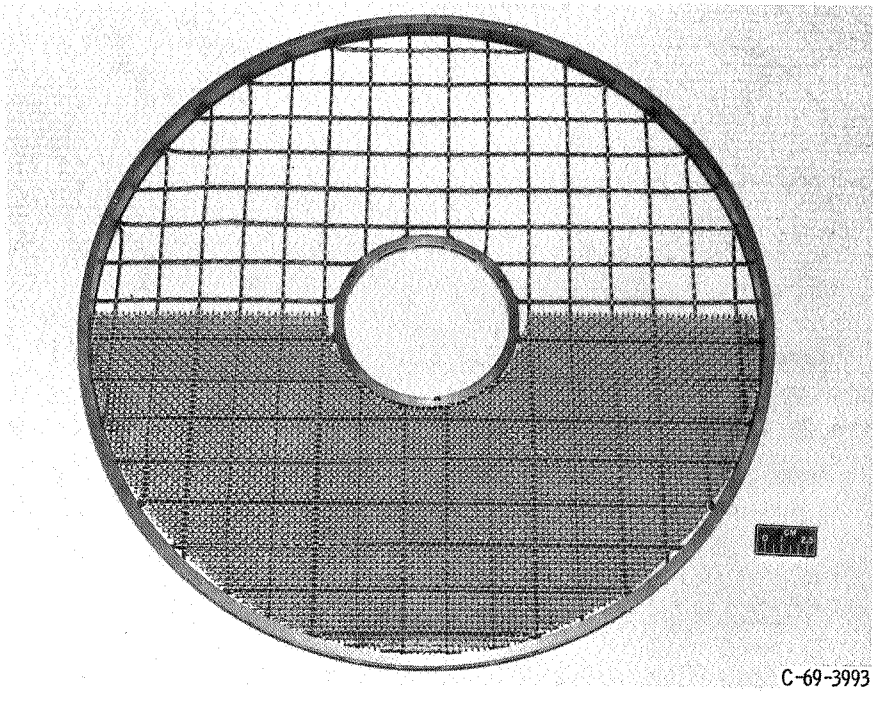

(d) Screen pattern 6 mounted on support grid.

Figure 1. - Concluded.

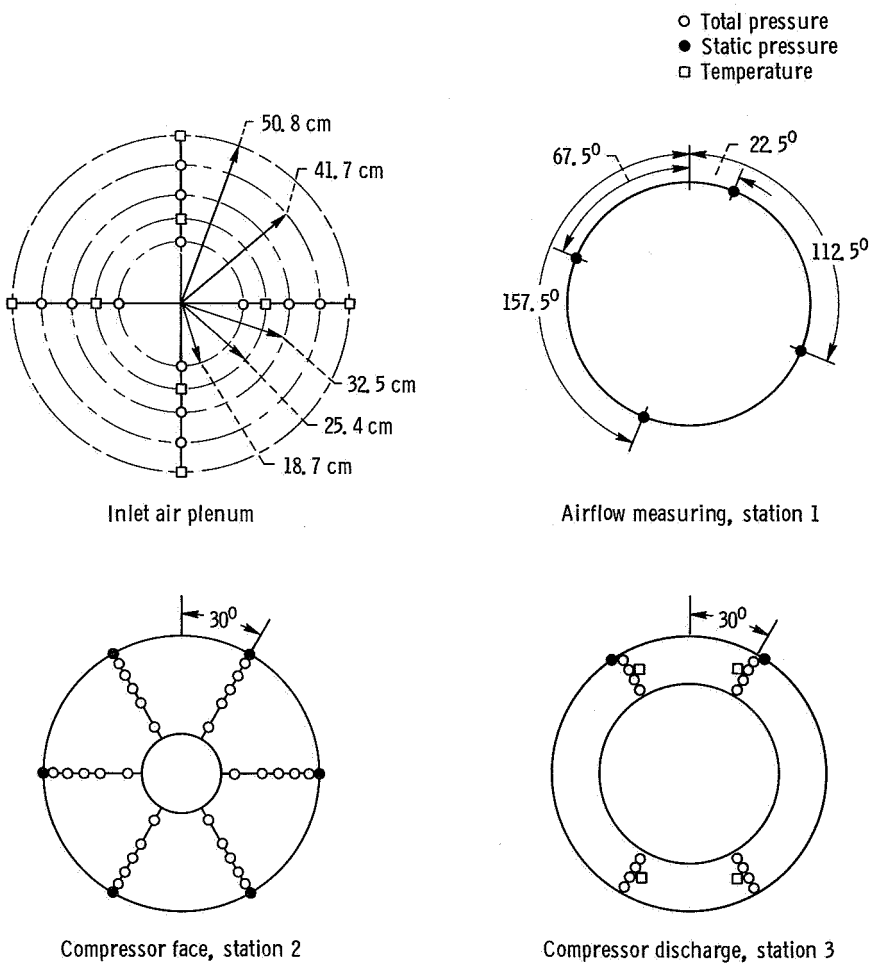

Figure 2. - Instrumentation schematic as viewed from upstream.

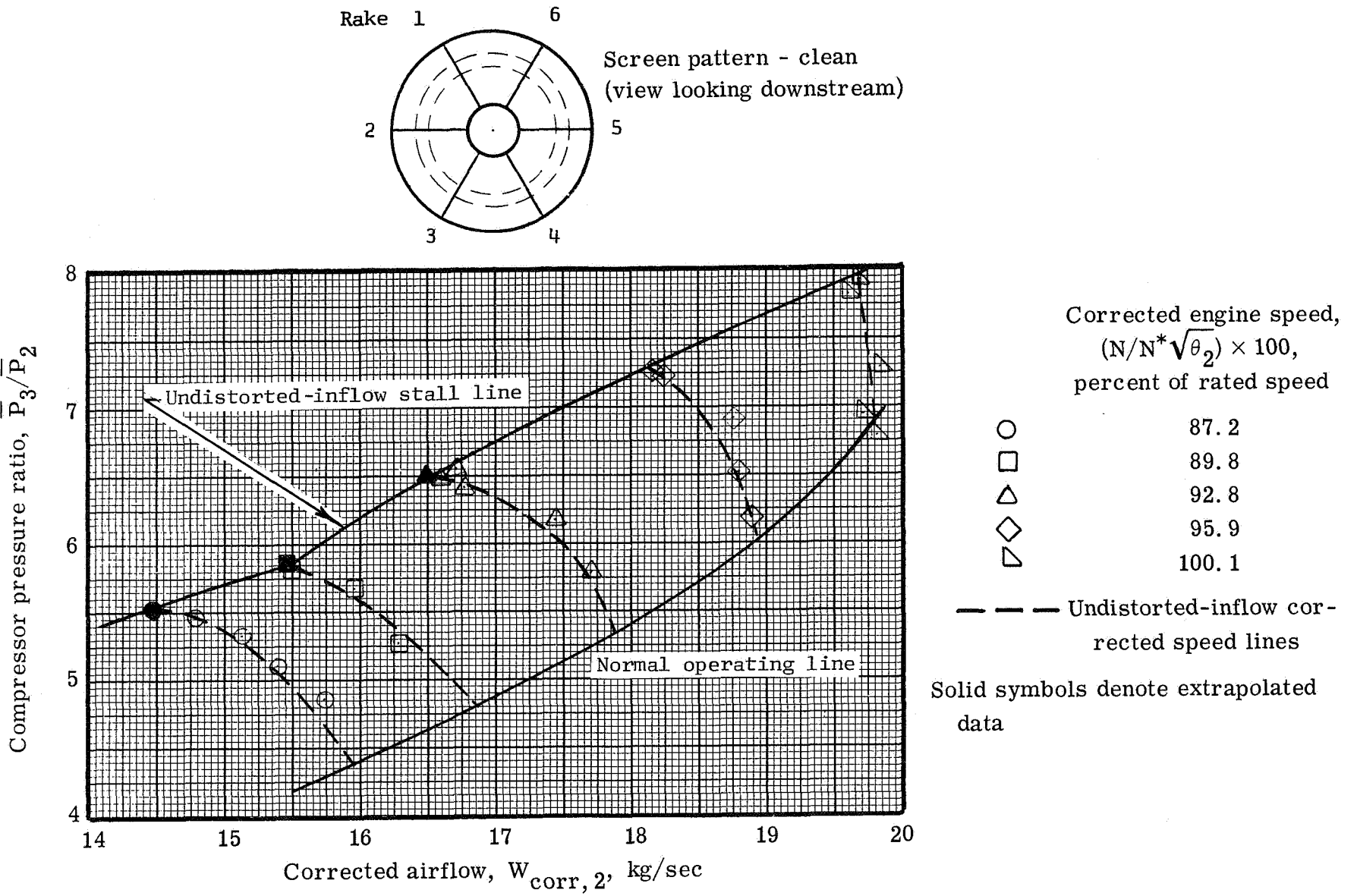

(a) Engine B map.

Figure 3. - Compressor performance with undistorted inflow.

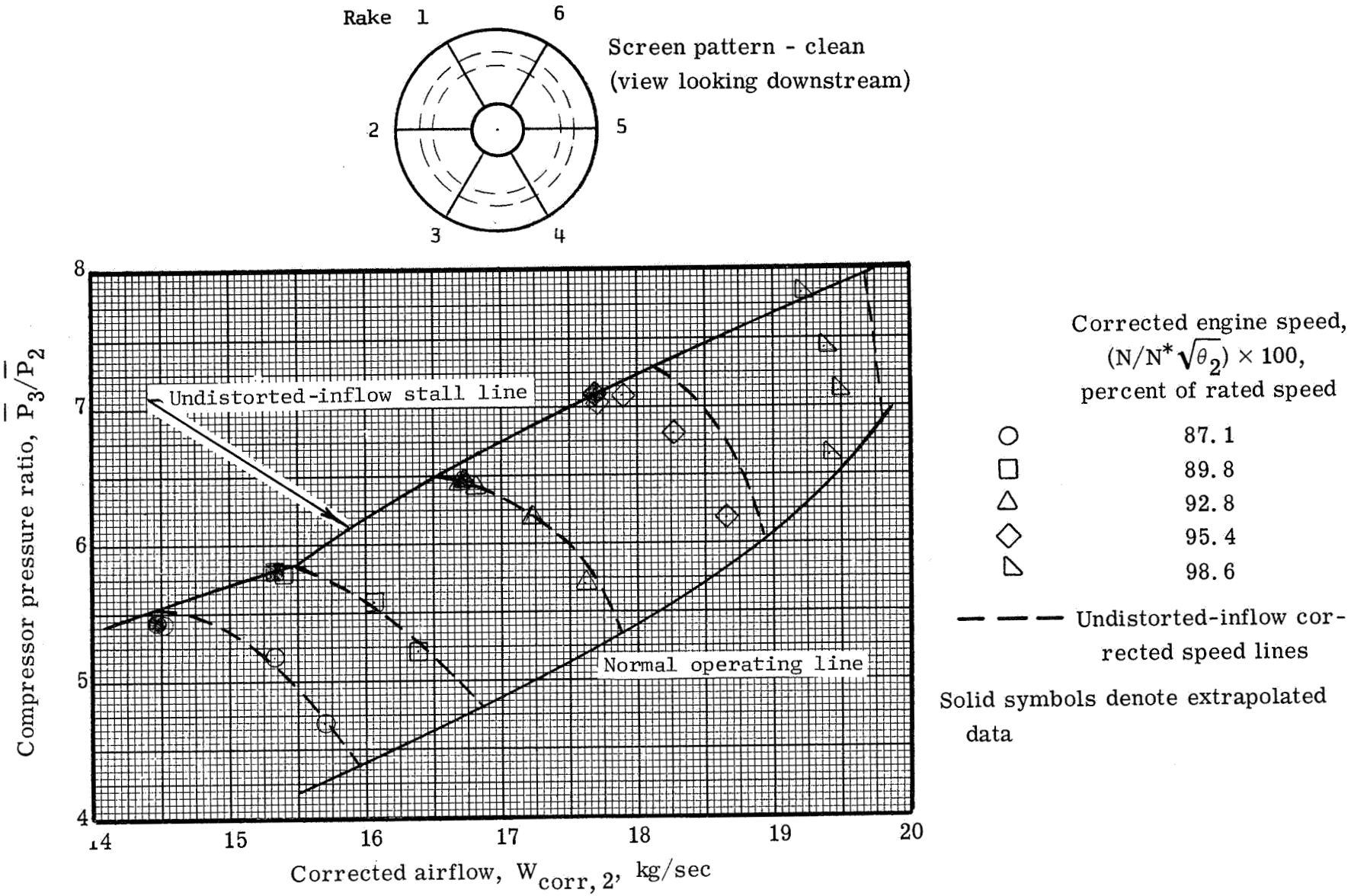

(b) Engine A map.

Figure 3. - Continued.

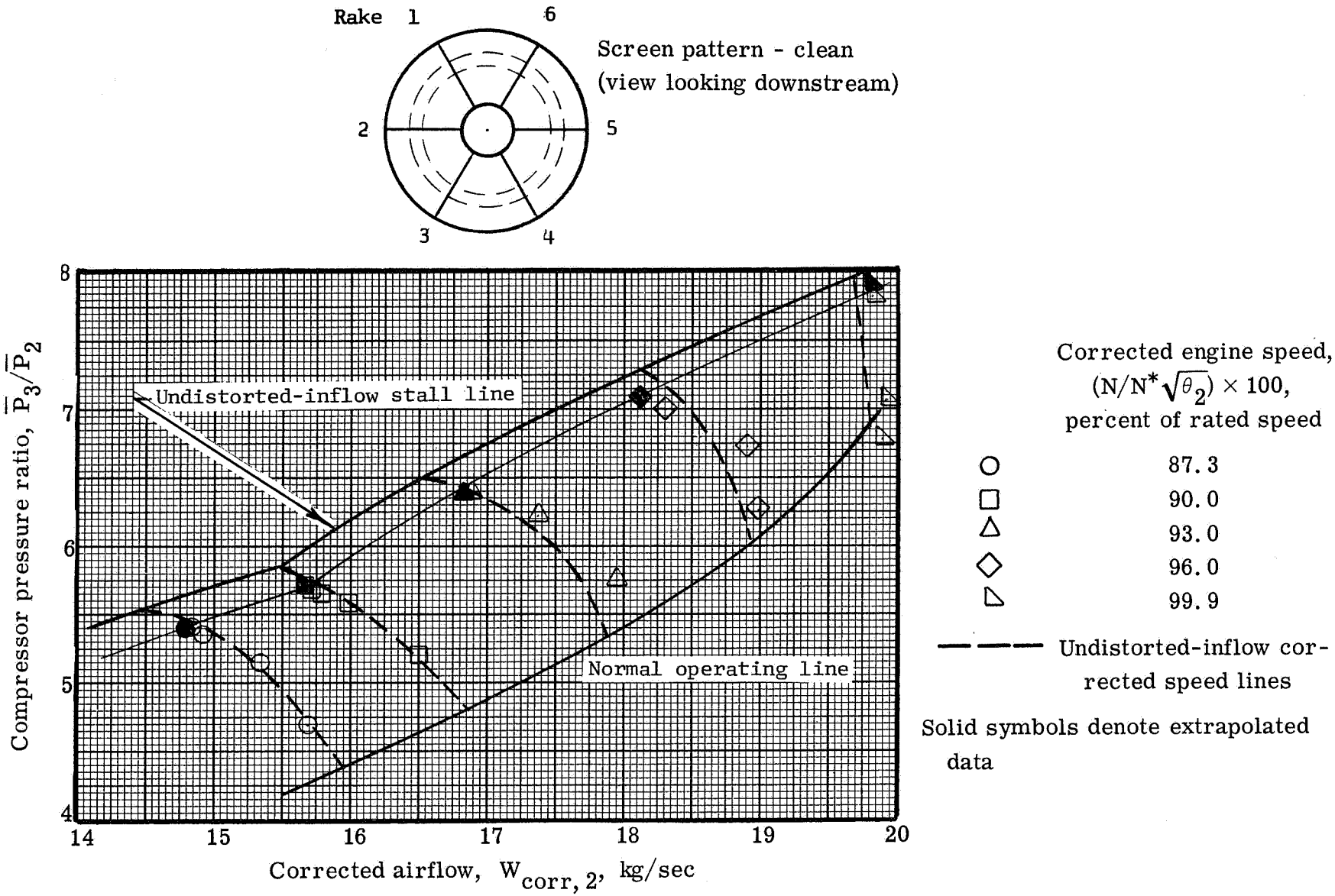

(c) 1969 Engine map (fig. 3, ref. 2).

Figure 3. - Concluded.

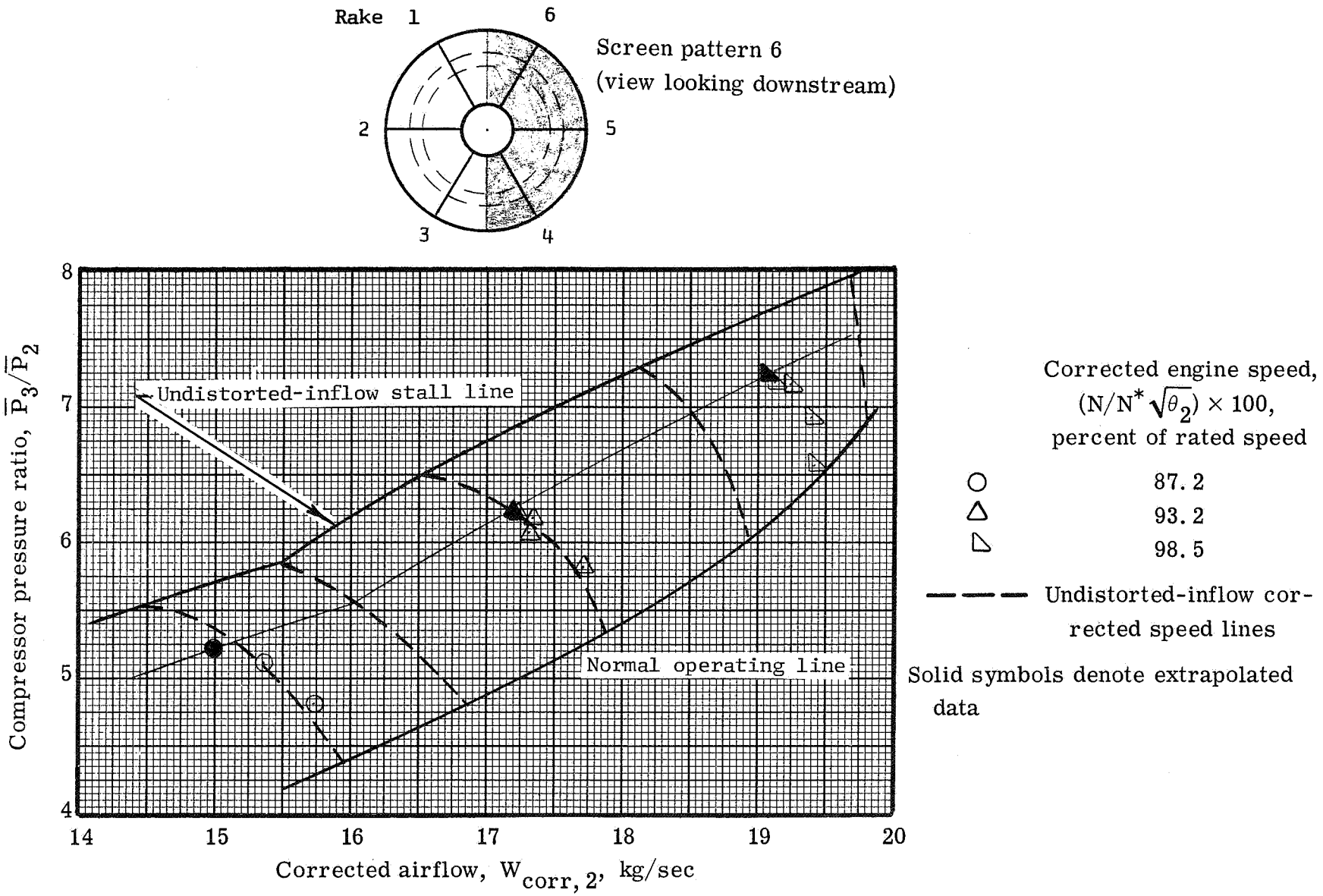

(a) 50.6-Percent-porosity screen; engine B.

Figure 4. - Compressor performance with 180° circumferential distortion.

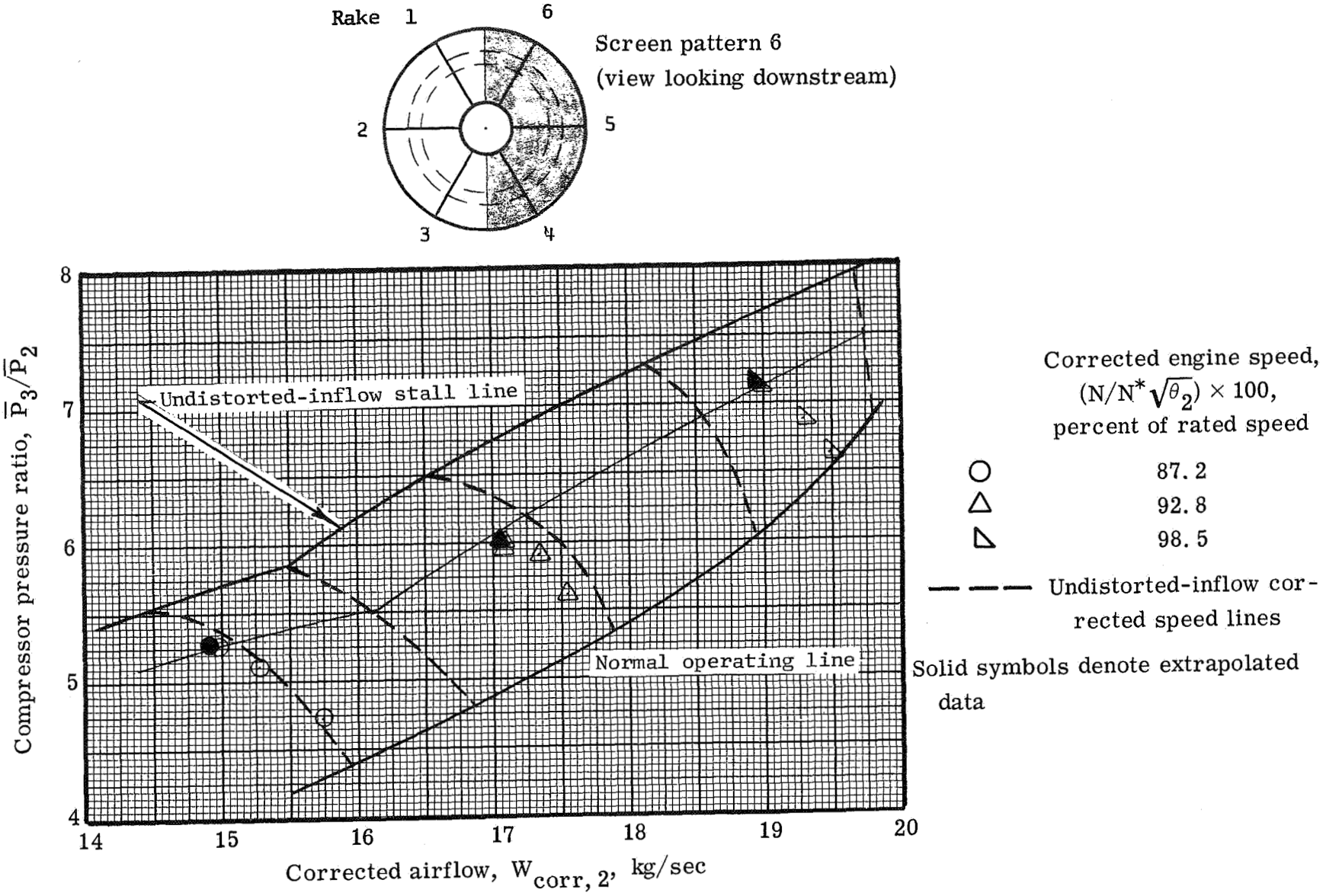

(b) 50.6-Percent-porosity screen; engine A.

Figure 4. - Continued.

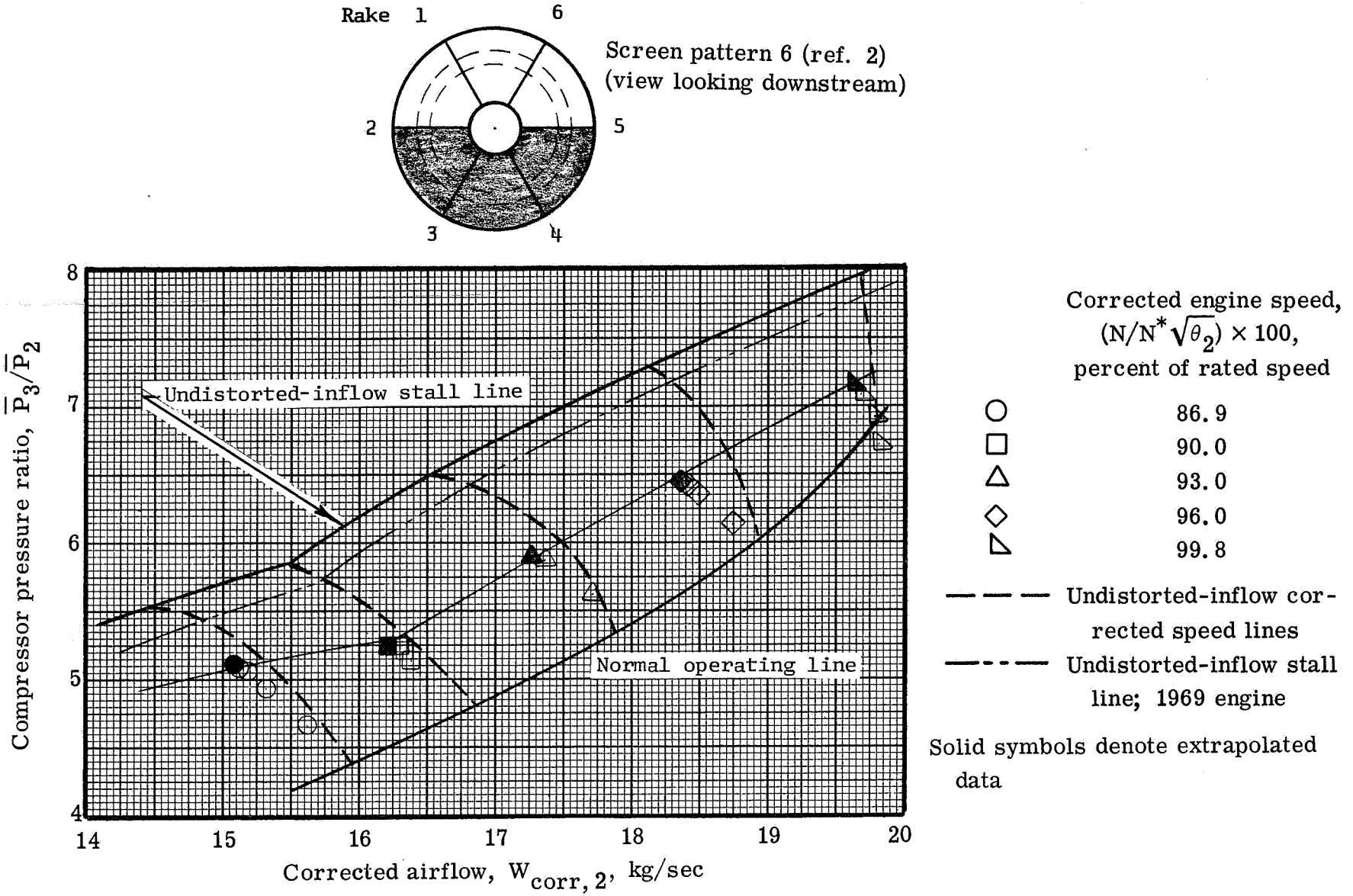

(c) 49.8-Percent-porosity screen; 1969 engine (ref. 2).

Figure 4. - Continued.

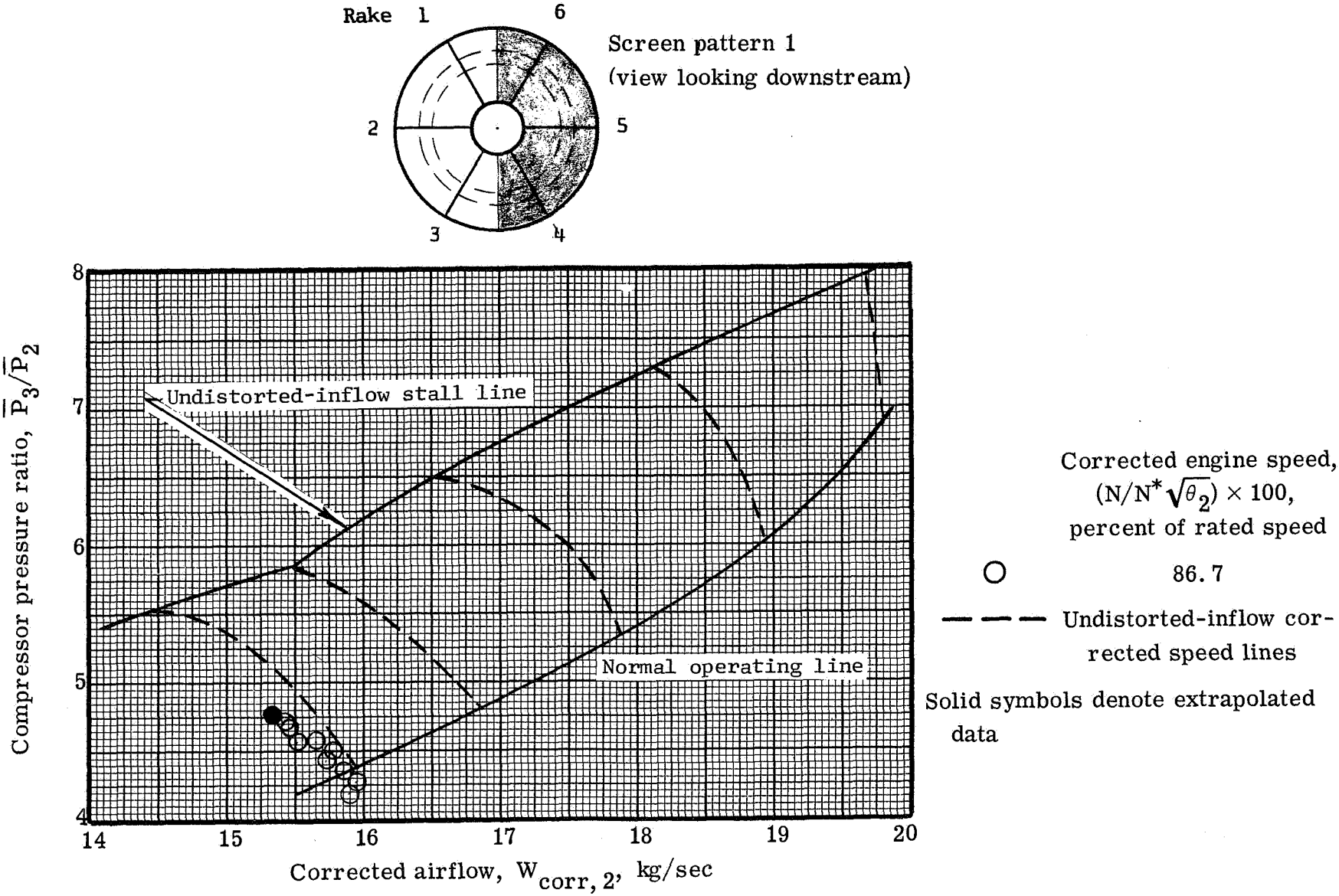

(d) 26.4-Percent-porosity screen; engine A.

Figure 4. - Concluded.

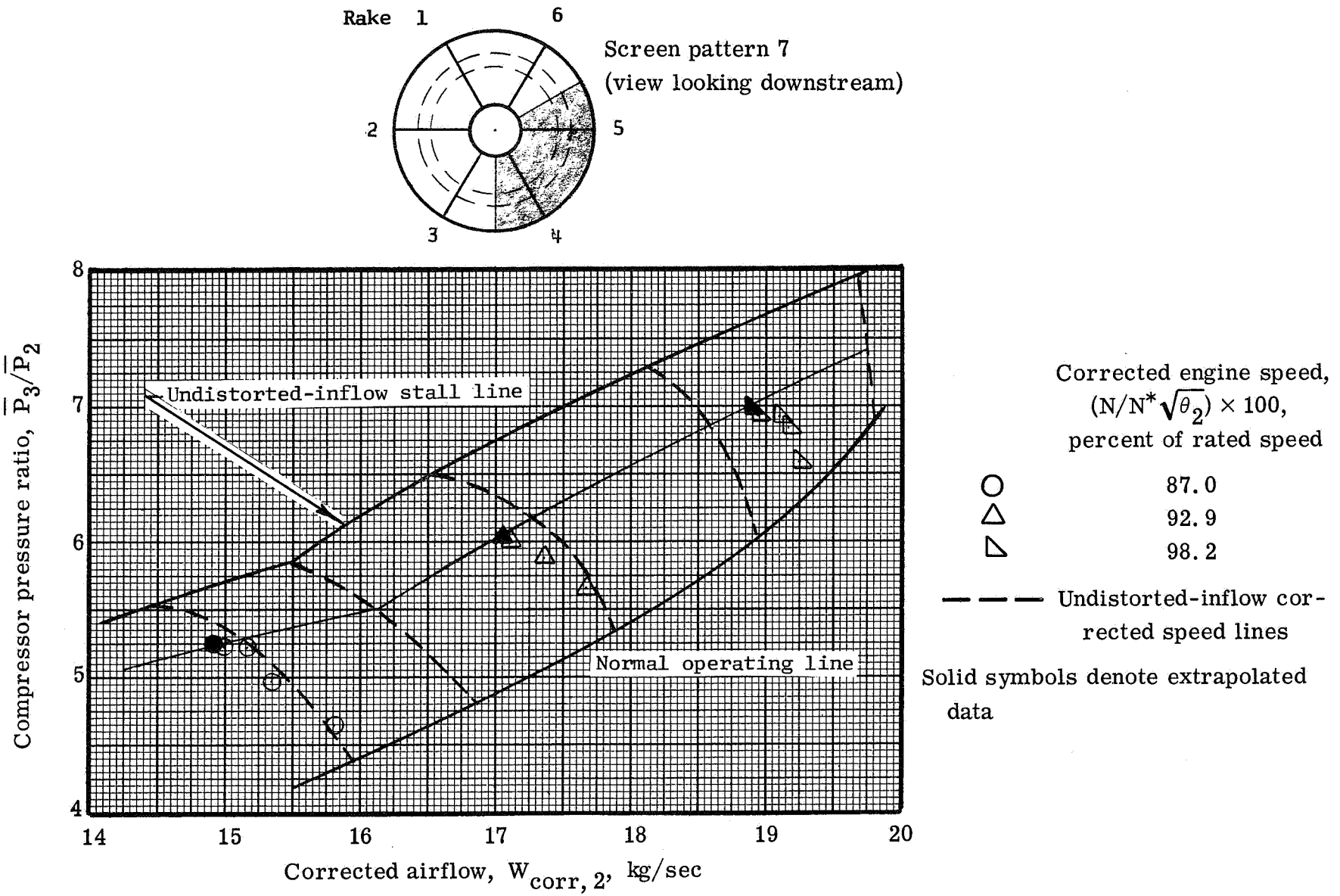

(a) 50.6-Percent-porosity screen; engine A.

Figure 5. - Compressor performance with 120° circumferential distortion.

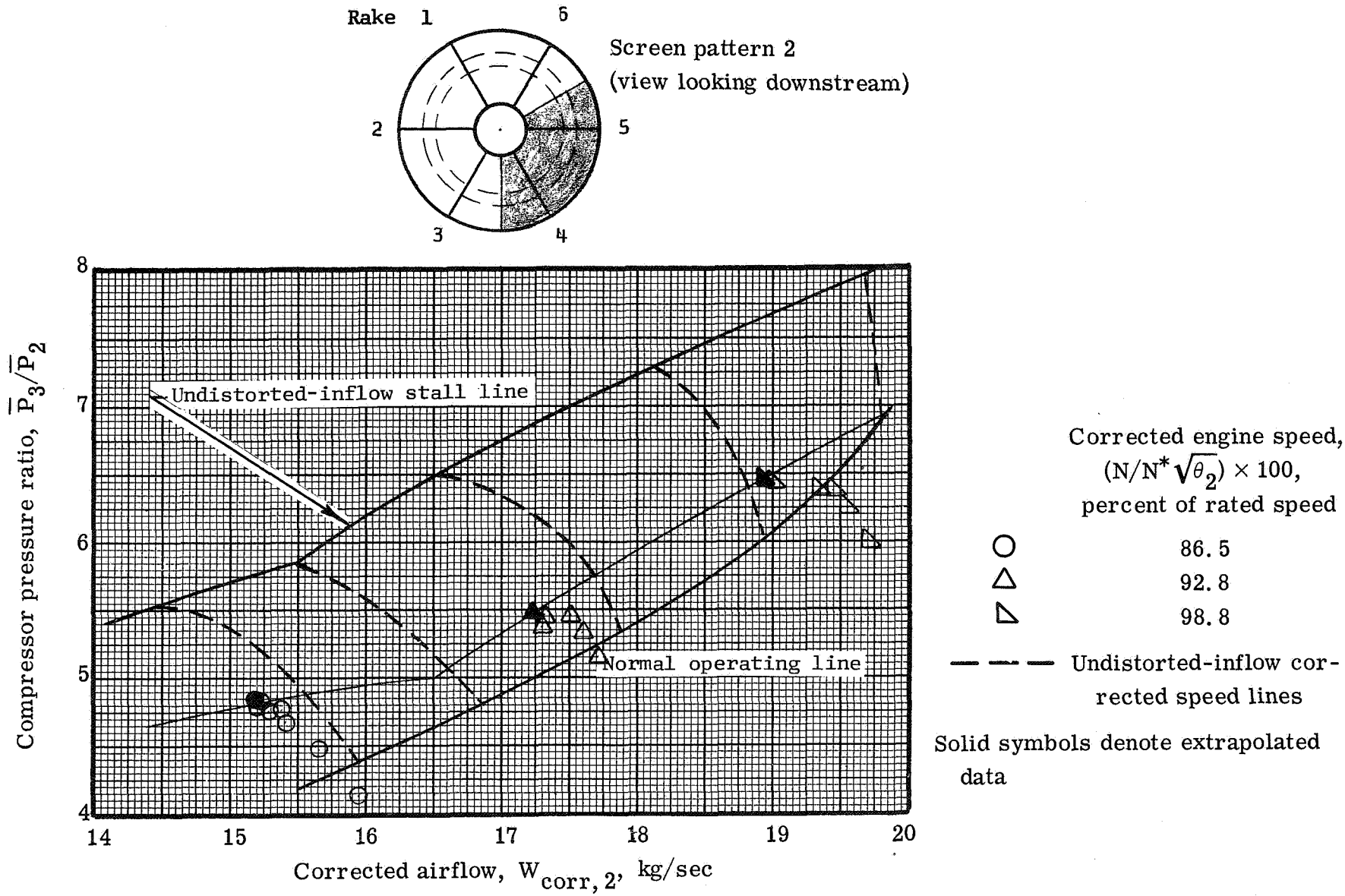

(b) 26.4-Percent-porosity screen; engine A.

Figure 5. - Concluded.

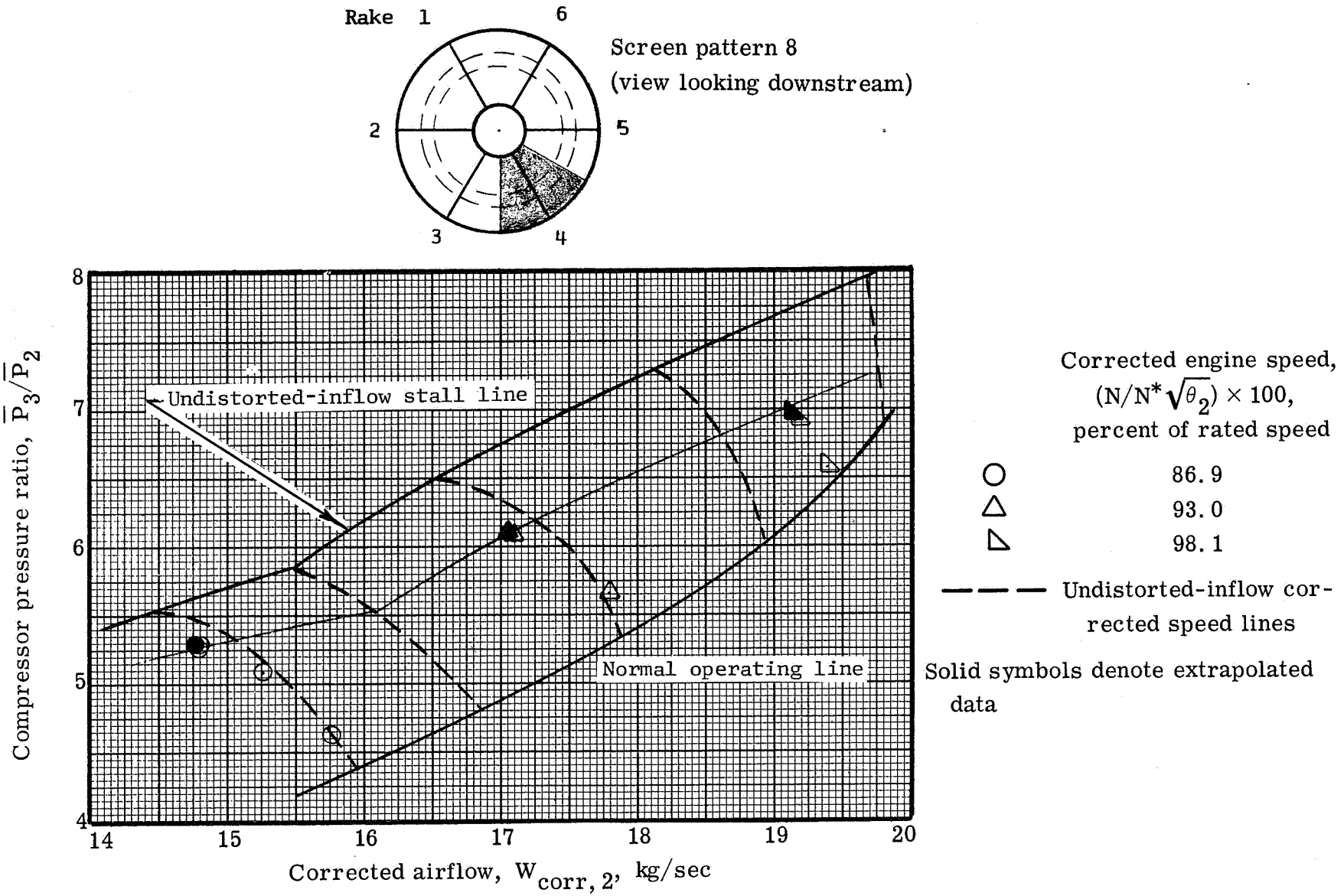

(a) 50.6-Percent-porosity screen; engine A.

Figure 6. - Compressor performance with 60° circumferential distortion.

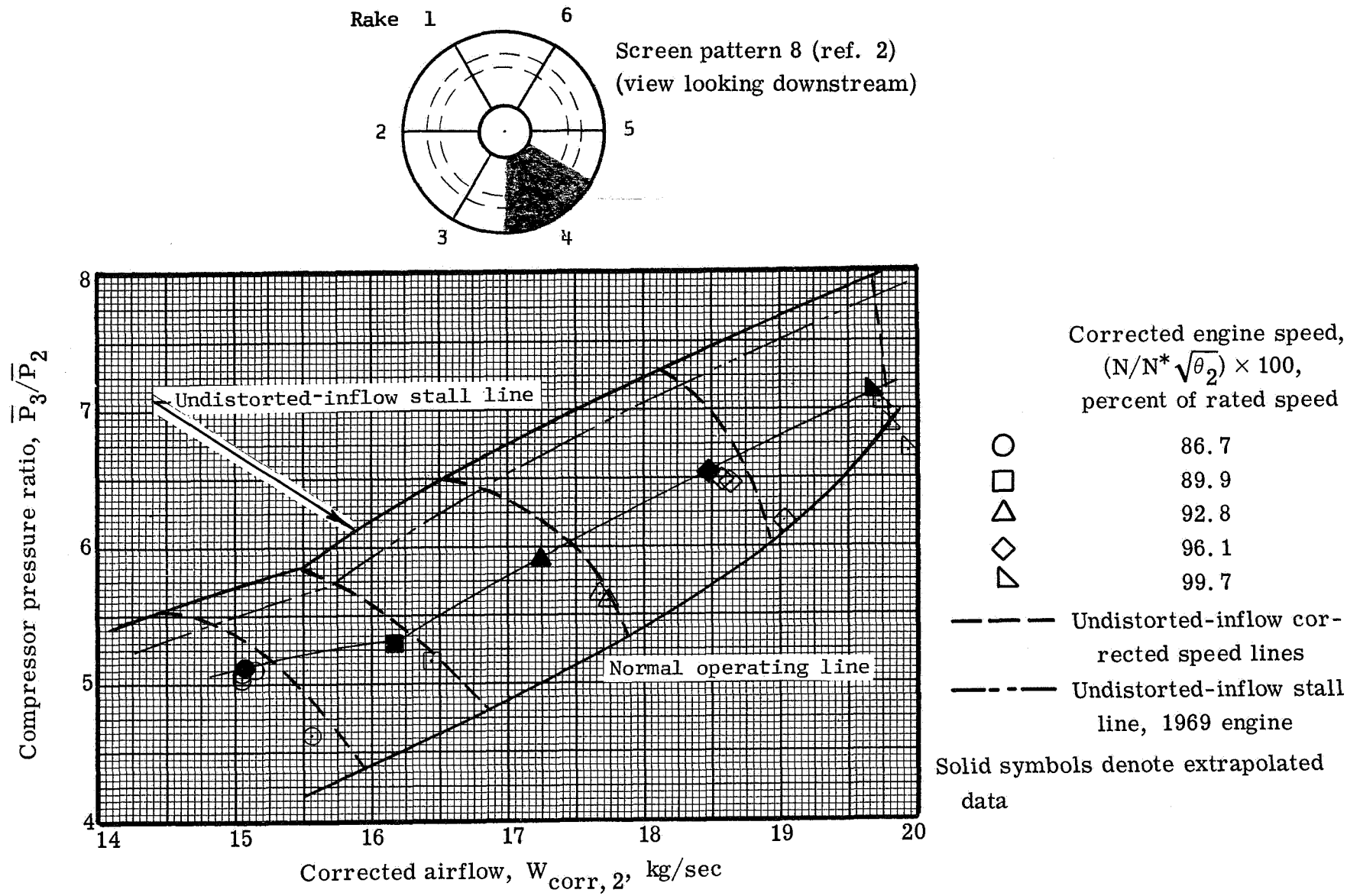

(b) 49.8-Percent-porosity screen; 1969 engine (ref. 2).

Figure 6. - Continued.

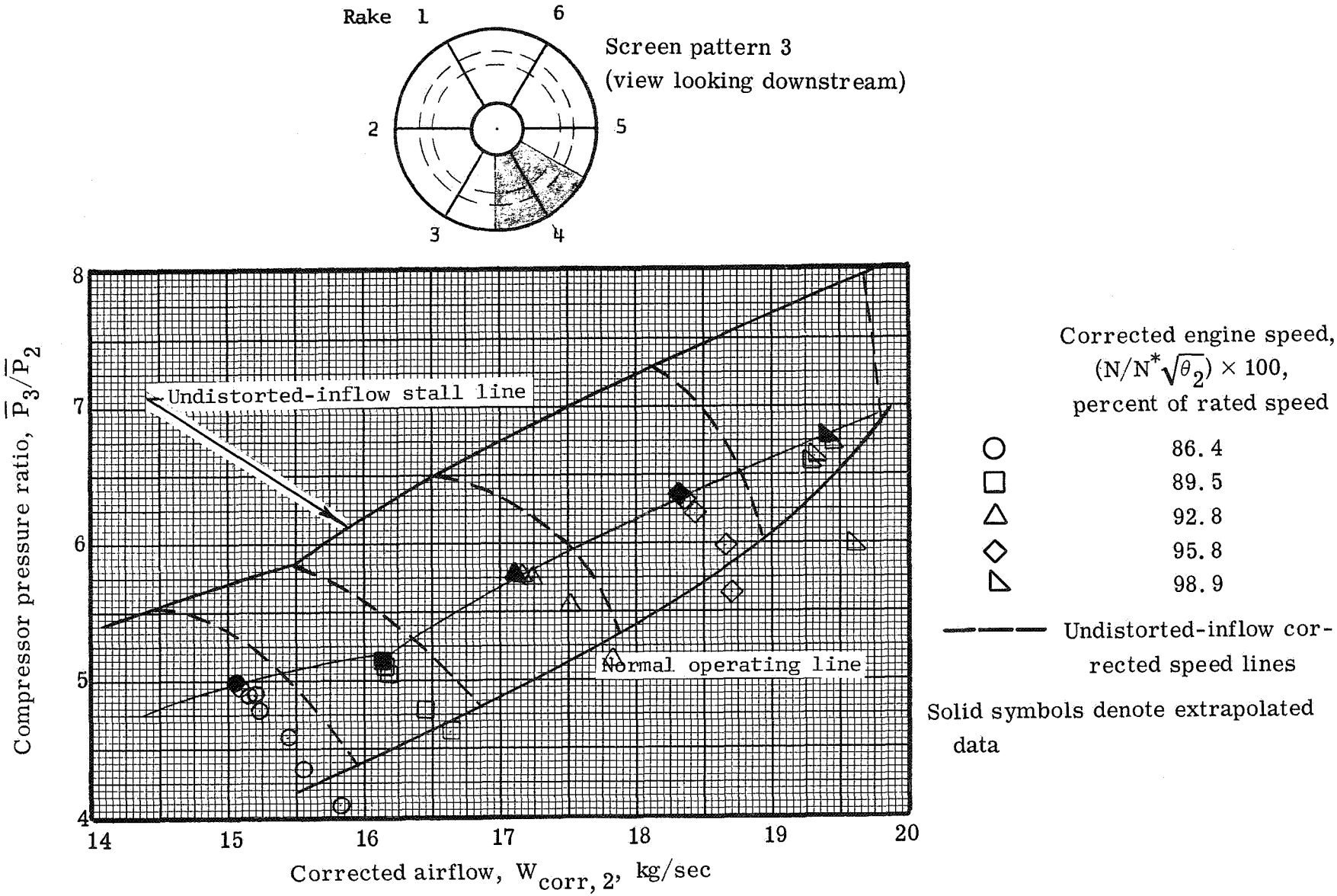

(c) 26.4-Percent-porosity screen; engine A.

Figure 6. - Concluded.

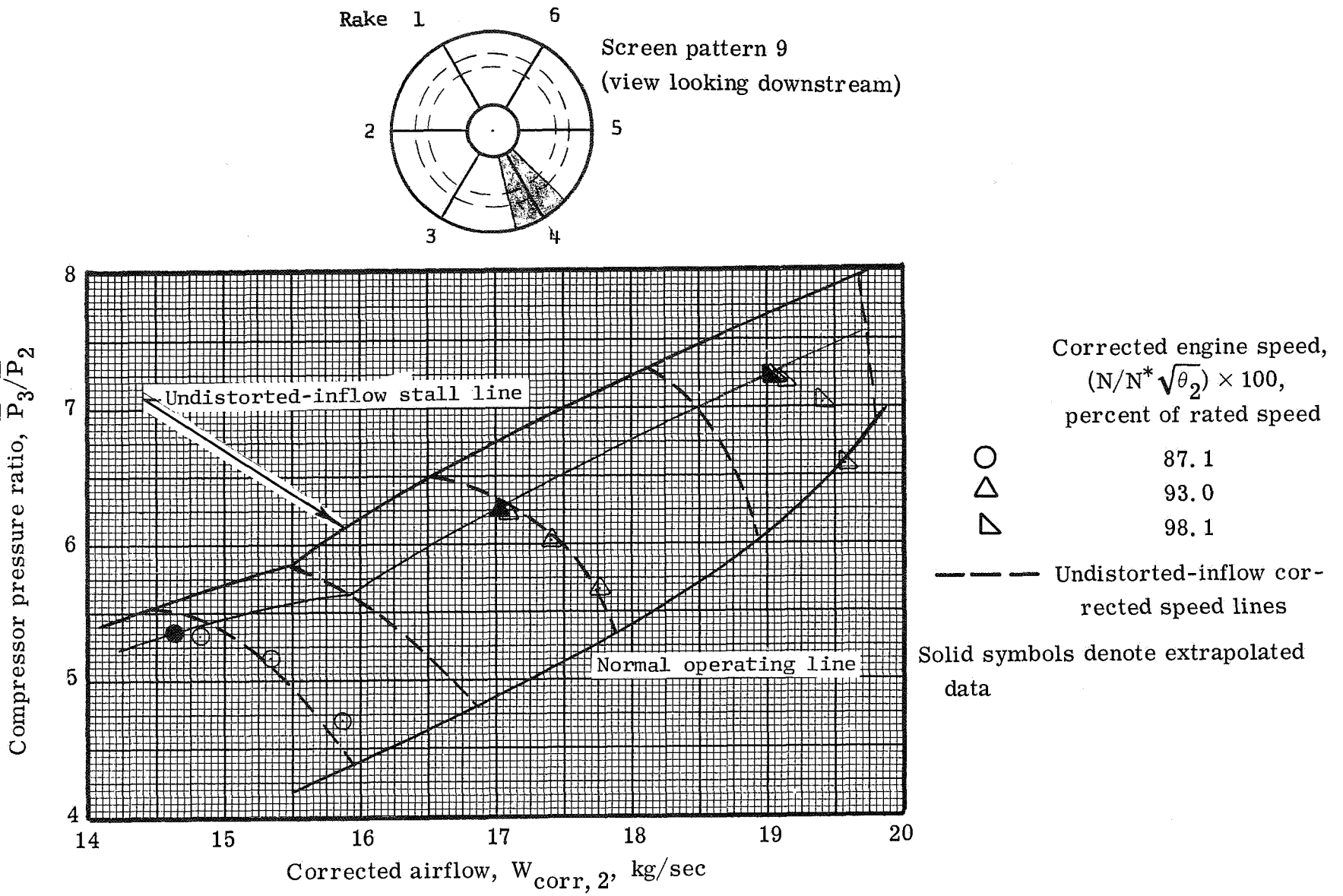

(a) 50.6-Percent-porosity screen; engine A.

Figure 7. - Compressor performance with 30^o circumferential distortion.

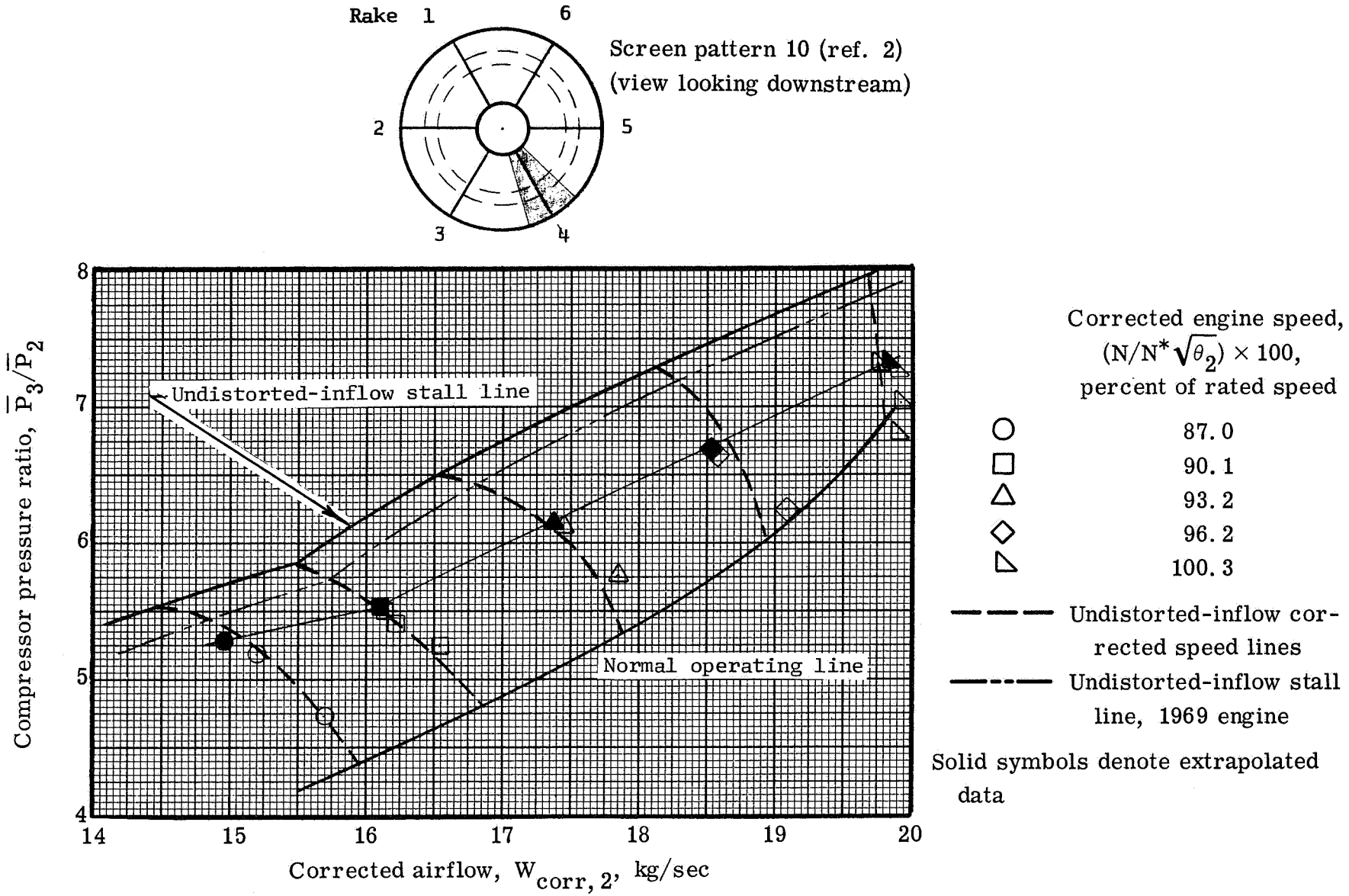

(b) 49.8-Percent-porosity screen; 1969 engine (ref. 2).

Figure 7. - Concluded.

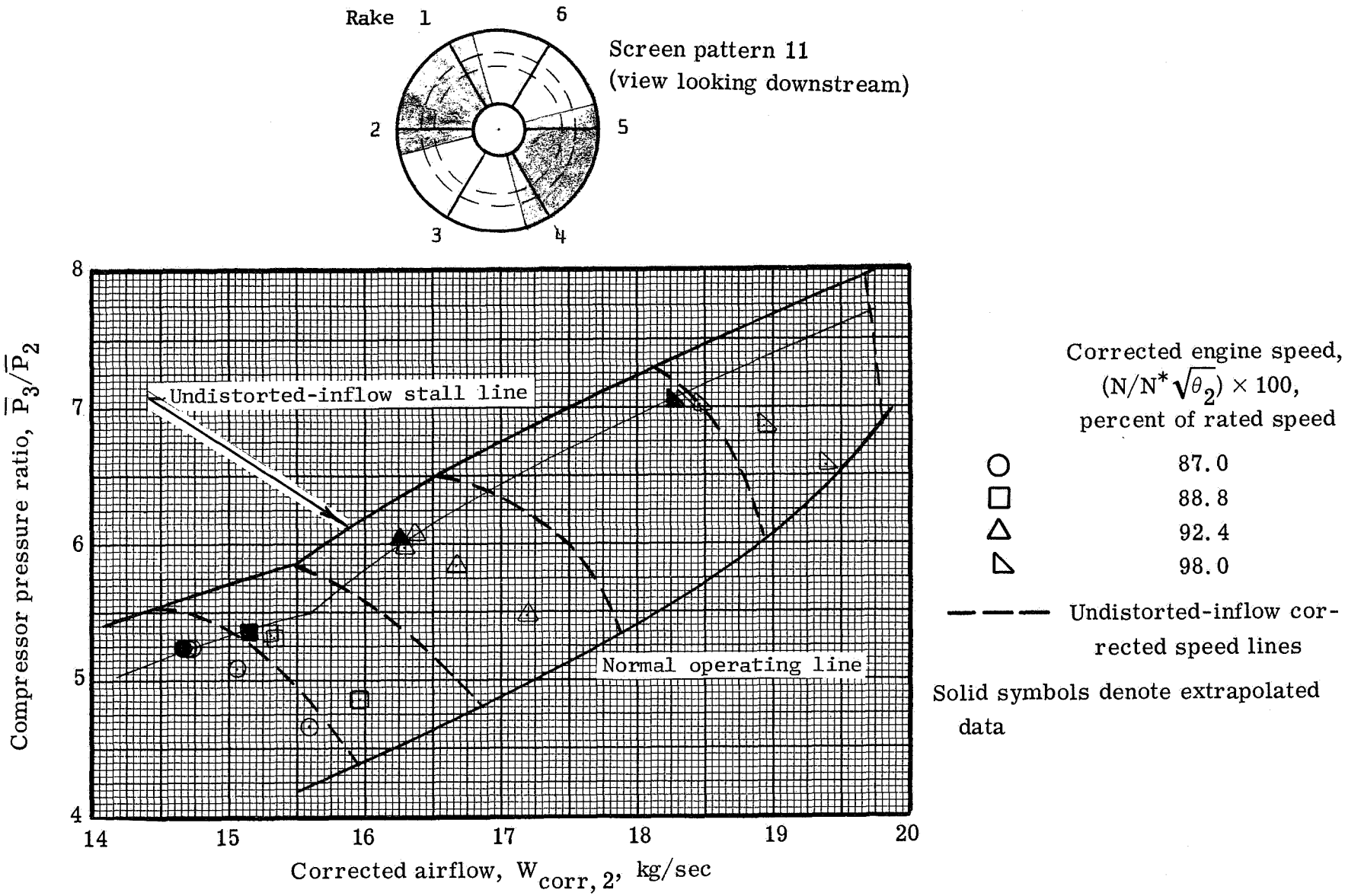

(a) 90° Spoiled sectors; engine A.

Figure 8. - Compressor performance with two-per-revolution circumferential distortion of 50.6-percent-porosity screen.

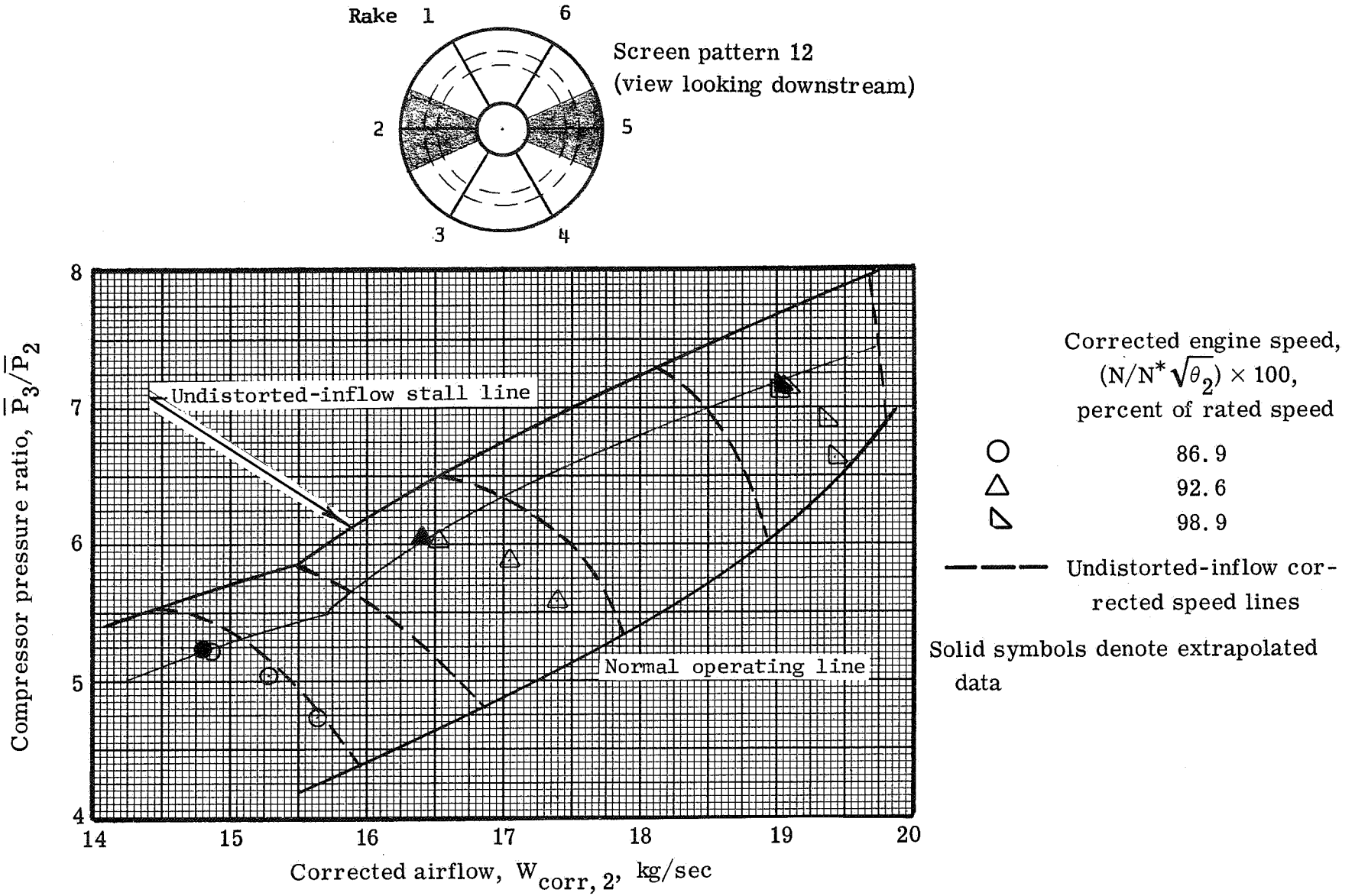

(b) 45° Spoiled sectors; engine A.

Figure 8. - Continued.

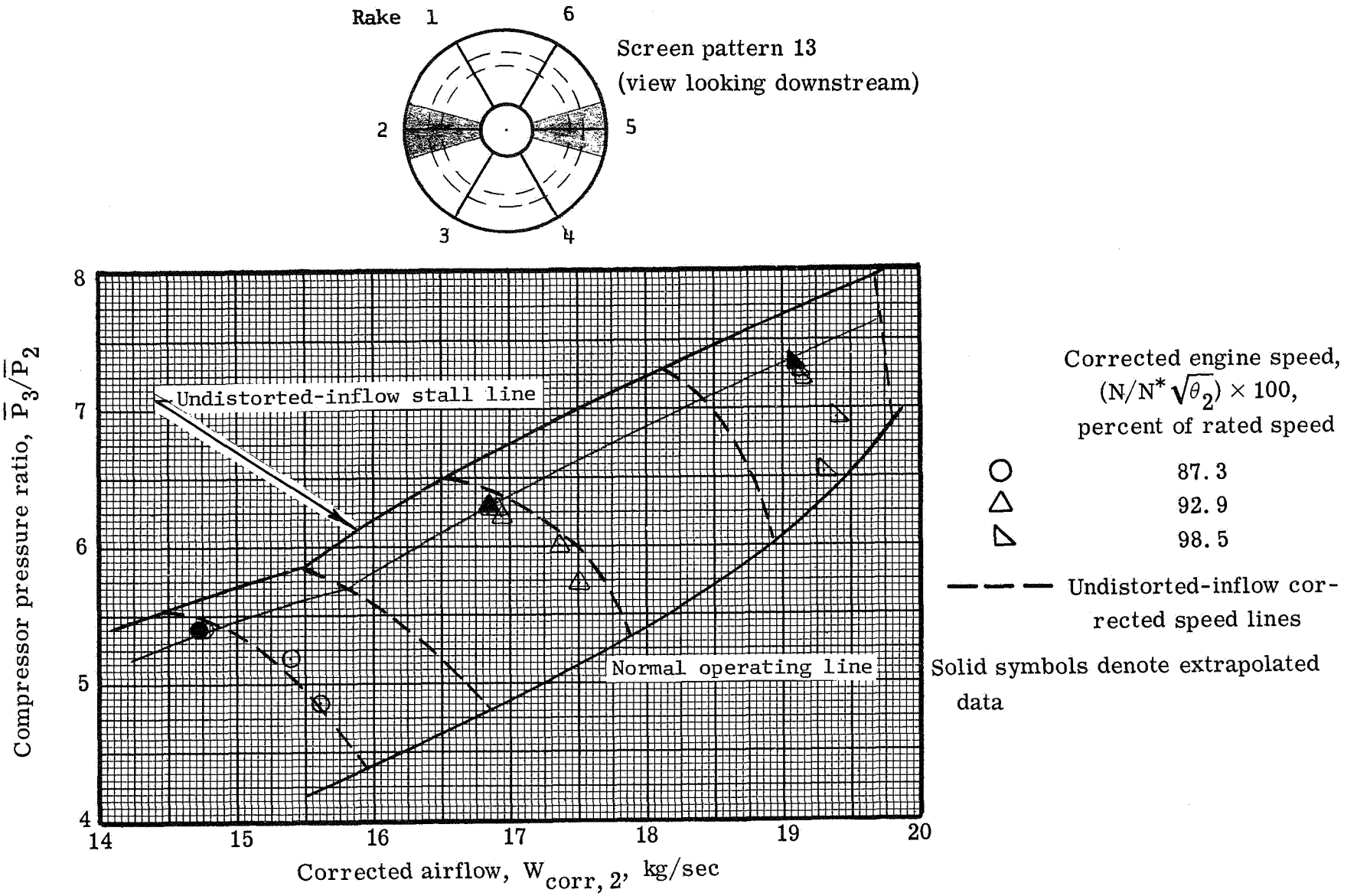

(c) 30° Spoiled sectors; engine B.

Figure 8. - Concluded.

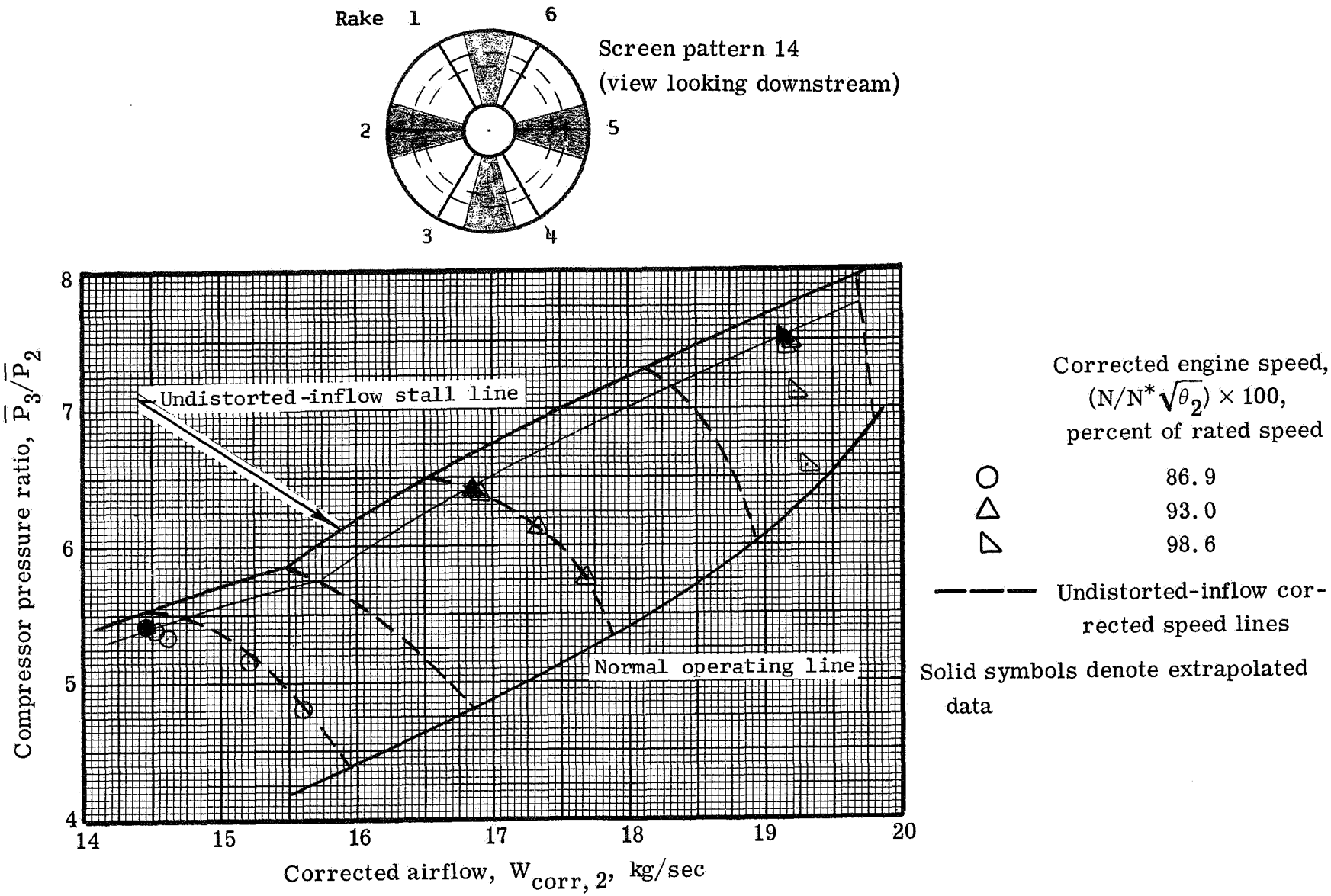

Figure 9. - Compressor performance with four-per-revolution circumferential distortion. 30° Spoiled sectors of 50.6-percent-porosity screen; engine B.

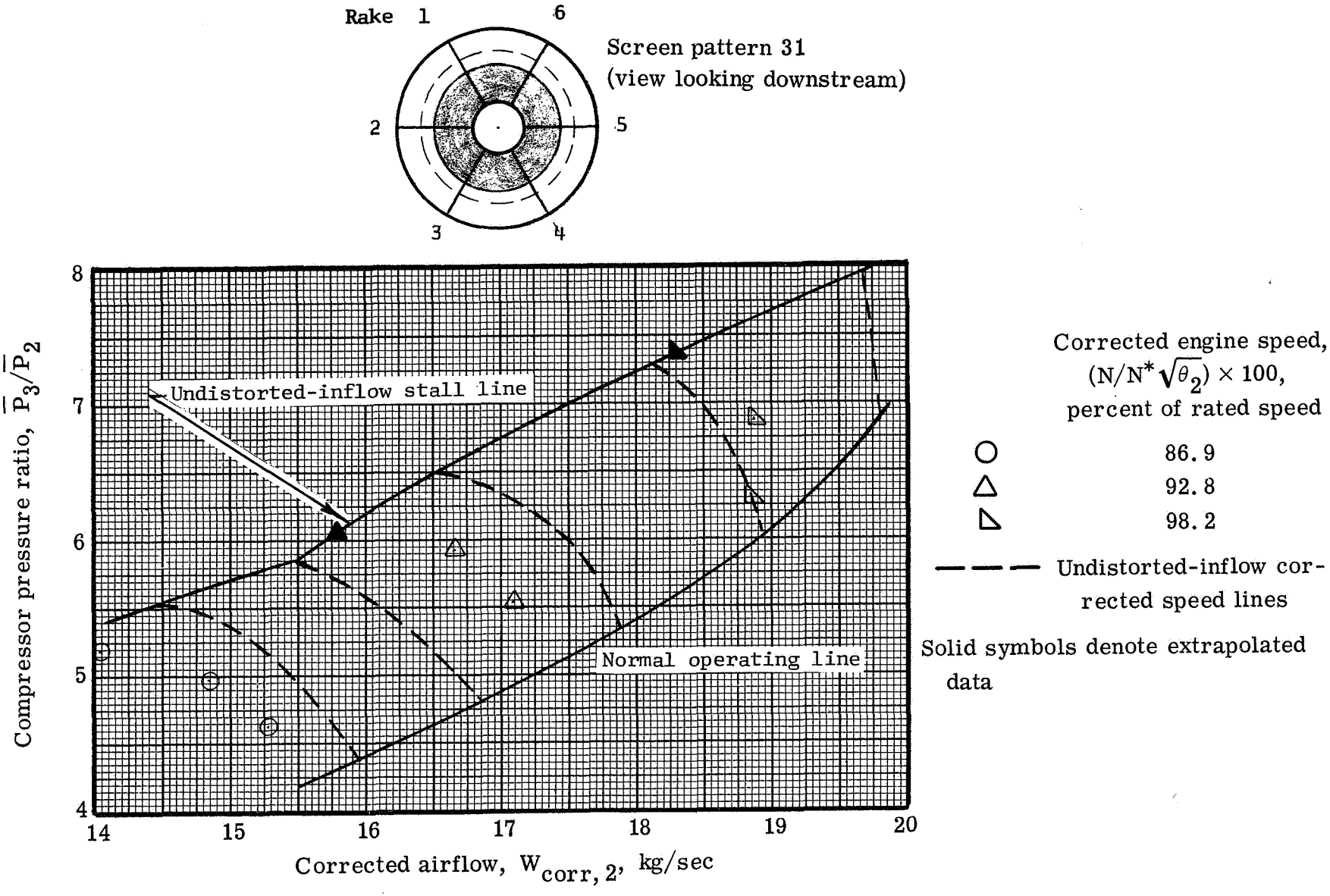

(a) 39.7-Percent-porosity screen; engine B.

Figure 10. - Compressor performance with hub radial distortion. Spoiled-area ratio, A_{SP}/A_2, 0.4.

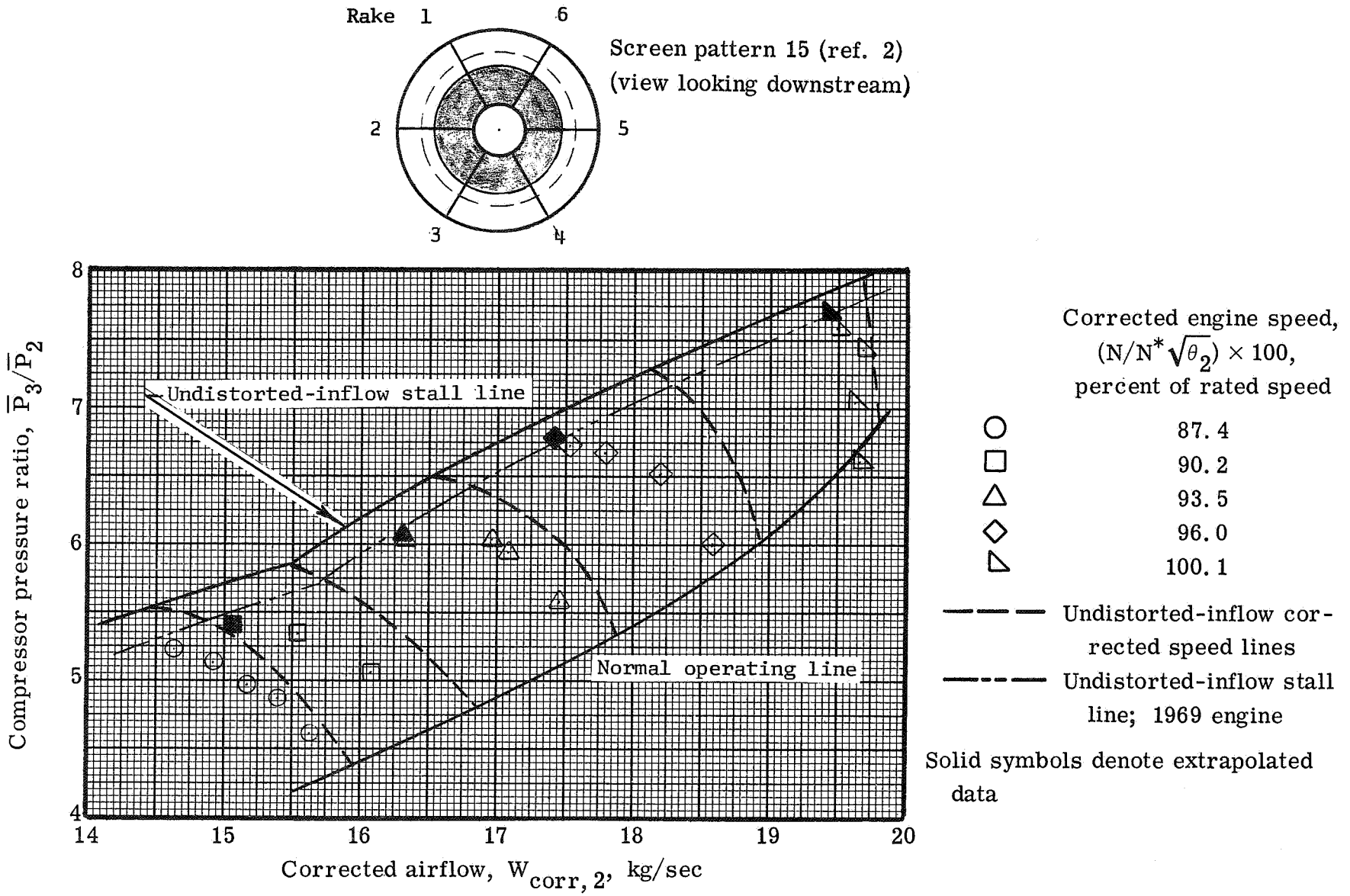

(b) 39.7-Percent-porosity screen; 1969 engine (ref. 2).

Figure 10. - Continued.

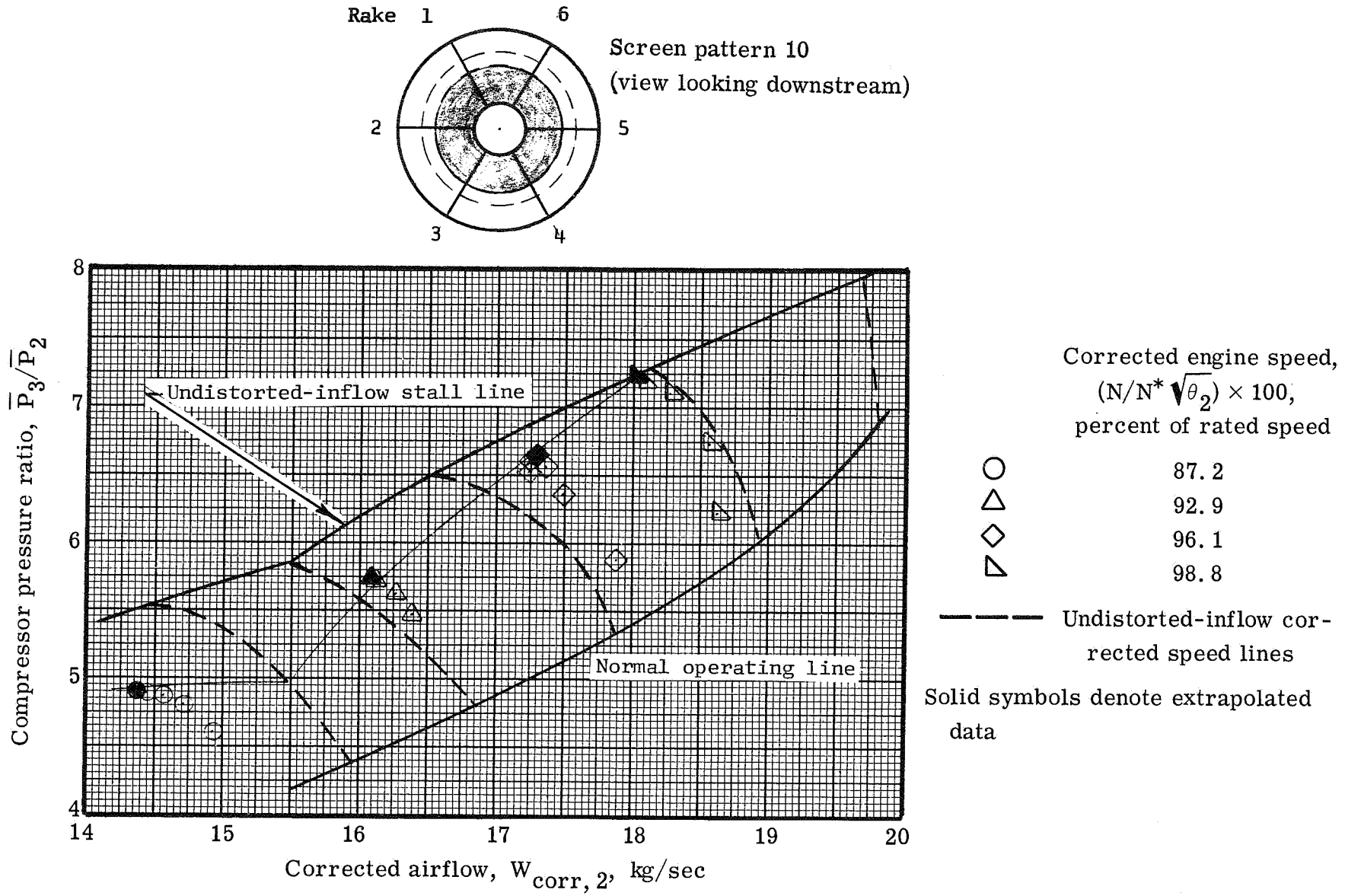

(c) 26.4-Percent-porosity screen; engine B.

Figure 10. - Continued.

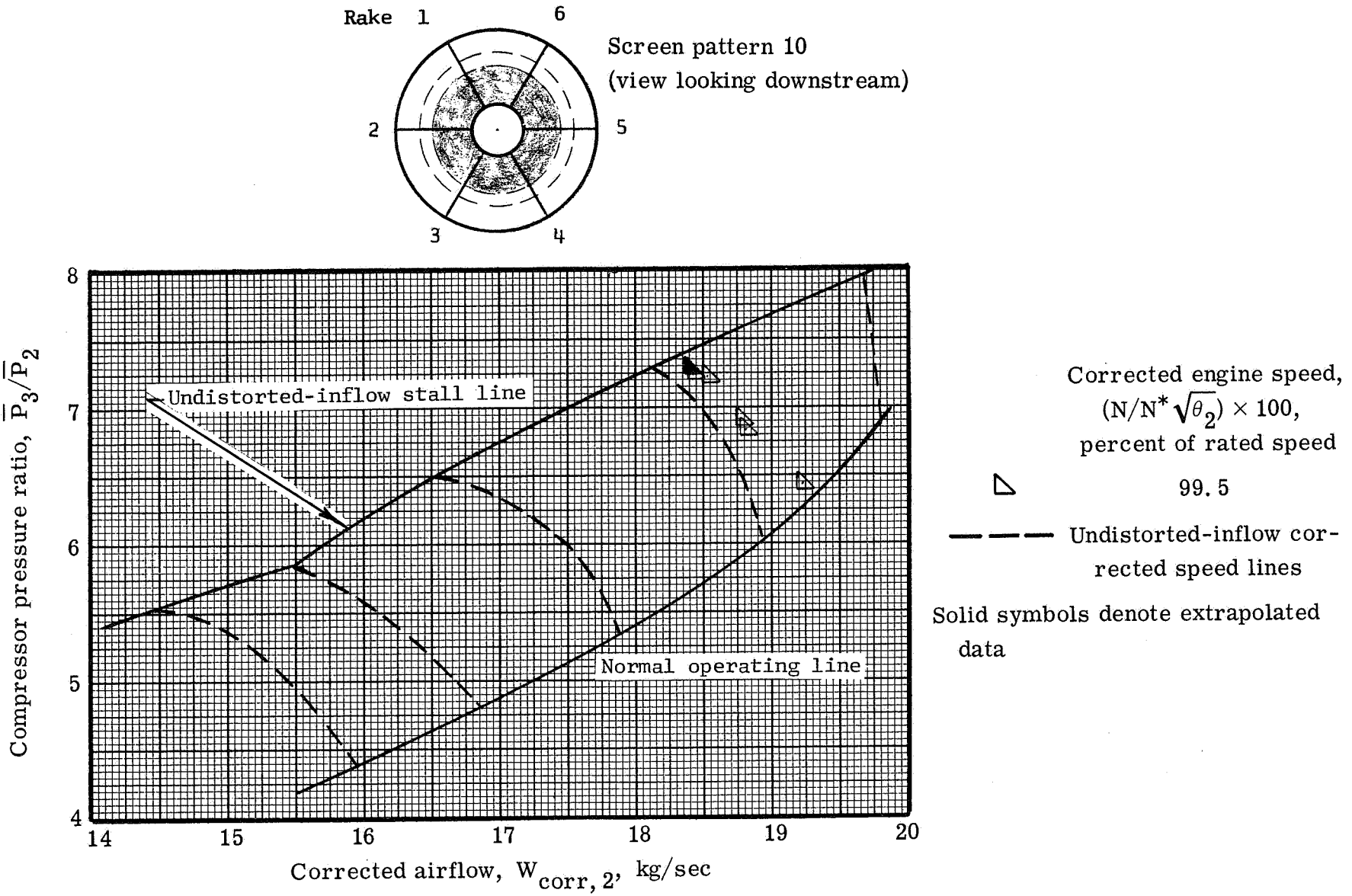

(d) 26.4-Percent-porosity screen; engine A.

Figure 10. - Concluded.

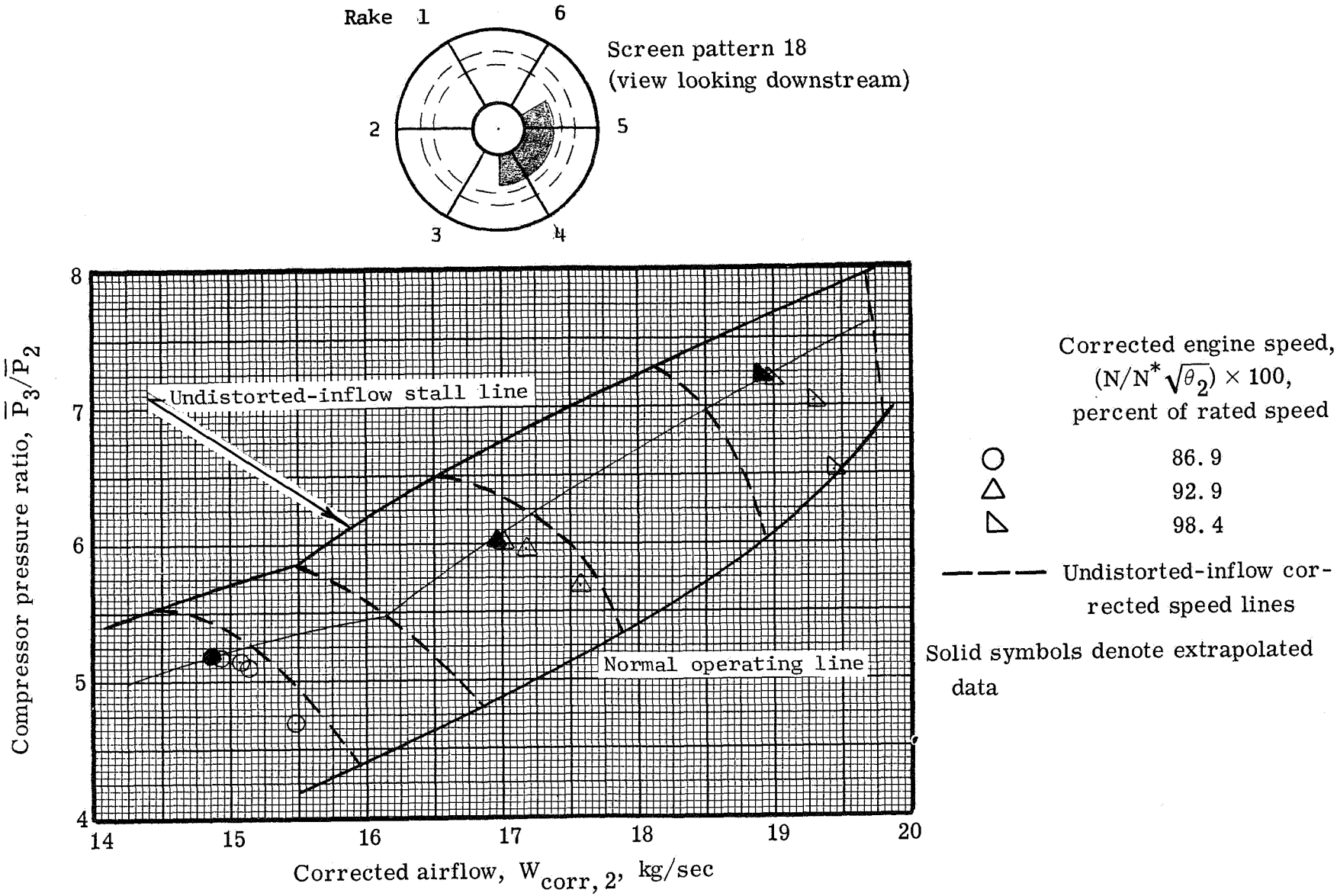

(a) 120° Spoiled sector; spoiled-area ratio, A_{SP}/A_2, 0.067; engine B.

Figure 11. - Compressor performance with partial hub radial distortion. 39.7-Percent-porosity screen.

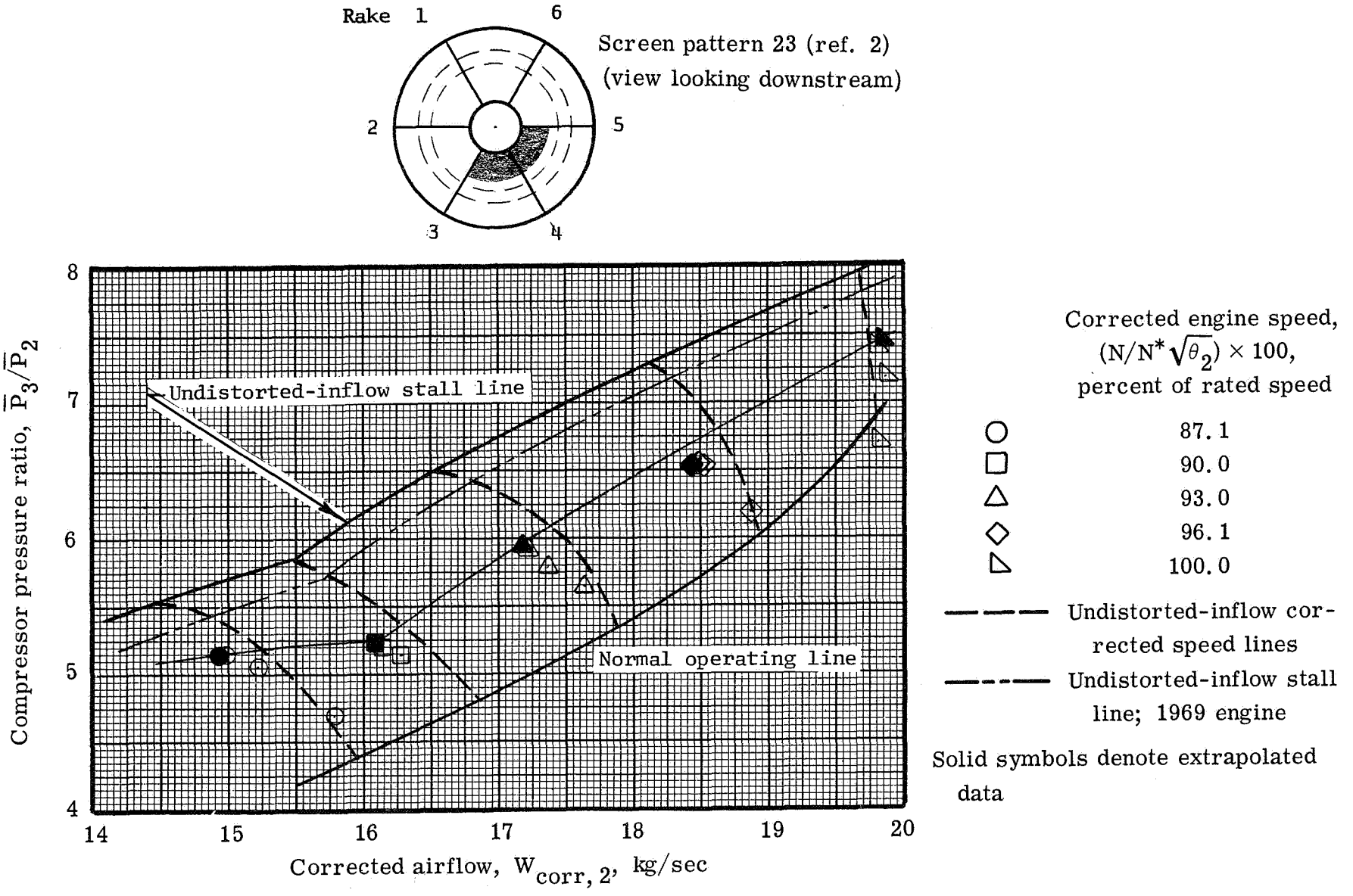

(b) 120° Spoiled sector; spoiled-area ratio, A_{SP}/A_2, 0.067; 1969 engine (ref. 2).

Figure 11. - Continued.

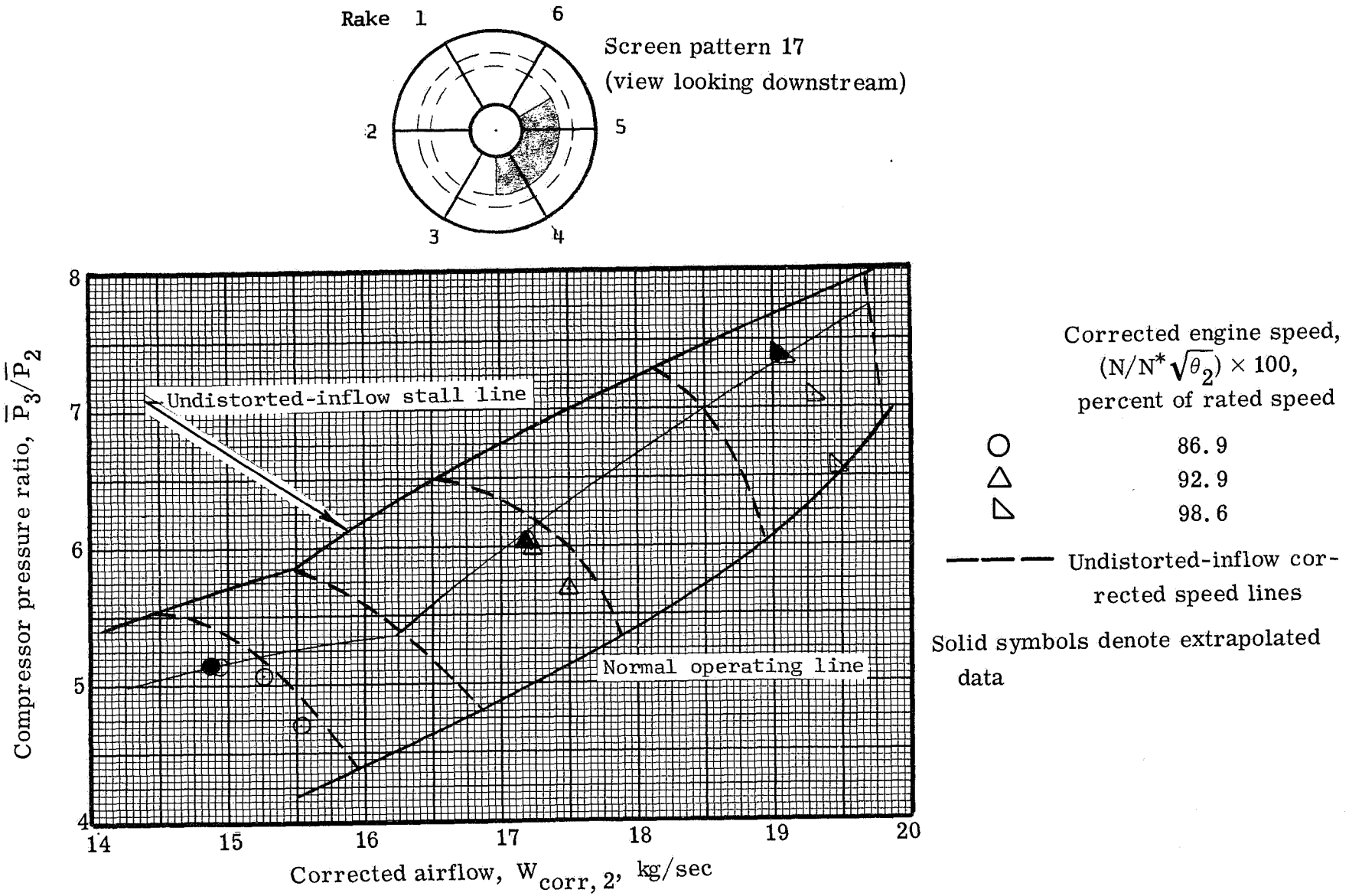

(c) 120° Spoiled sector; spoiled-area ratio, A_{SP}/A_2, 0.113; engine B.

Figure 11. - Continued.

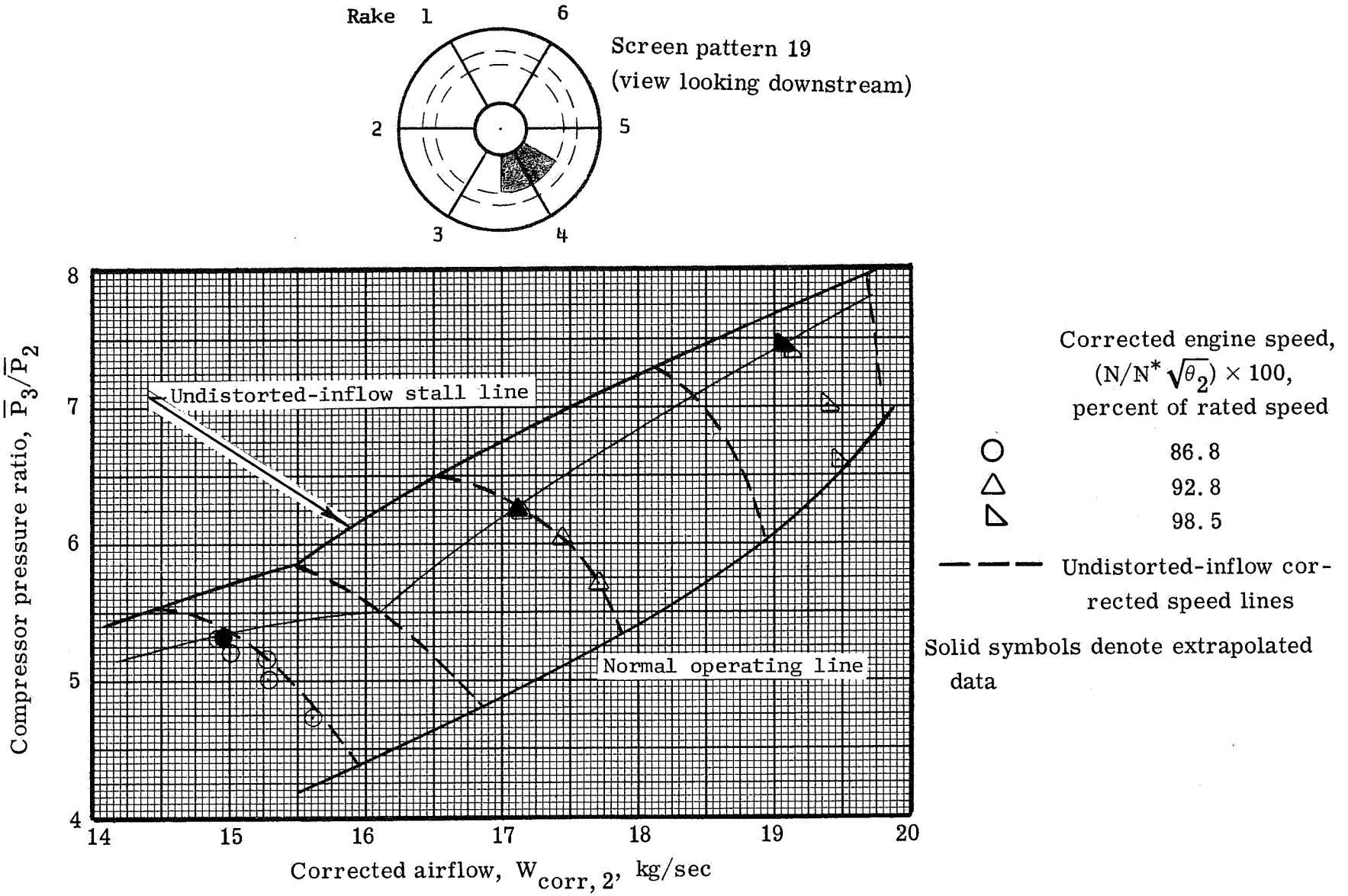

(d) 60^o Spoiled sector; spoiled-area ratio, A_{SP}/A_2, 0.057; engine B.

Figure 11. - Continued.

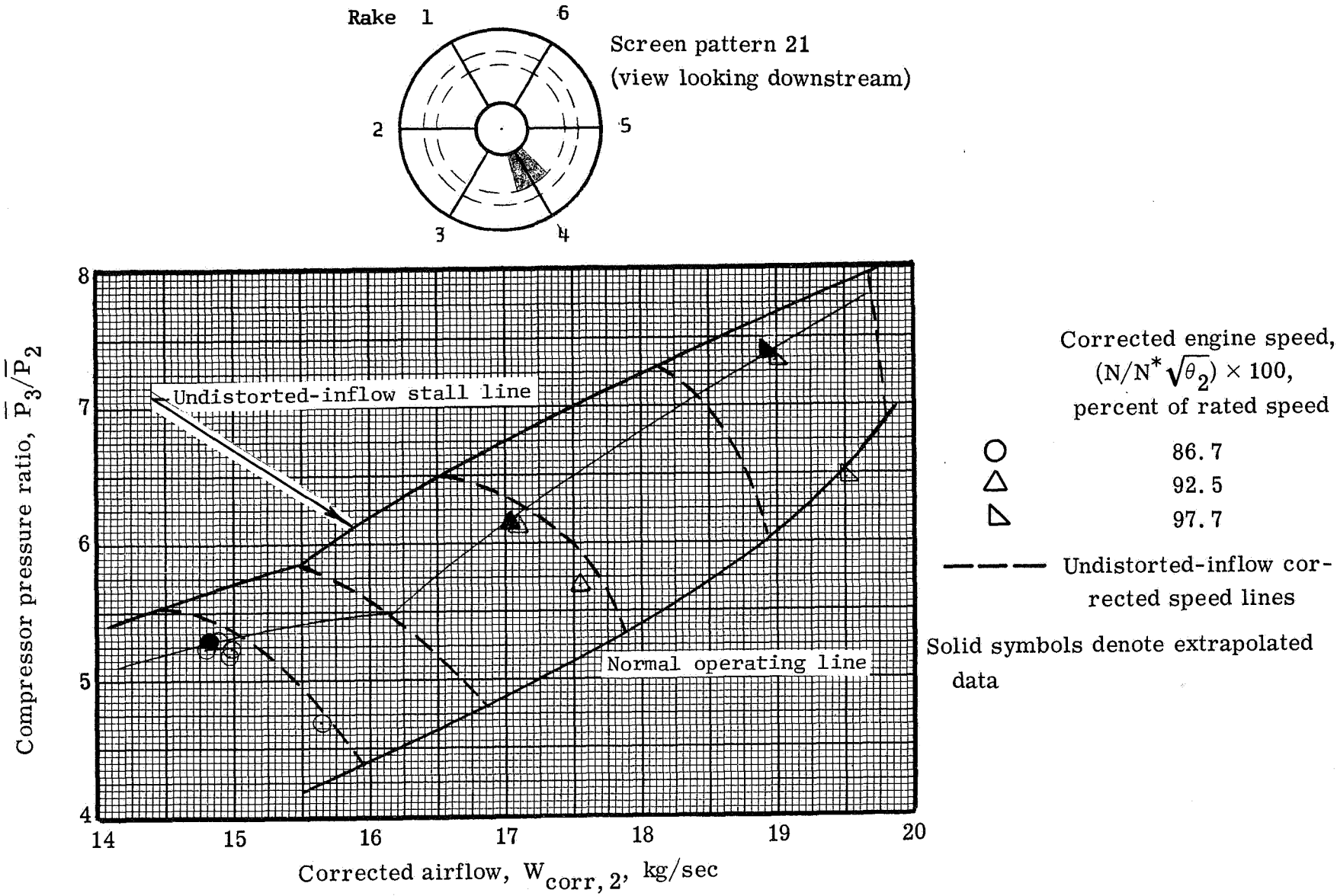

(e) 30^o Spoiled sector; spoiled-area ratio, A_{SP}/A_2, 0.028; engine B.

Figure 11. - Concluded.

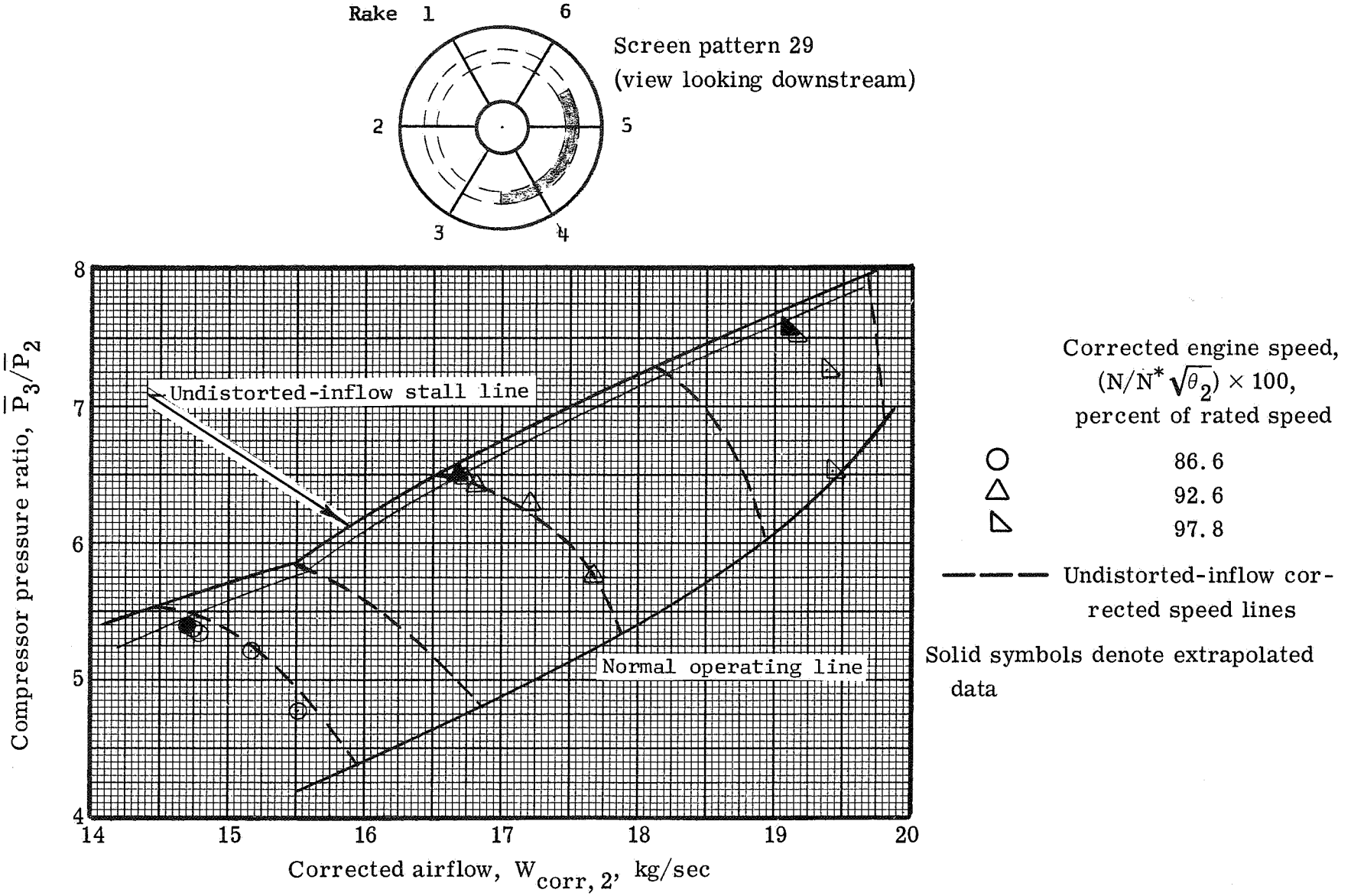

Figure 12. - Compressor performance with partial mid-span radial distortion. 120° Spoiled sector; 39.7-percent-porosity screen; spoiled-area ratio, A_{SP}/A_2, 0.087; engine B.

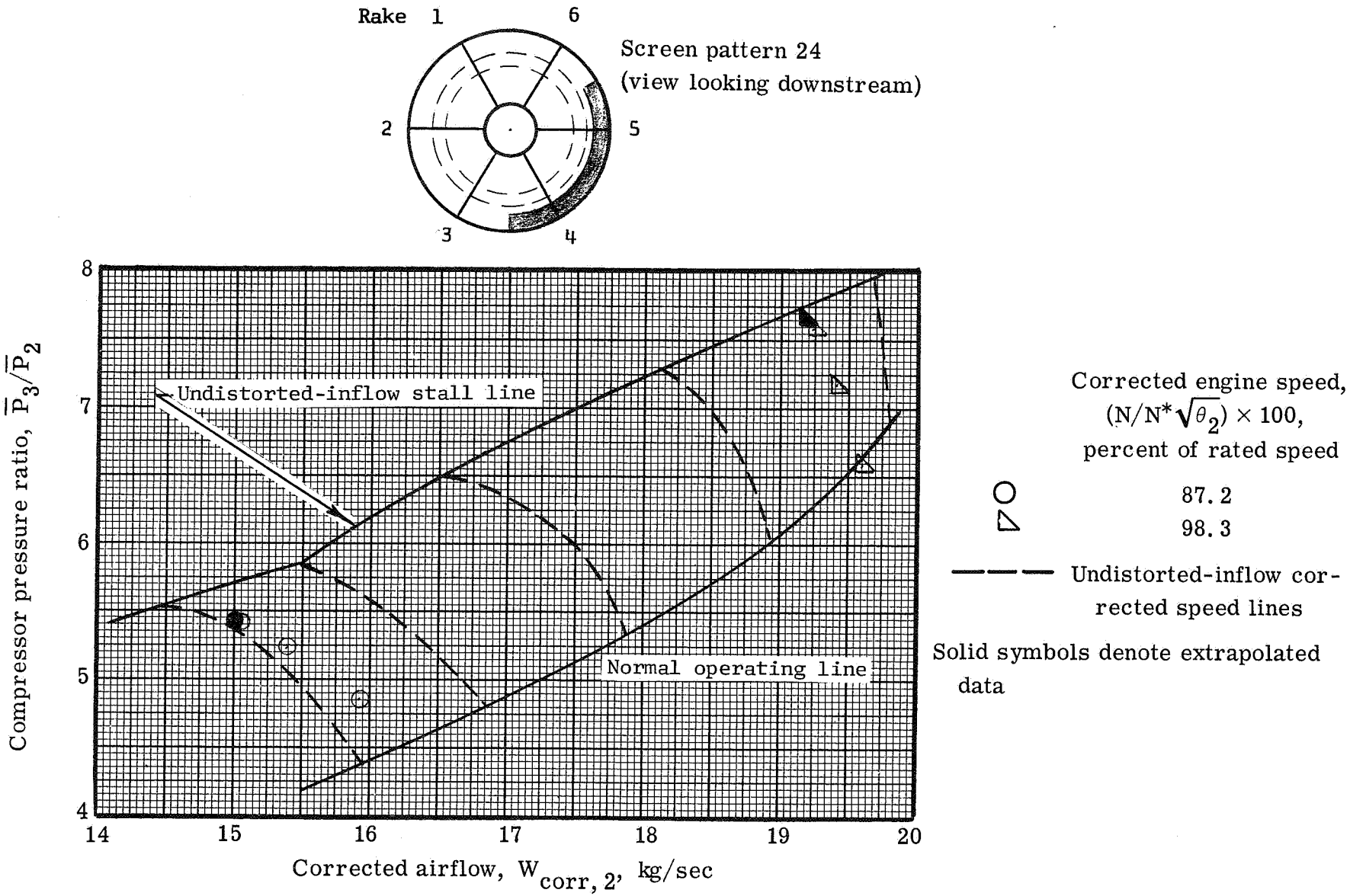

(a) 120^o Spoiled sector; spoiled-area ratio, A_{SP}/A_2, 0.067; engine B.

Figure 13. - Compressor performance with partial tip radial distortion. 39.7-Percent-porosity screen.

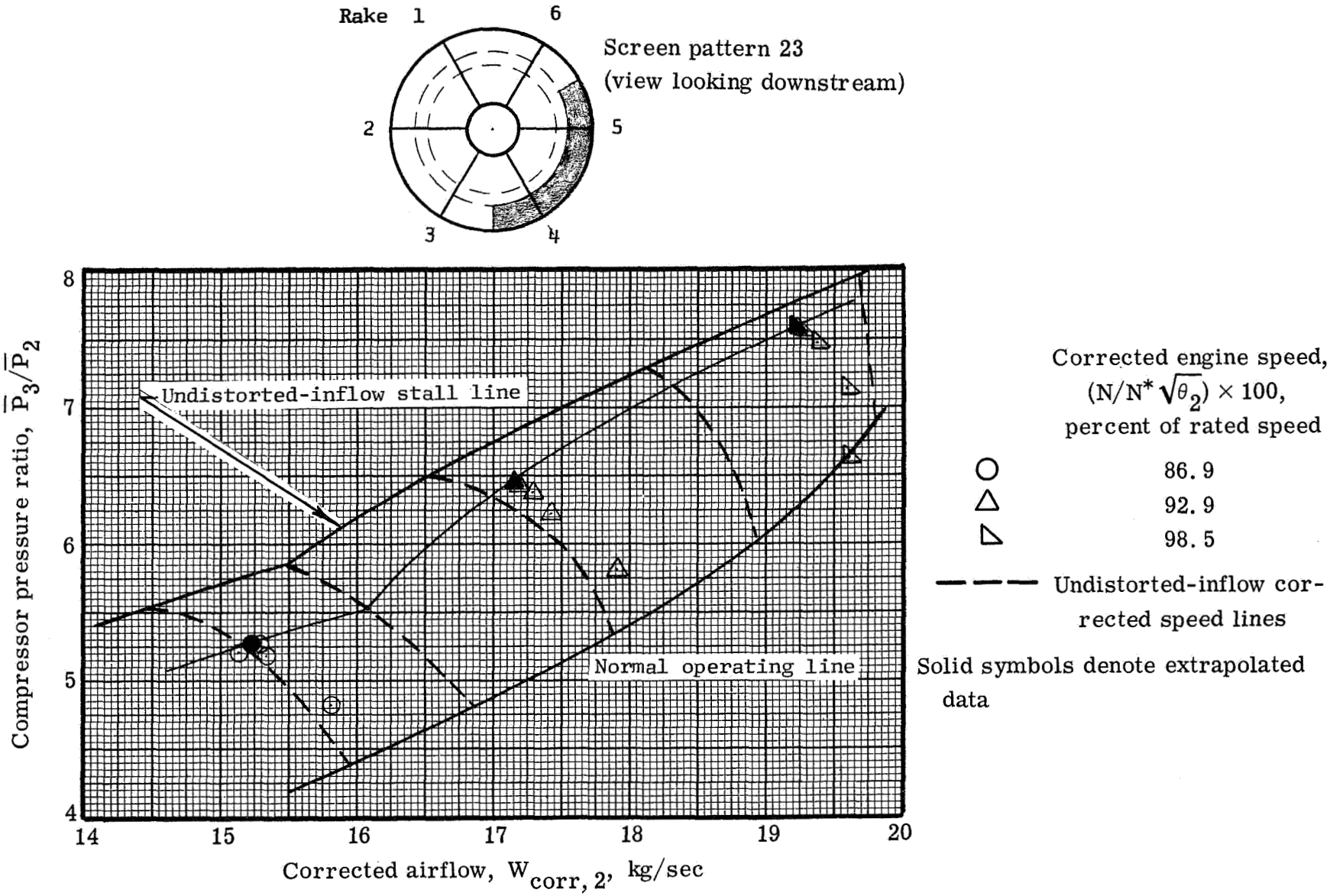

(b) 120° Spoiled sector; spoiled-area ratio, A_{SP}/A_2, 0.133; engine B.

Figure 13. - Continued.

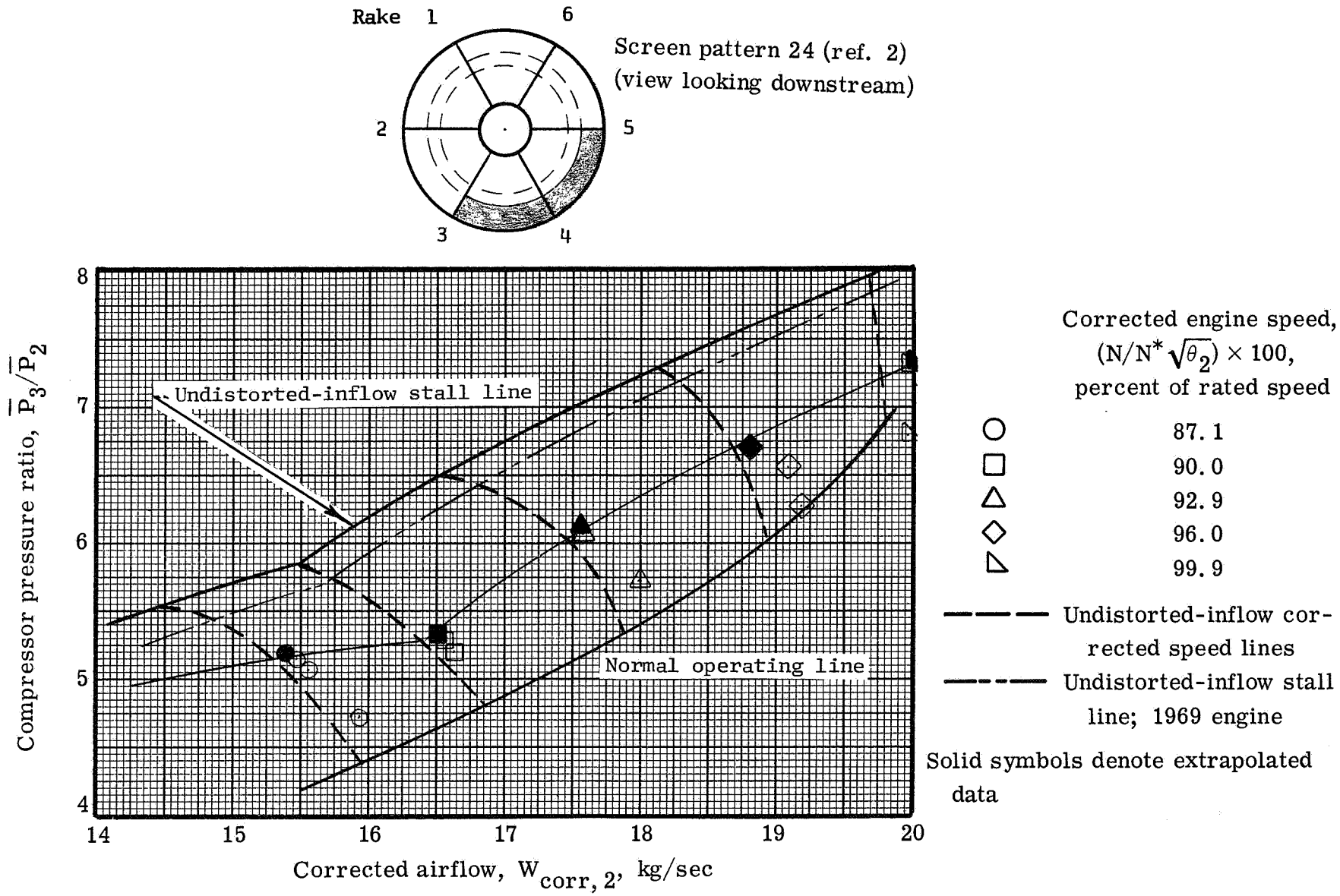

(c) 120° Spoiled sector; spoiled-area ratio, A_{SP}/A_2, 0.133; 1969 engine (ref. 2).

Figure 13. - Continued.

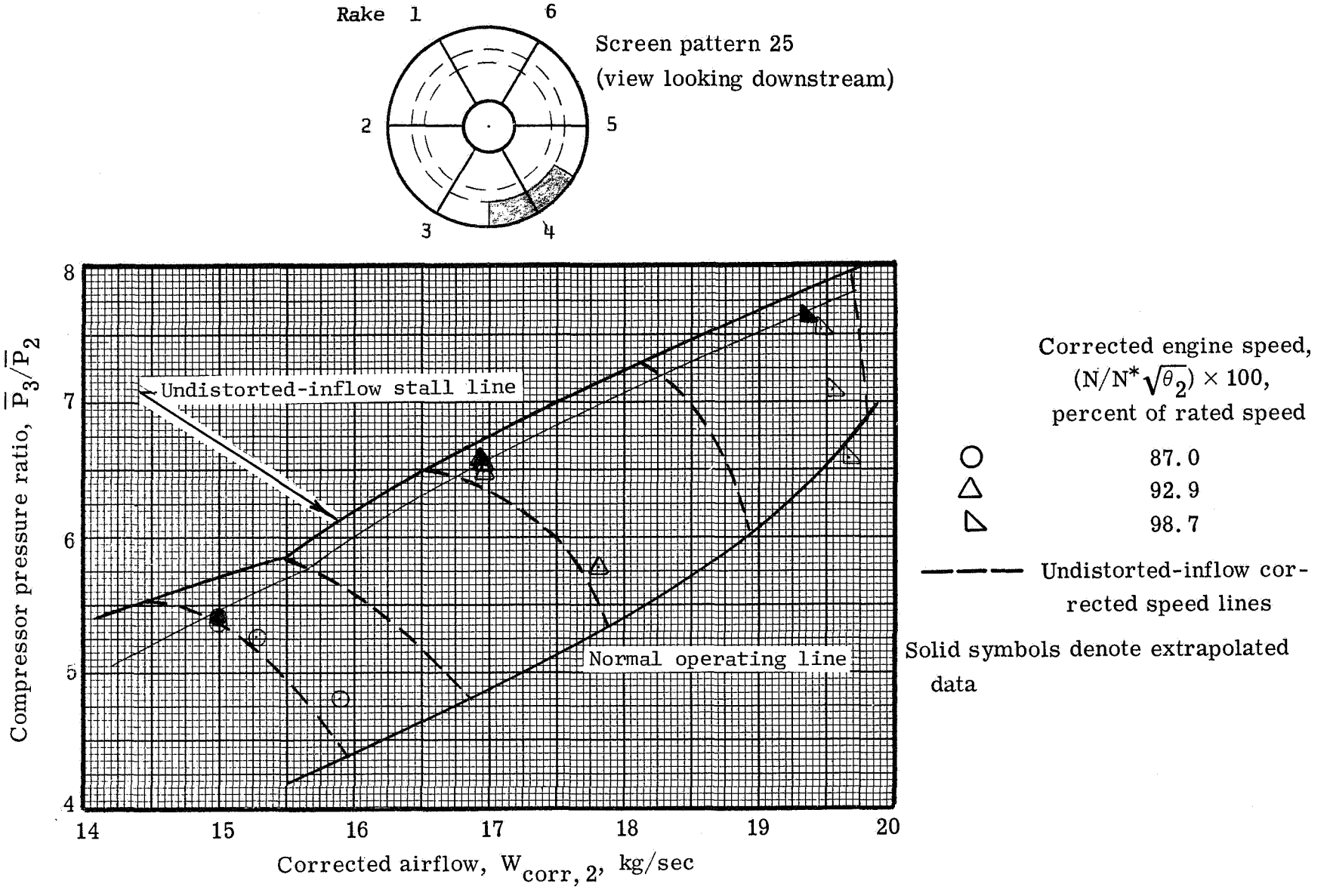

(d) 60° Spoiled sector; spoiled-area ratio, A_{SP}/A_2, 0.067; engine B.

Figure 13. - Concluded.

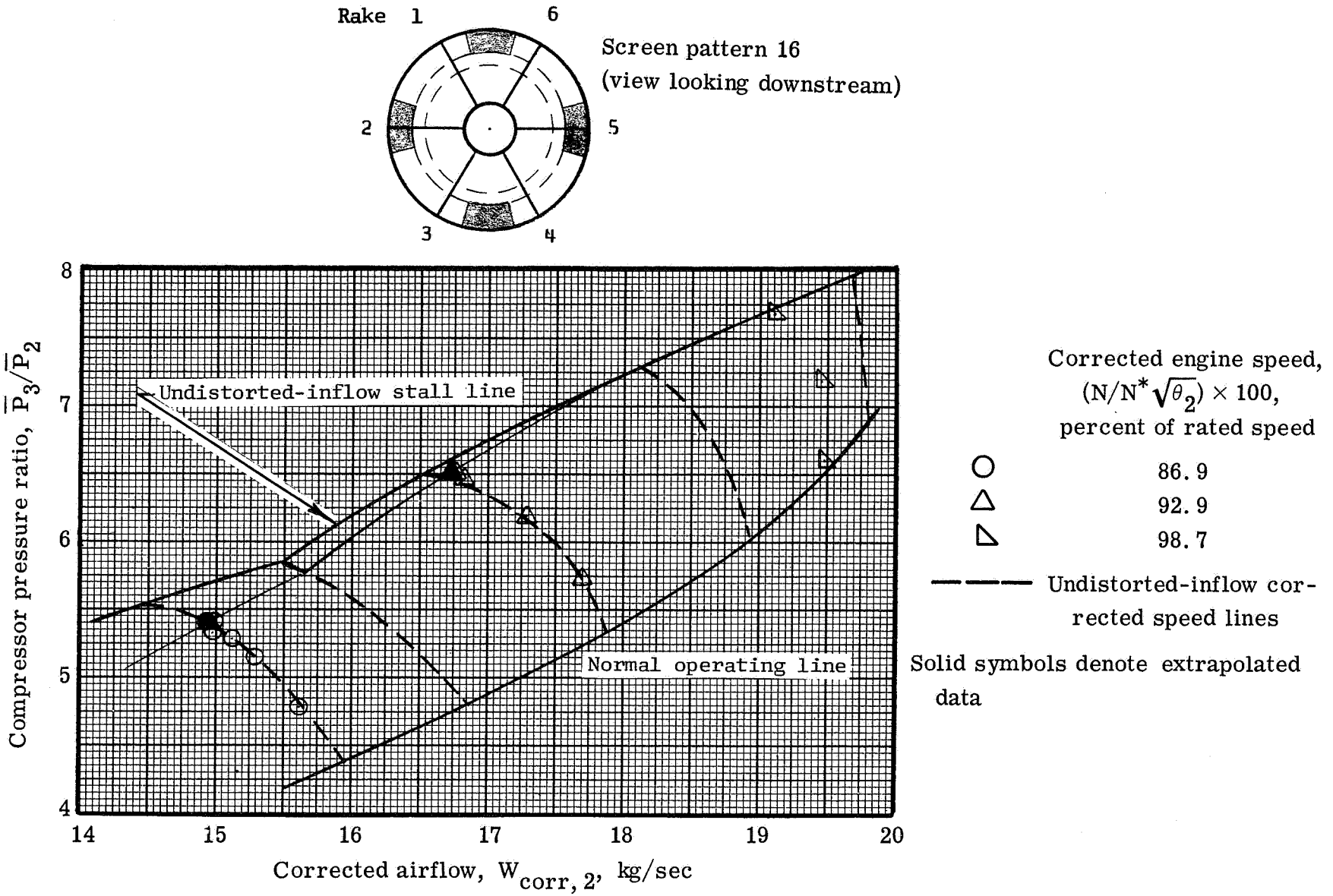

Figure 14. - Compressor performance with four-per-revolution partial tip radial distortion. 30^o Spoiled sectors; 50.6-percent-porosity screen; spoiled-area ratio, A_{SP}/A_2, 0.133; engine B.

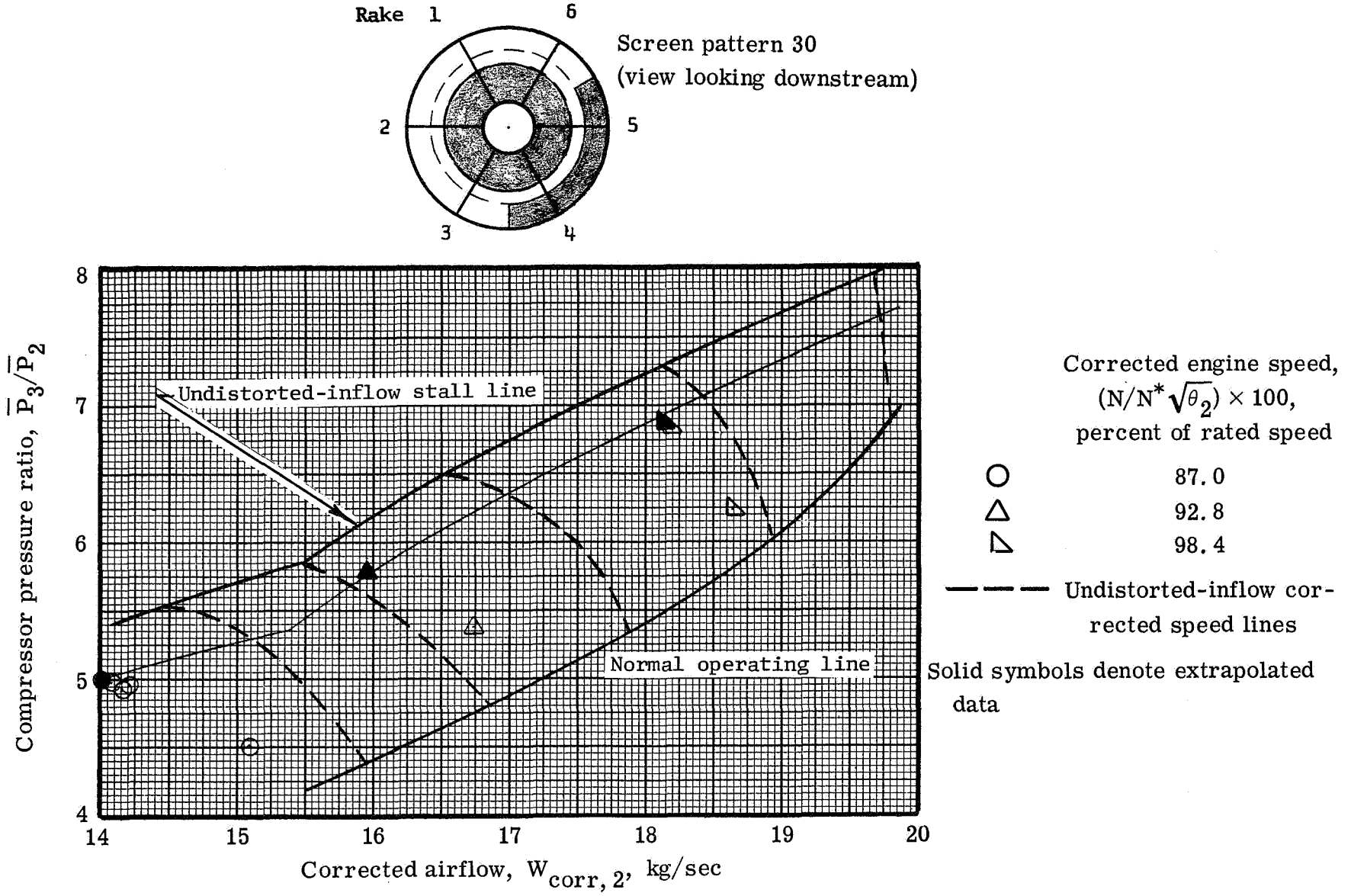

(a) Hub radial: 26.4-percent-porosity screen; tip radial: spoiled-area ratio, A_{SP}/A_2, 0.133.

Figure 15. - Compressor performance with a combined hub radial - 120° partial tip radial distortion; engine B. Hub radial: spoiled-area ratio, A_{SP}/A_2, 0.4; partial tip radial: 39.7-percent-porosity screen.

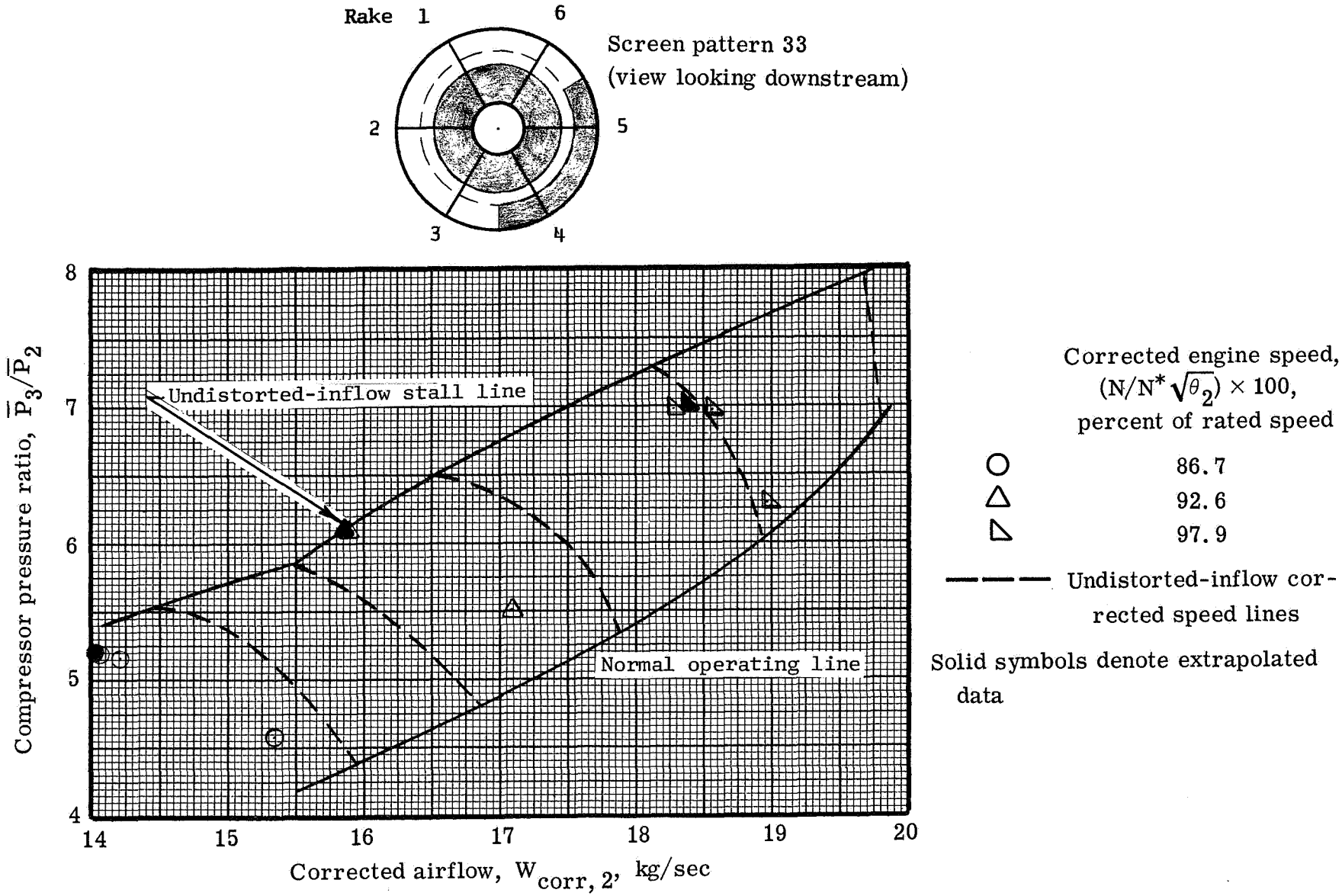

(b) Hub radial: 39.7-percent-porosity screen; partial tip radial: spoiled-area ratio, A_{SP}/A_2, 0.133.

Figure 15. - Continued.

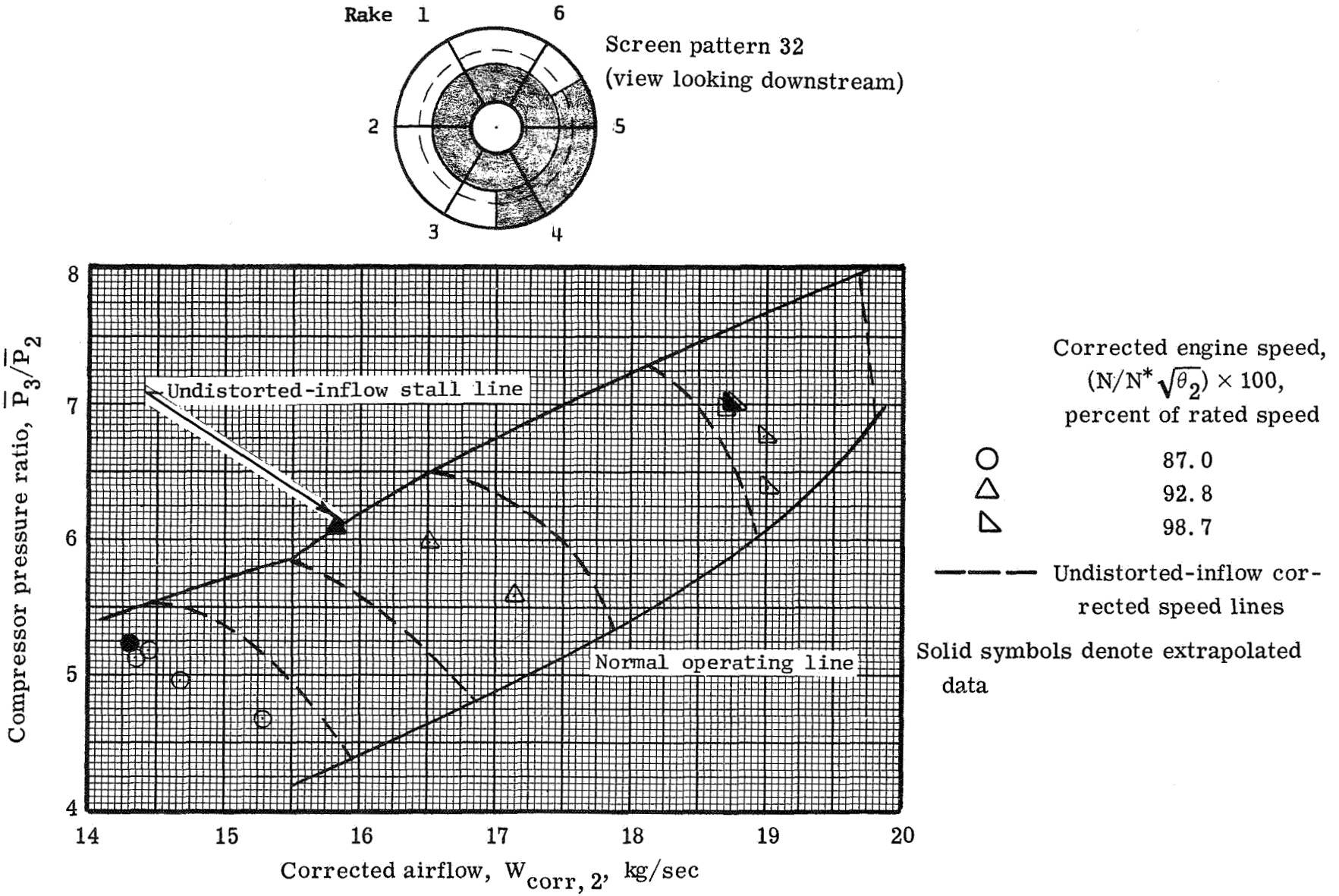

(c) Hub radial: 39.7-percent-porosity screen; partial tip radial: spoiled-area ratio, A_{SP}/A_2, 0.200.

Figure 15. - Concluded.

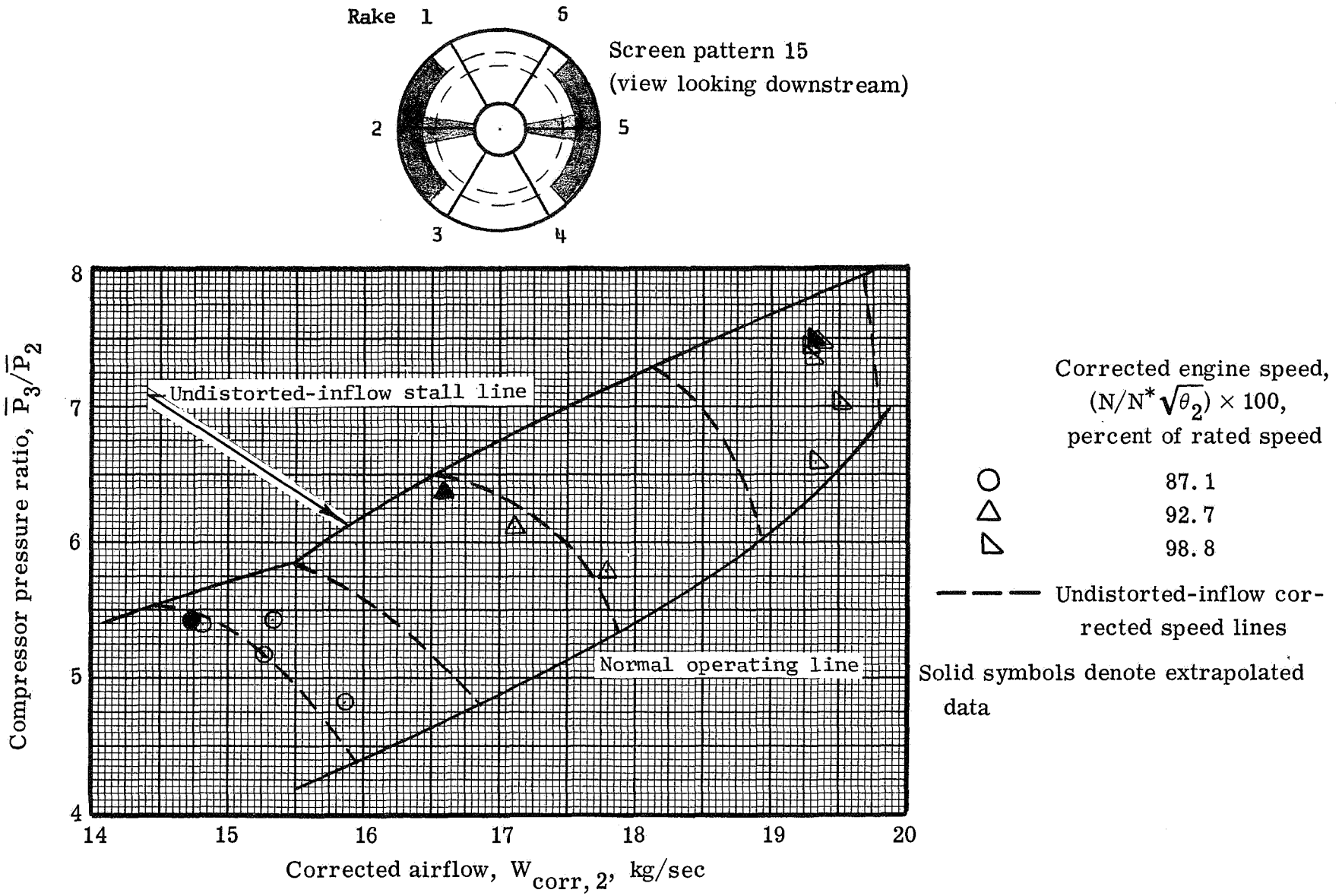

Figure 16. - Compressor performance with a two-per-revolution combined 20° circumferential sector - 90° partial tip radial sector; engine B. Circumferential sectors: 57.4-percent-porosity screens; spoiled-area ratio, A_{SP}/A_2, 0.089; partial tip radial sectors: 50.6-percent-porosity screens; spoiled-area ratio, A_{SP}/A_2, 0.100.

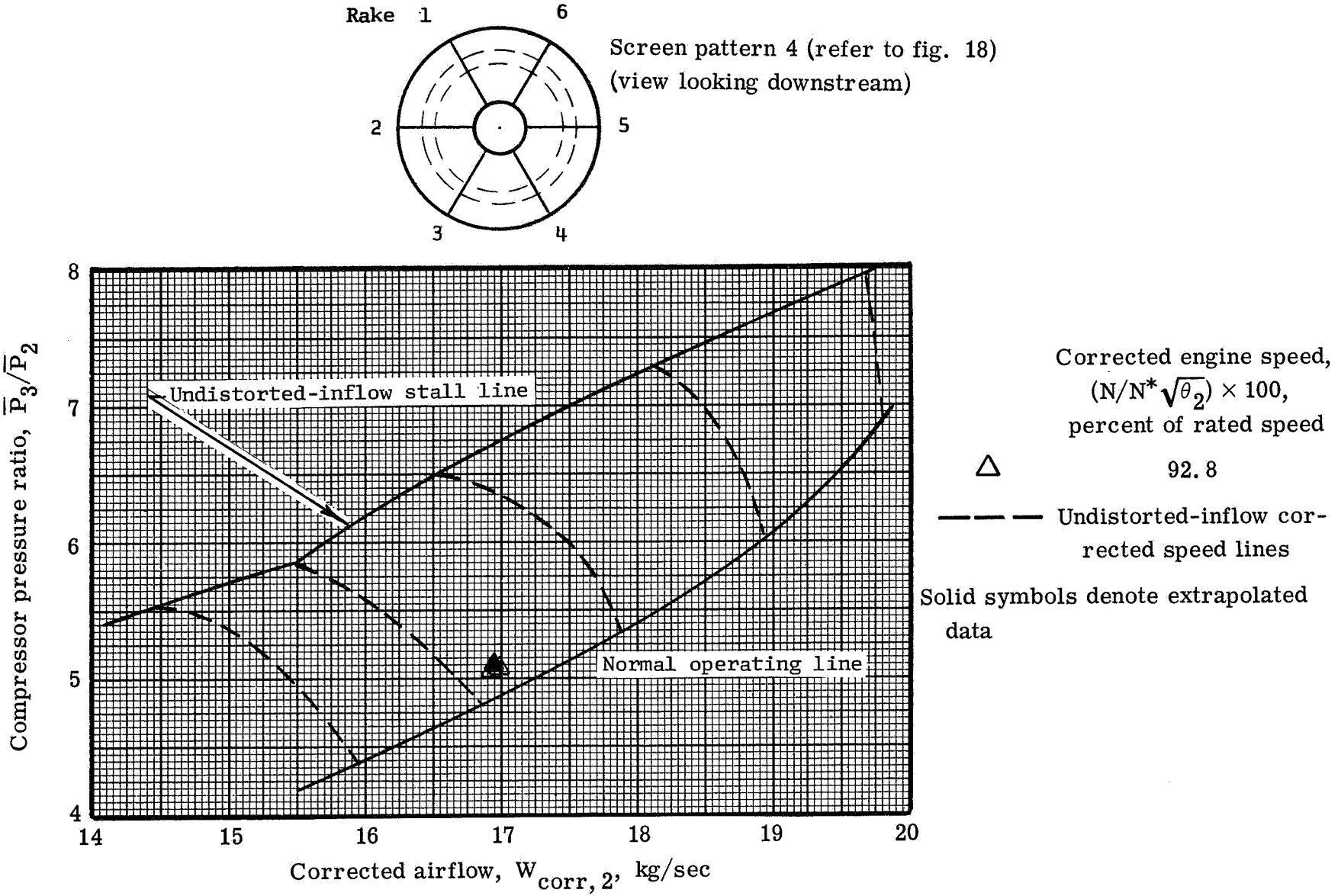

(a) Stall point at angular displacement α of 5^o (ref. 1).

Figure 17. - Compressor performance with simulated peak instantaneous distortion pattern.

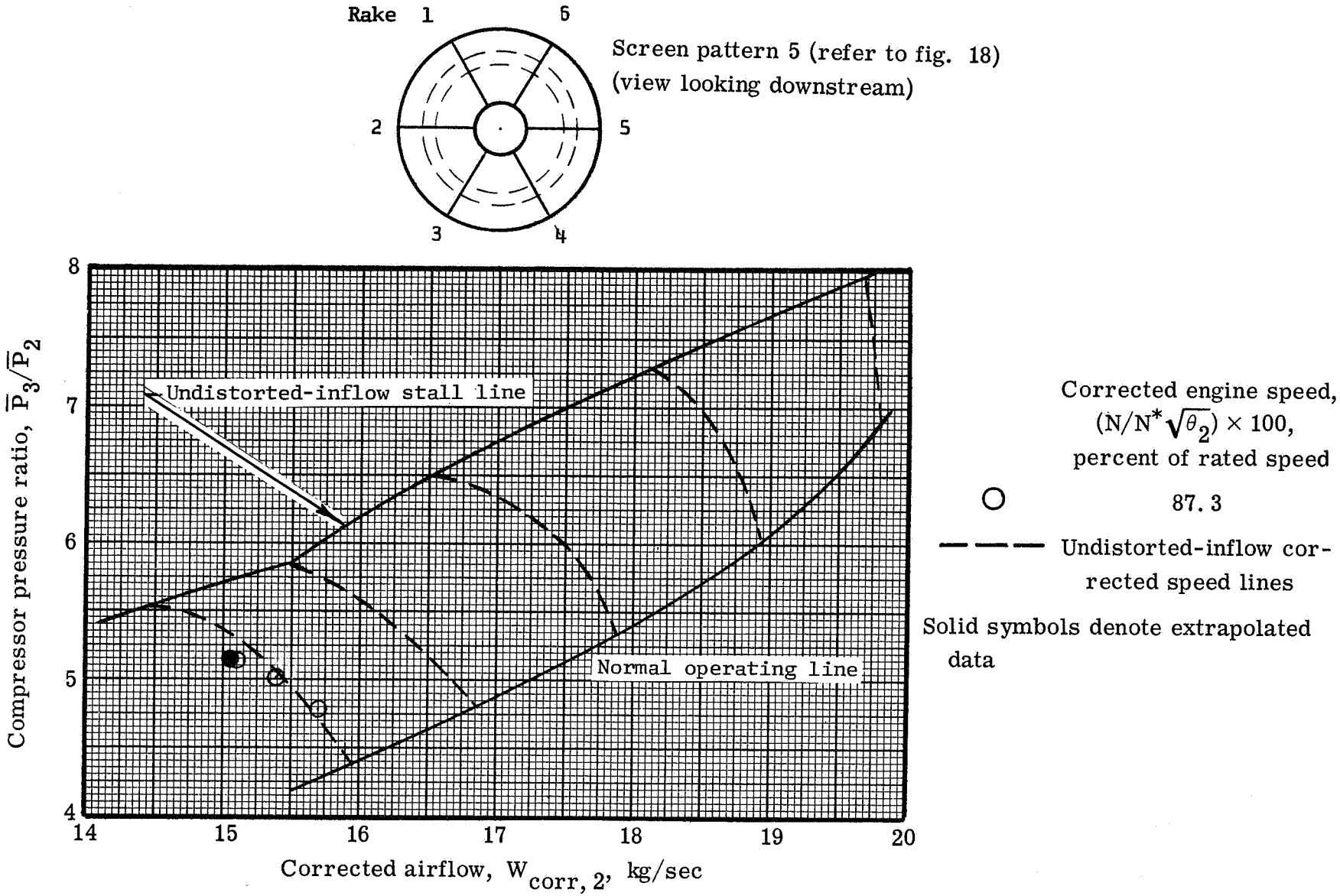

(b) Stall point at angular displacement α of 0^o (ref. 1).

Figure 17. - Concluded.

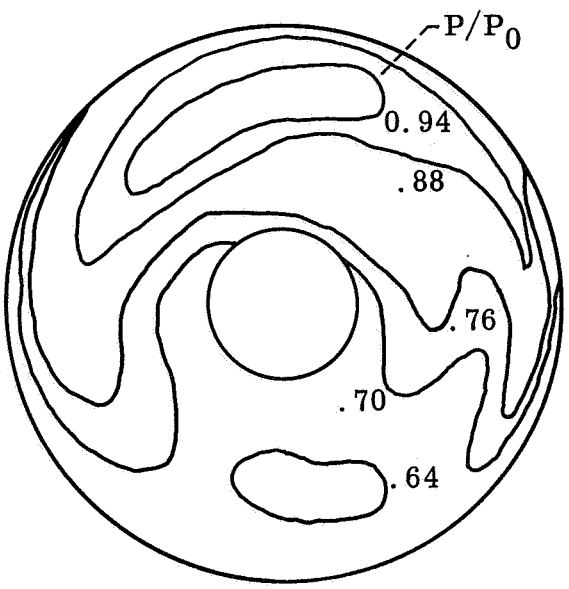

Peak instantaneous distortion; stall point at angular displacement α of 5^{o} (fig. 10(b), ref. 1); distortion index, DPCWR, 0.148.

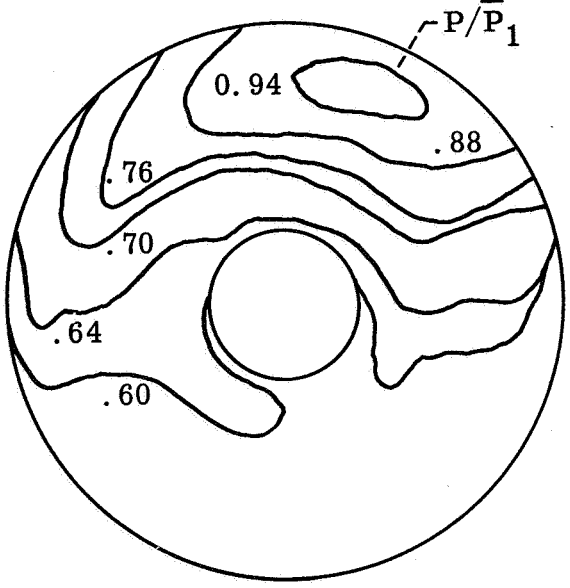

Screen simulation of stall point at $\alpha = 5^{o}$; screen pattern 4; DPCWR = 0.201.

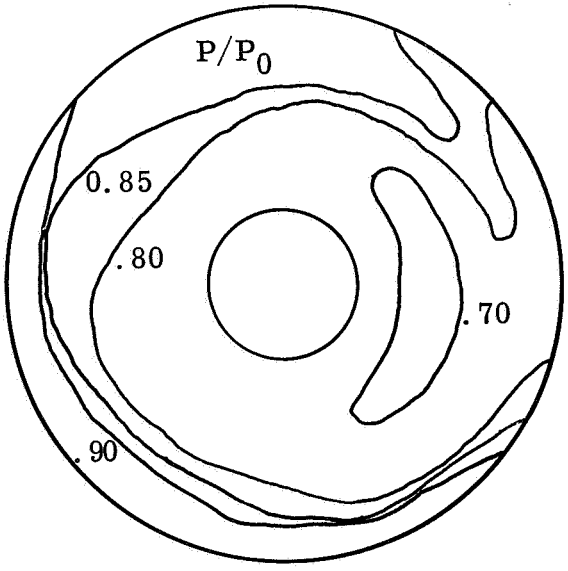

Peak instantaneous distortion; stall point at $\alpha = 0^{o}$ (fig. 10(a), ref. 1); DPCWR = 0.100.

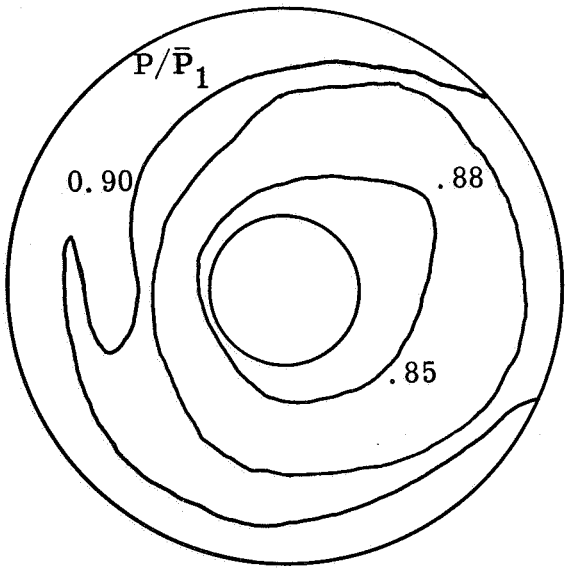

Screen simulation of stall point at $\alpha = 0^{o}$; screen pattern 5; DPCWR = 0.048.

Figure 18. - Compressor face total-pressure contours resulting from screen patterns 4 and 5.

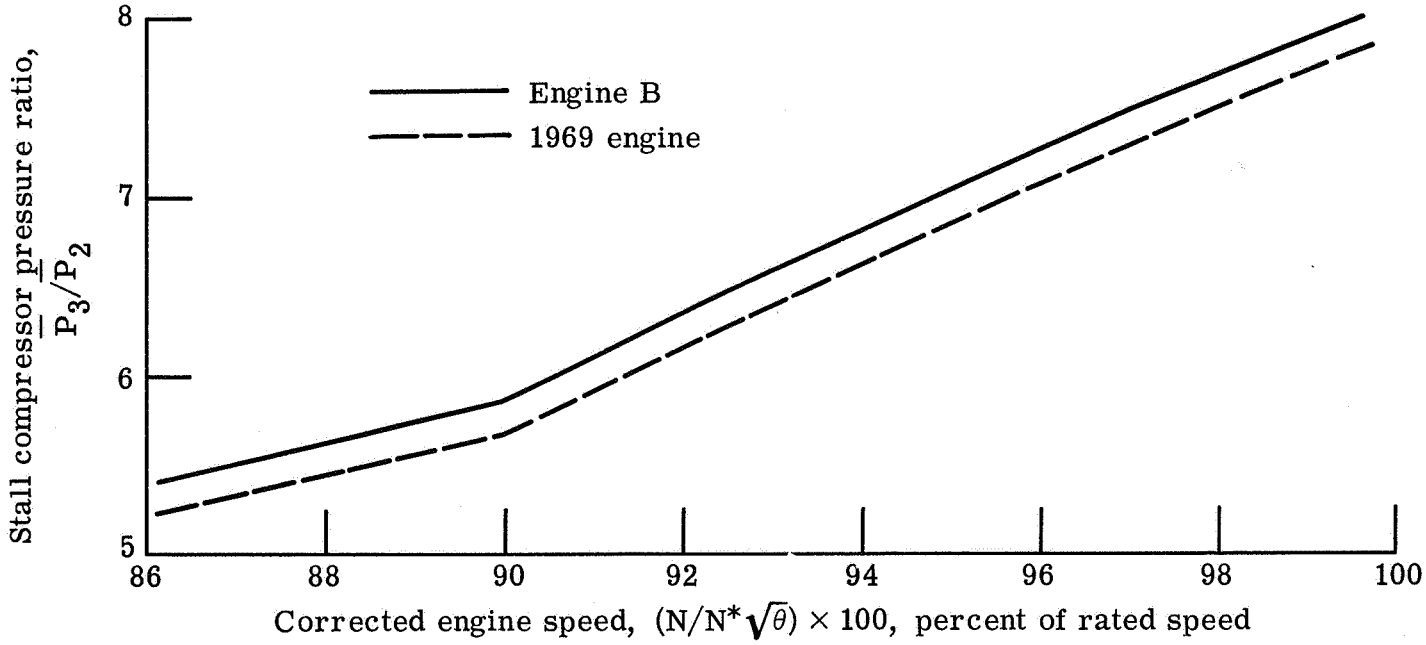

Figure 19. - Compressor pressure ratio at stall for undistorted inflow as a function of corrected engine speed.

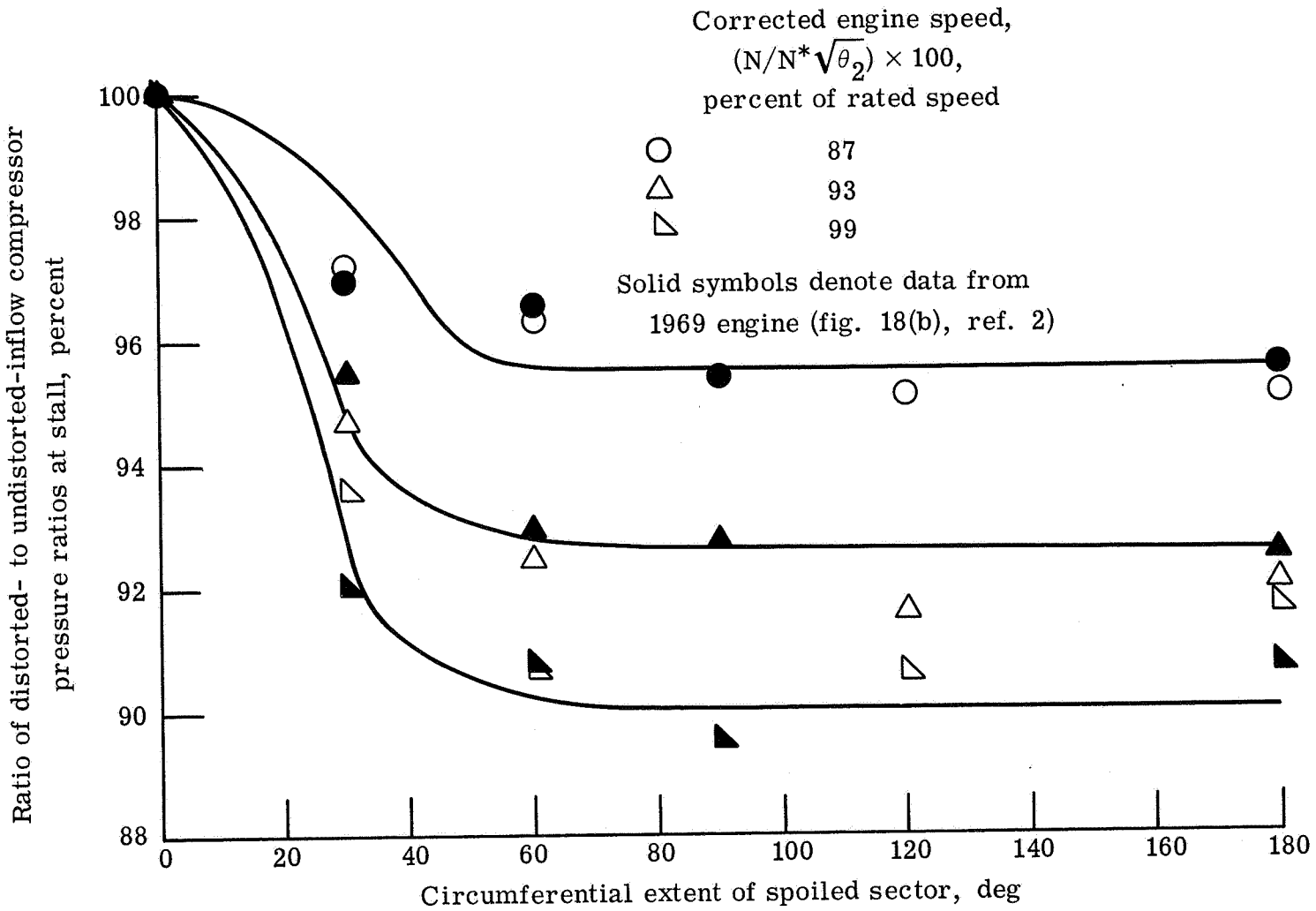

(a) One-per-revolution circumferential distortions.

Figure 20. - Effect of angle of circumferential spoiling on compressor stall. 50.6-Percent-porosity screen; engines A and B.

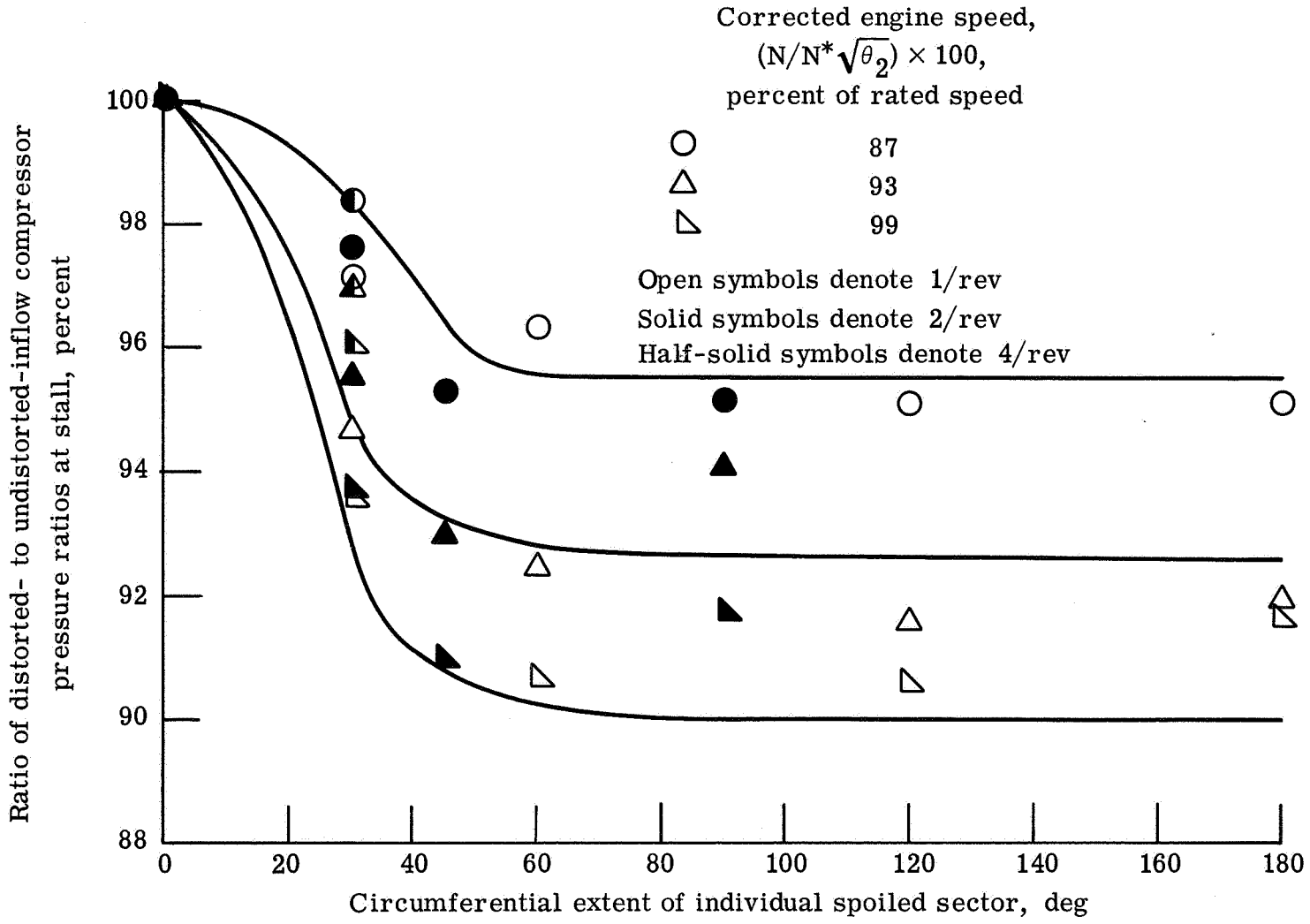

(b) Multiple-per-revolution circumferential distortions.

Figure 20. - Concluded.

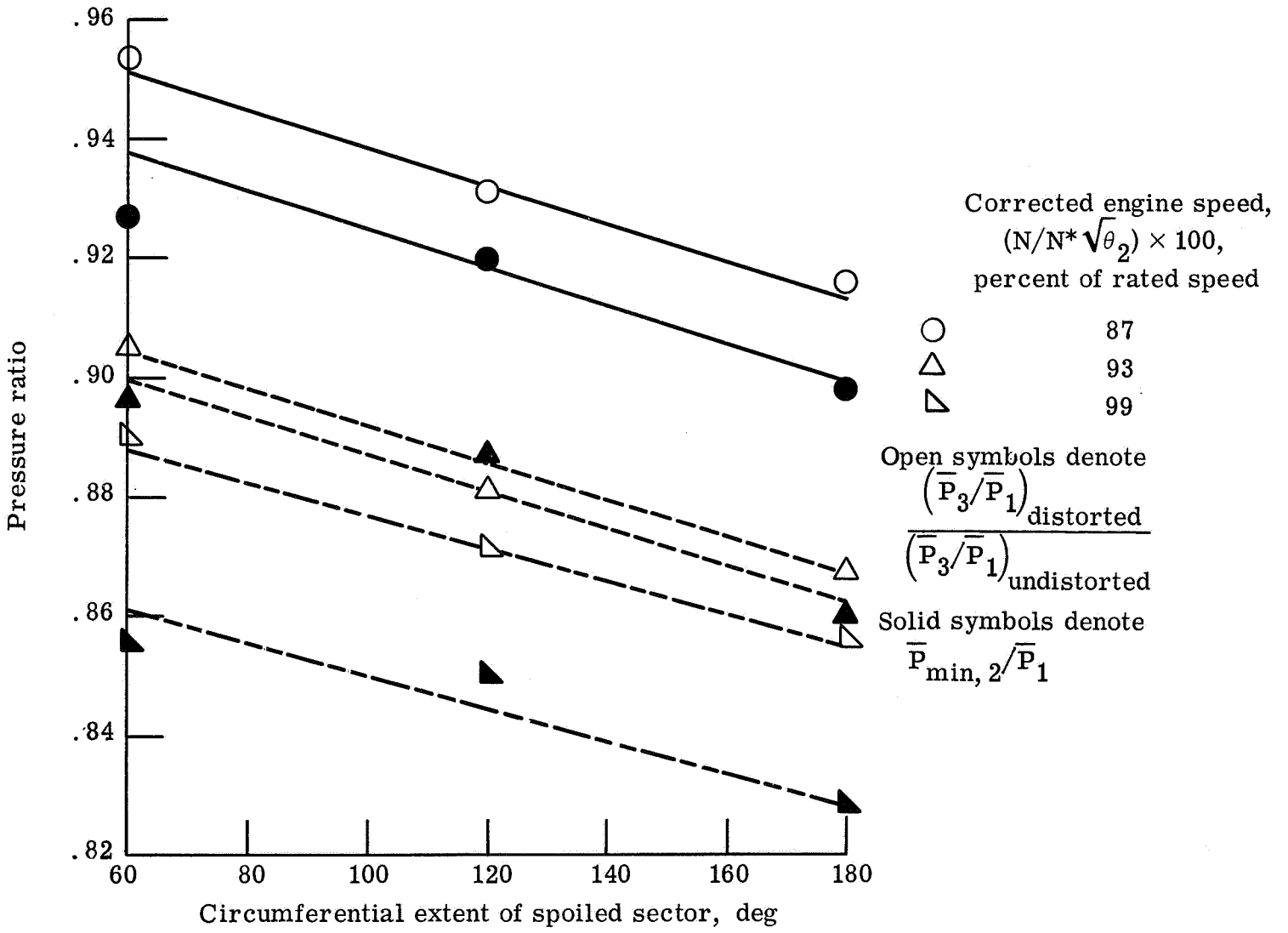

Figure 21. - Effect of angle of one-per-revolution circumferential spoiling on compressor face minimum pressure and compressor discharge average pressure. 50.6-Percent-porosity screen; engine A.

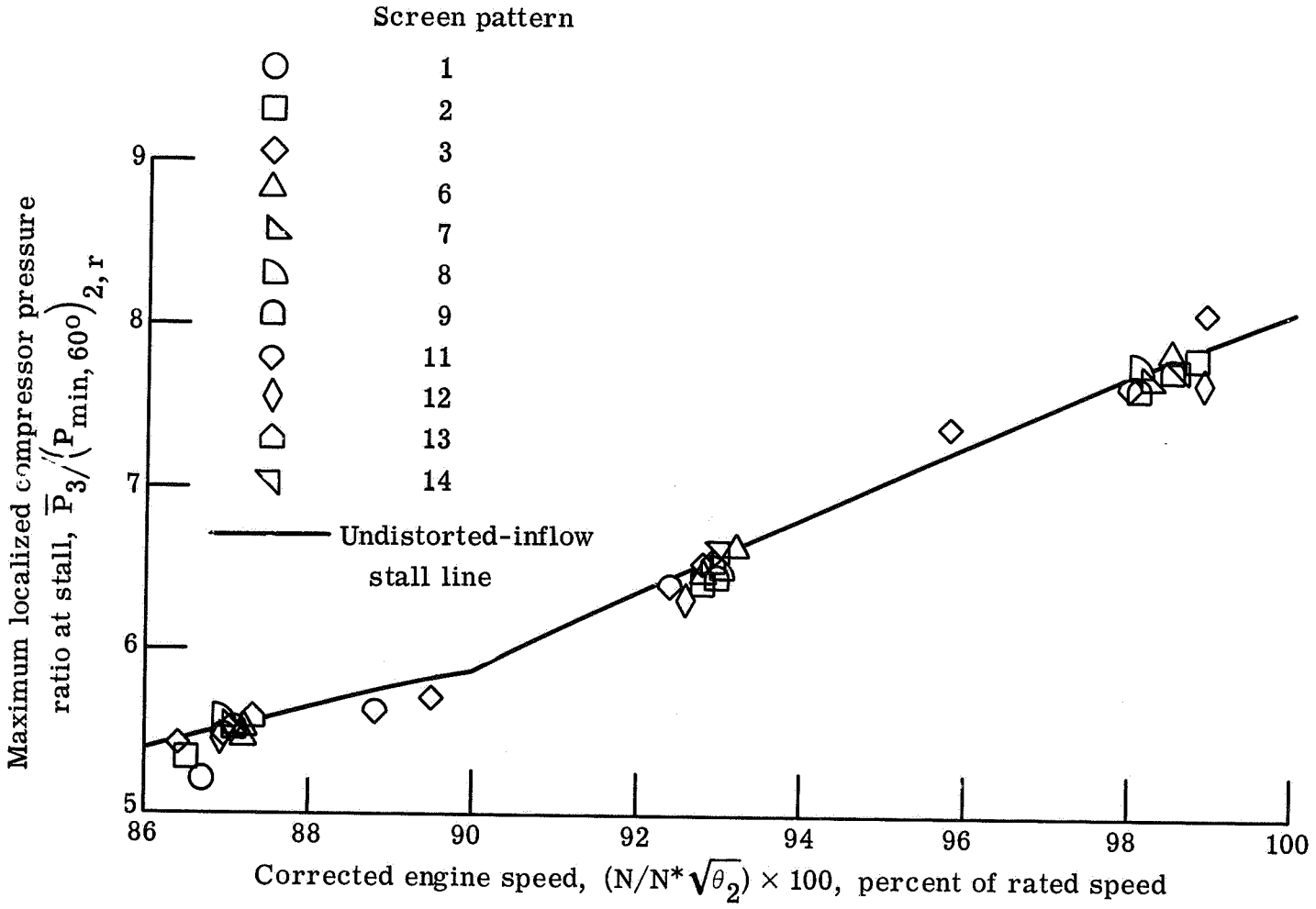

(a) Engines A and B.

Figure 22. - Maximum localized compressor pressure ratio at stall for single- and multiple-per-revolution circumferential distortions.

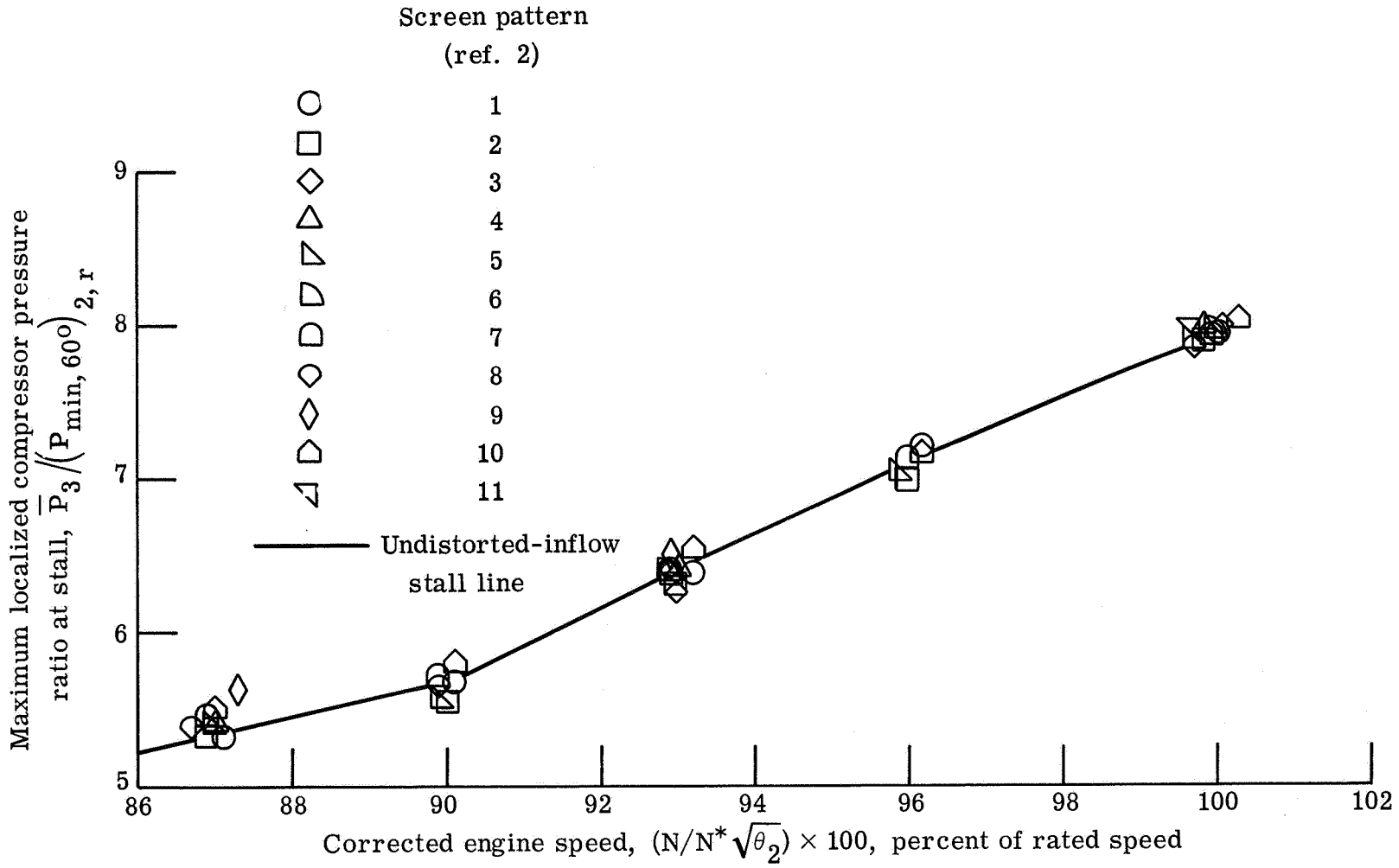

(b) 1969 Engine.

Figure 22. - Concluded.

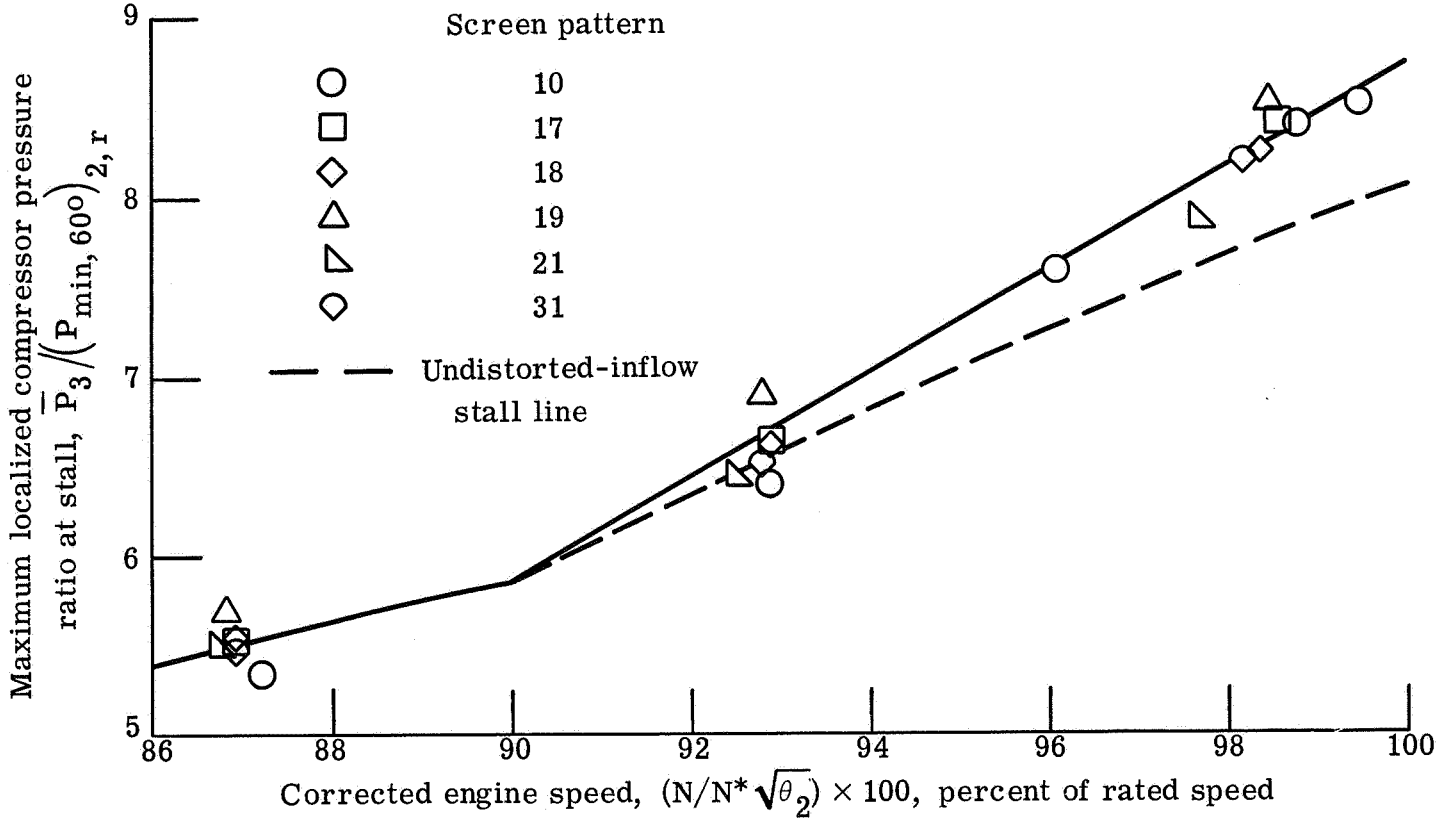

(a) Engines A and B.

Figure 23. - Maximum localized compressor pressure ratio at stall for pure and partial hub radial distortions.

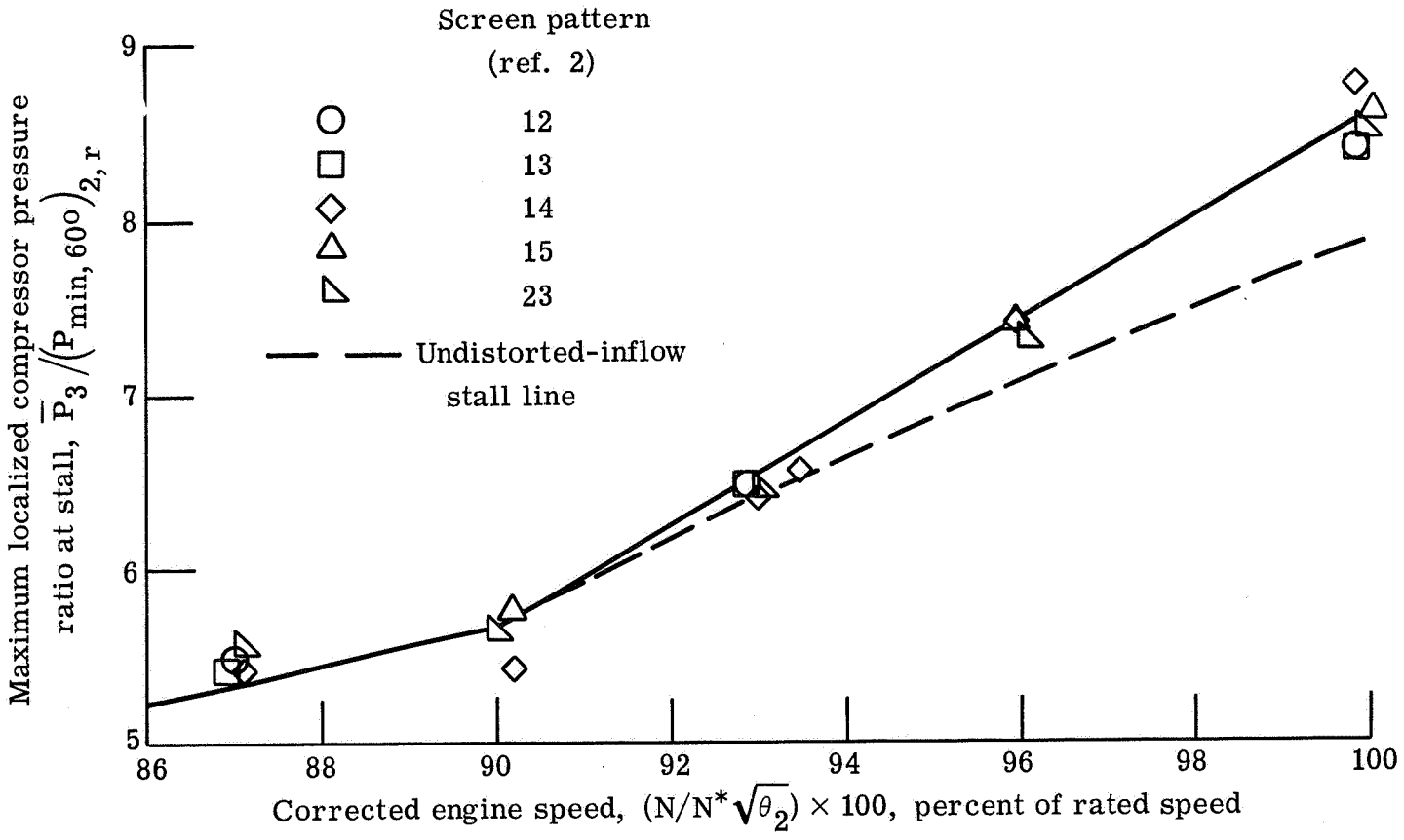

(b) 1969 Engine.

Figure 23. - Concluded.

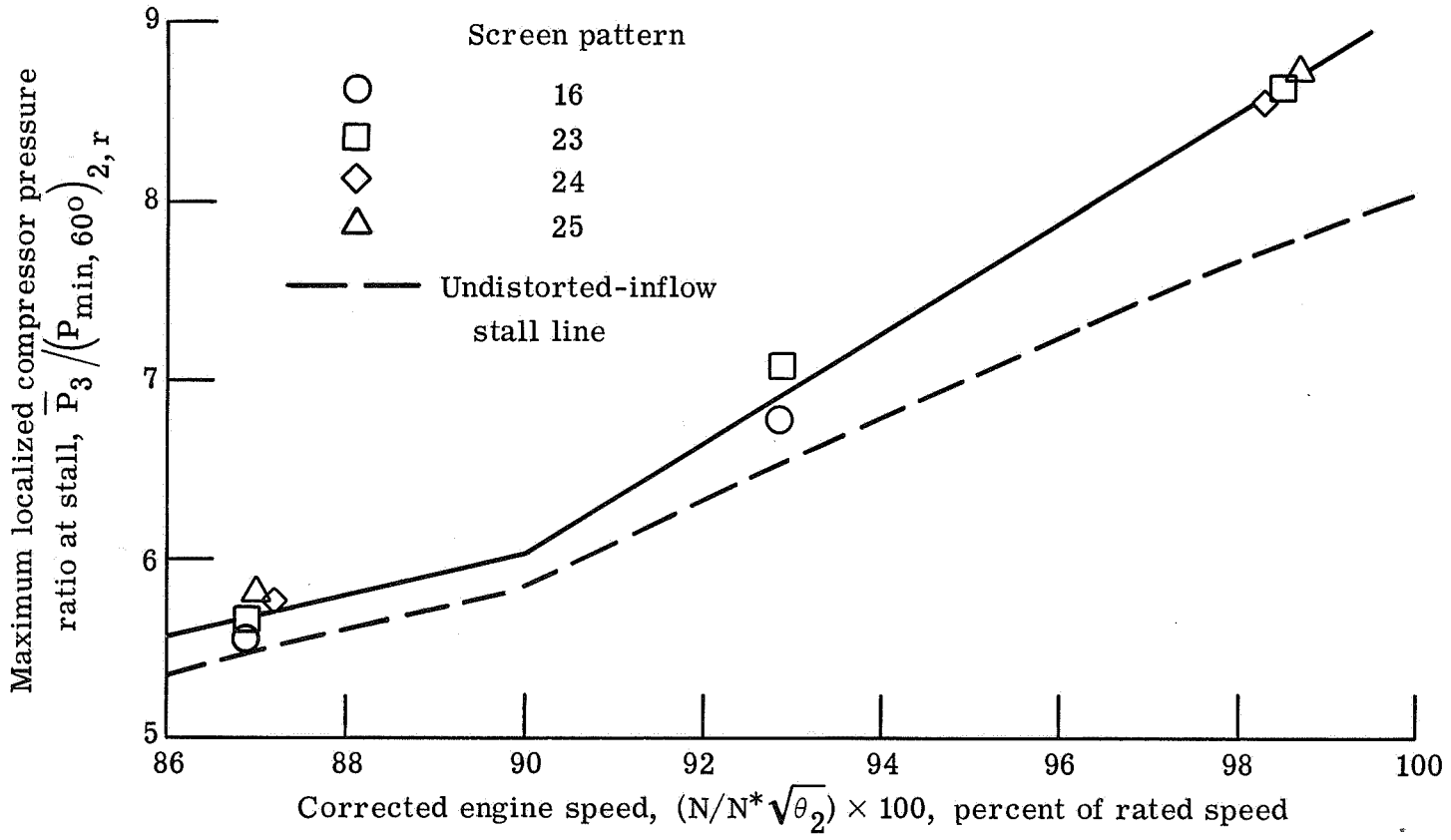

(a) Engine B.

Figure 24. - Maximum localized compressor pressure ratio at stall for pure and partial tip radial distortions.

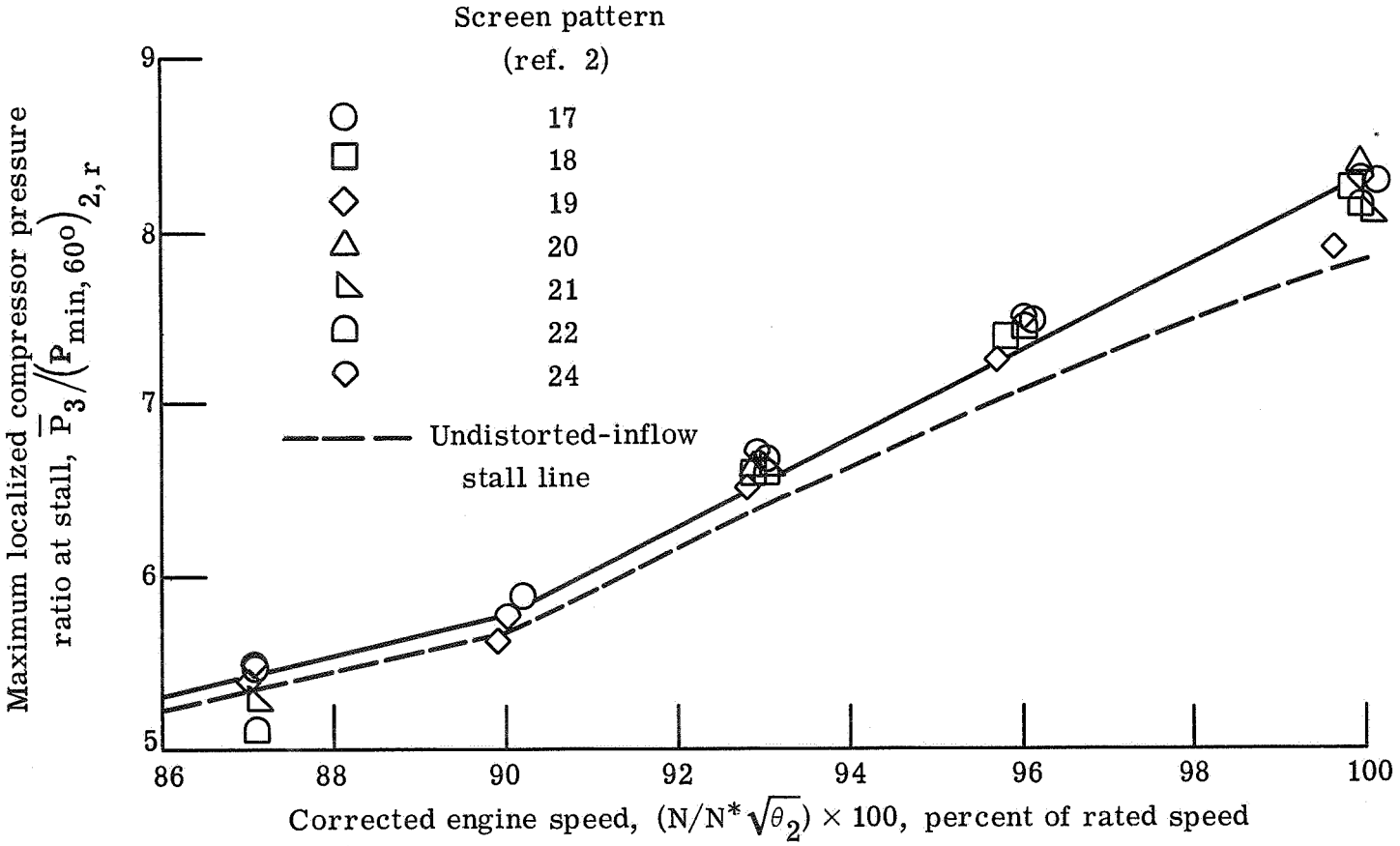

(b) 1969 Engine.

Figure 24. - Concluded.

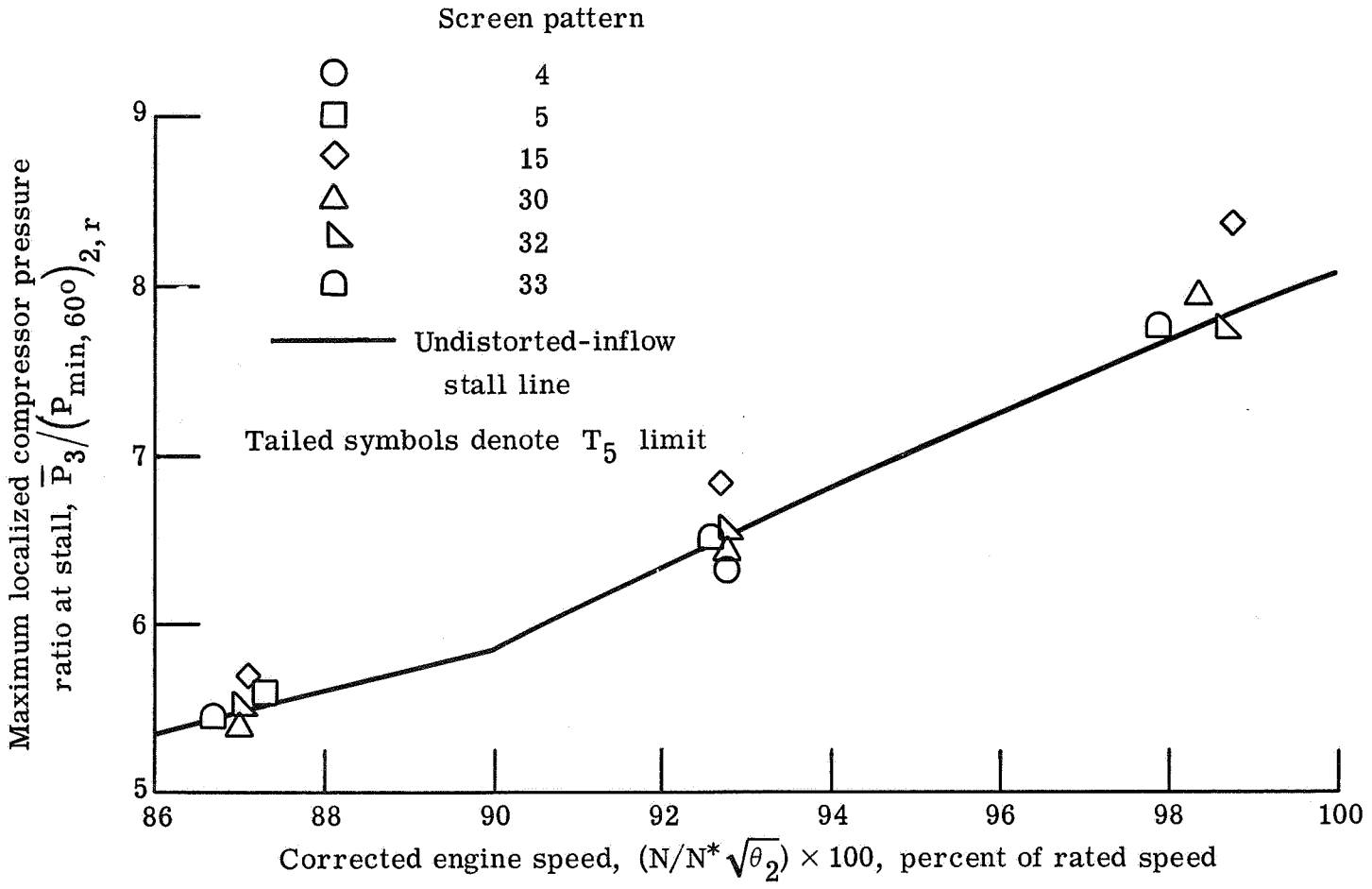

(a) Engines A and B.

Figure 25. - Maximum localized compressor pressure ratio at stall for combined radial and circumferential distortions.

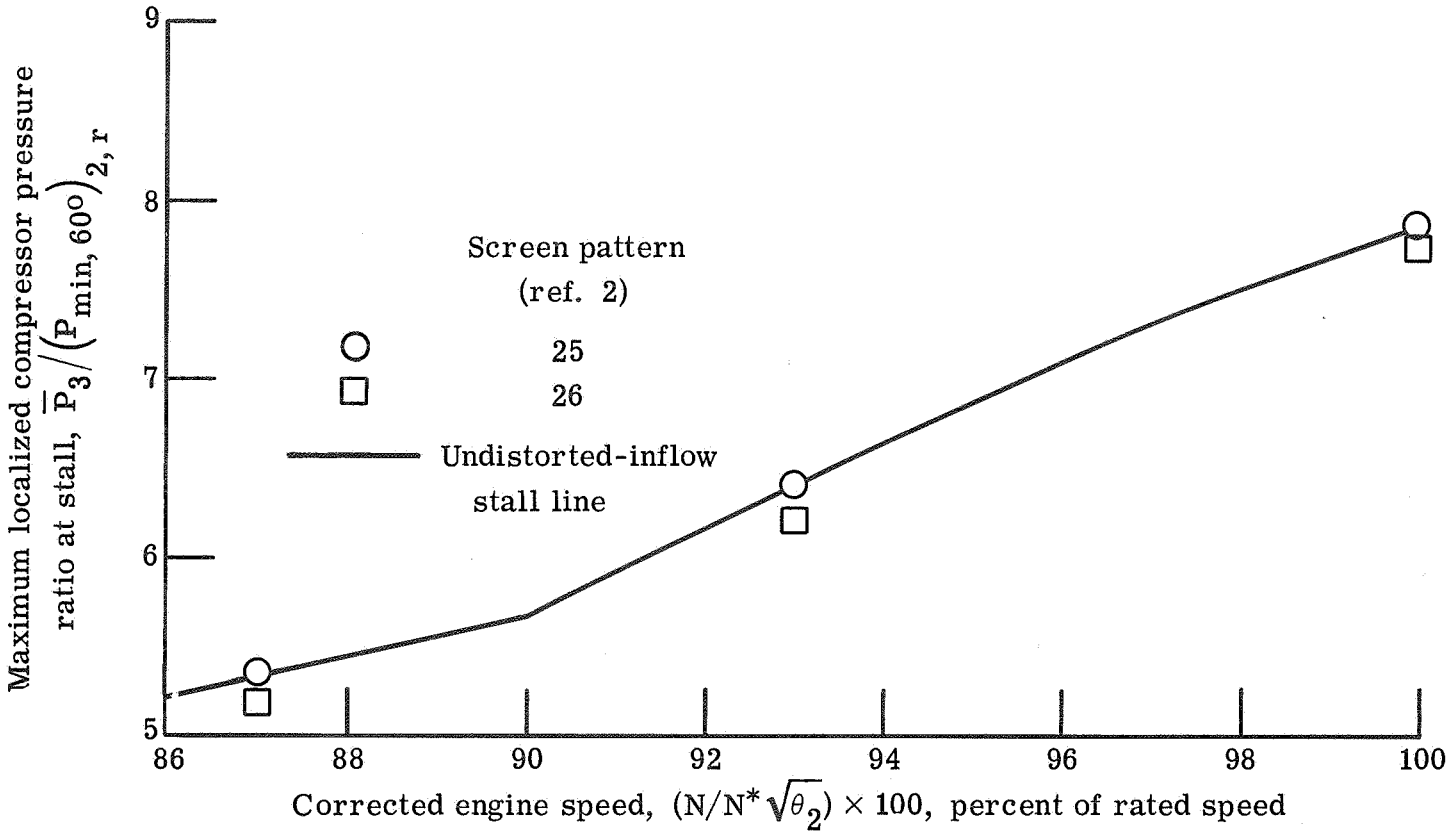

(b) 1969 Engine.

Figure 25. - Concluded.

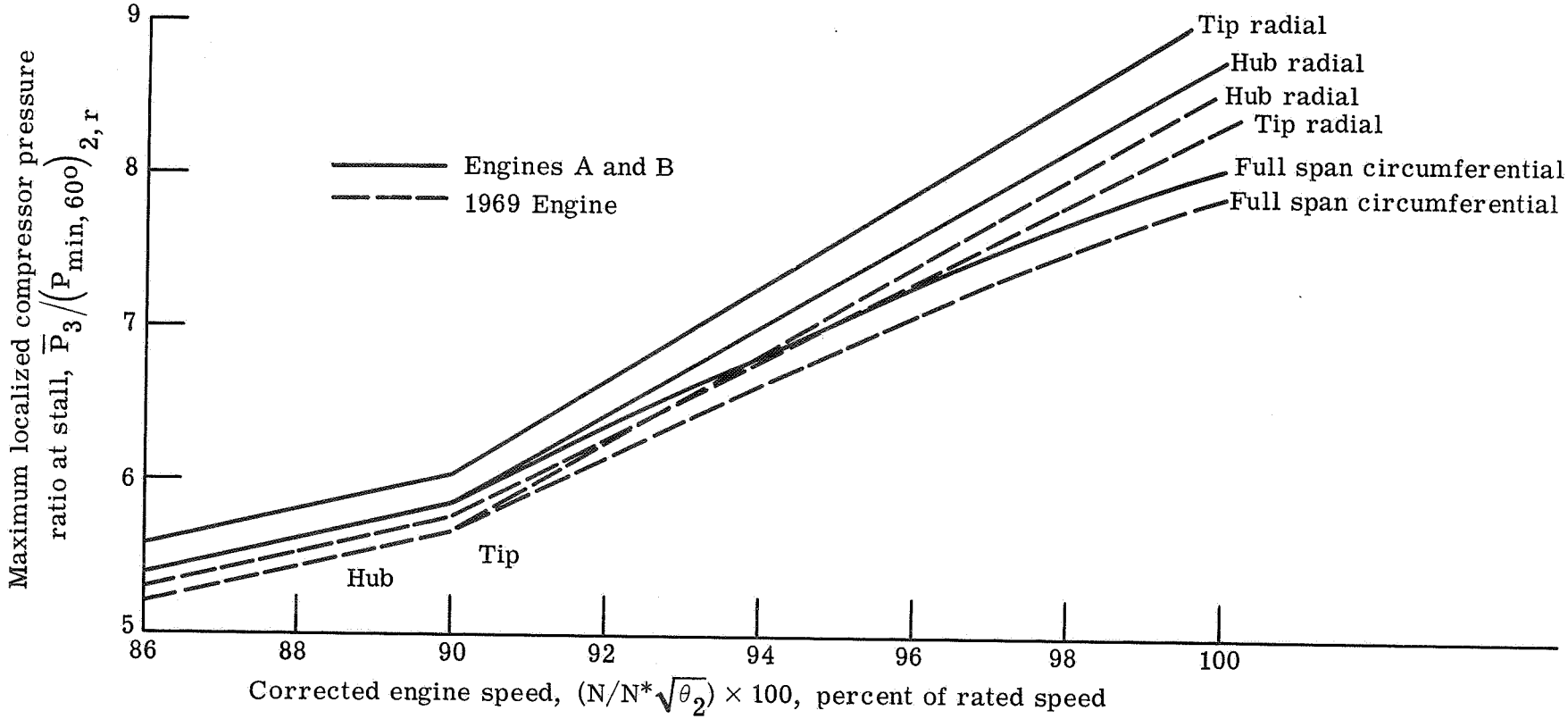

Figure 26. - Summary of localized compressor pressure ratios at stall.

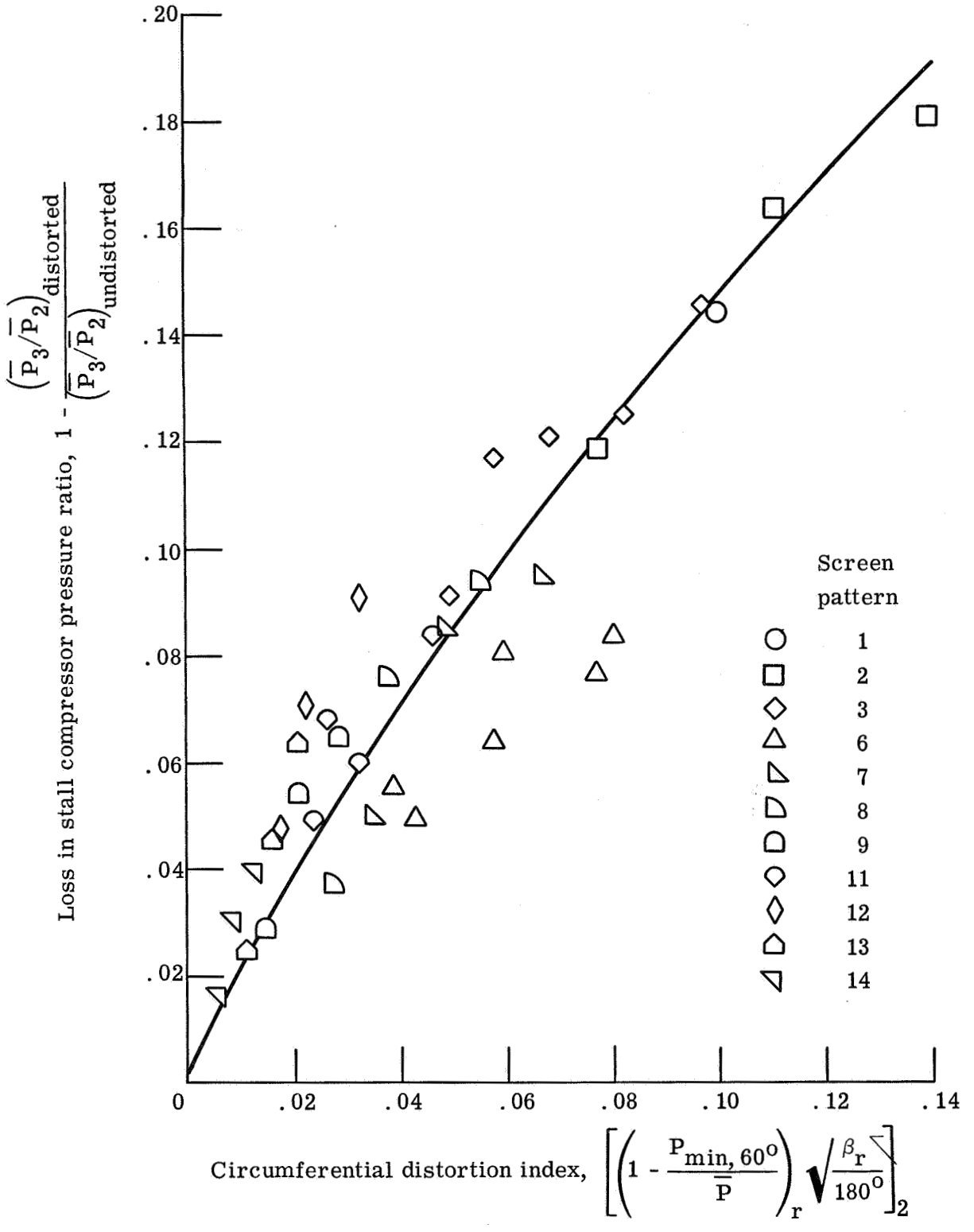

(a) Single- and multiple-per-revolution distortion patterns.

Figure 27. - Correlation of compressor pressure ratio at stall with circumferential distortion.

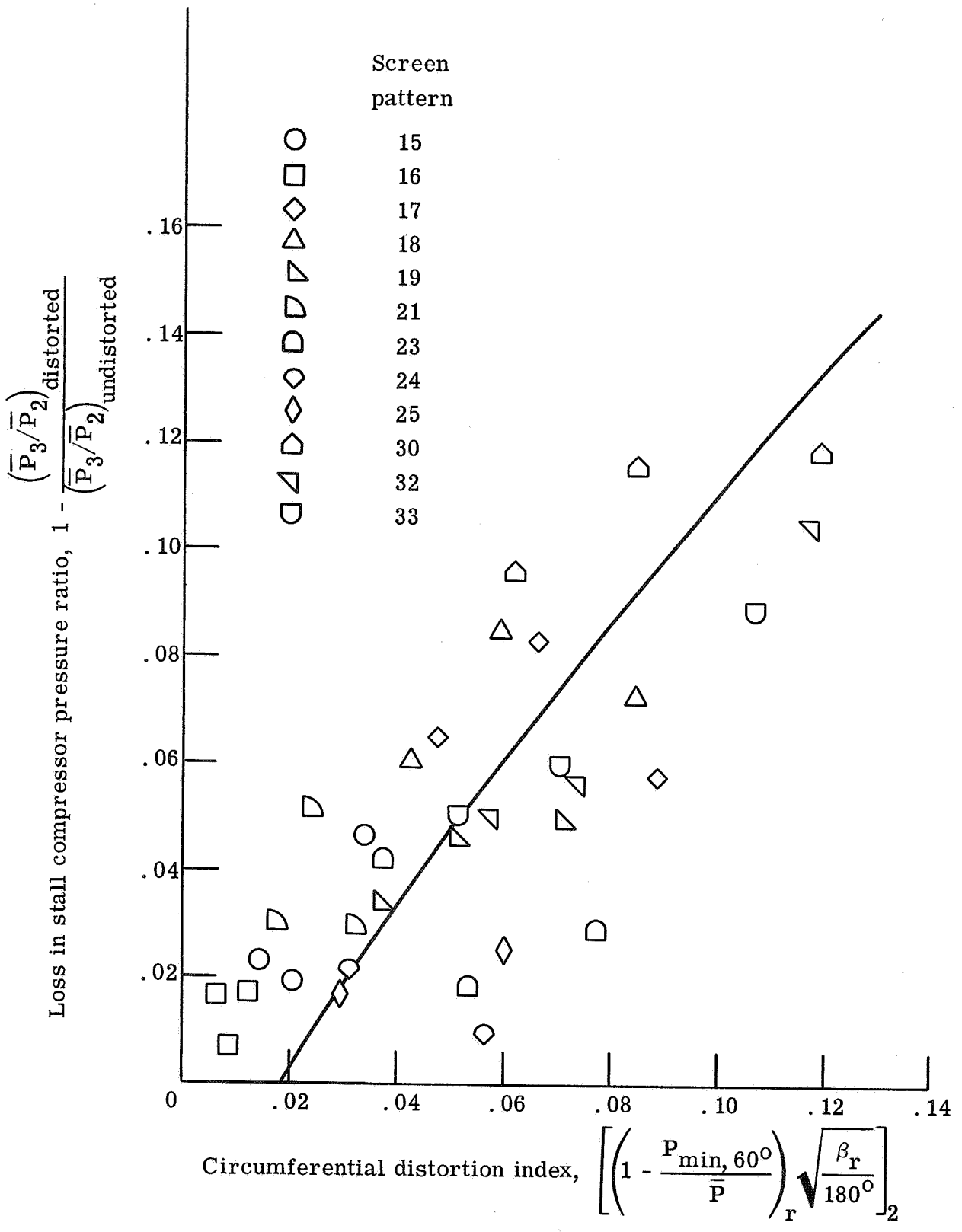

(b) Partial radial and combined distortion patterns.

Figure 27. - Concluded.

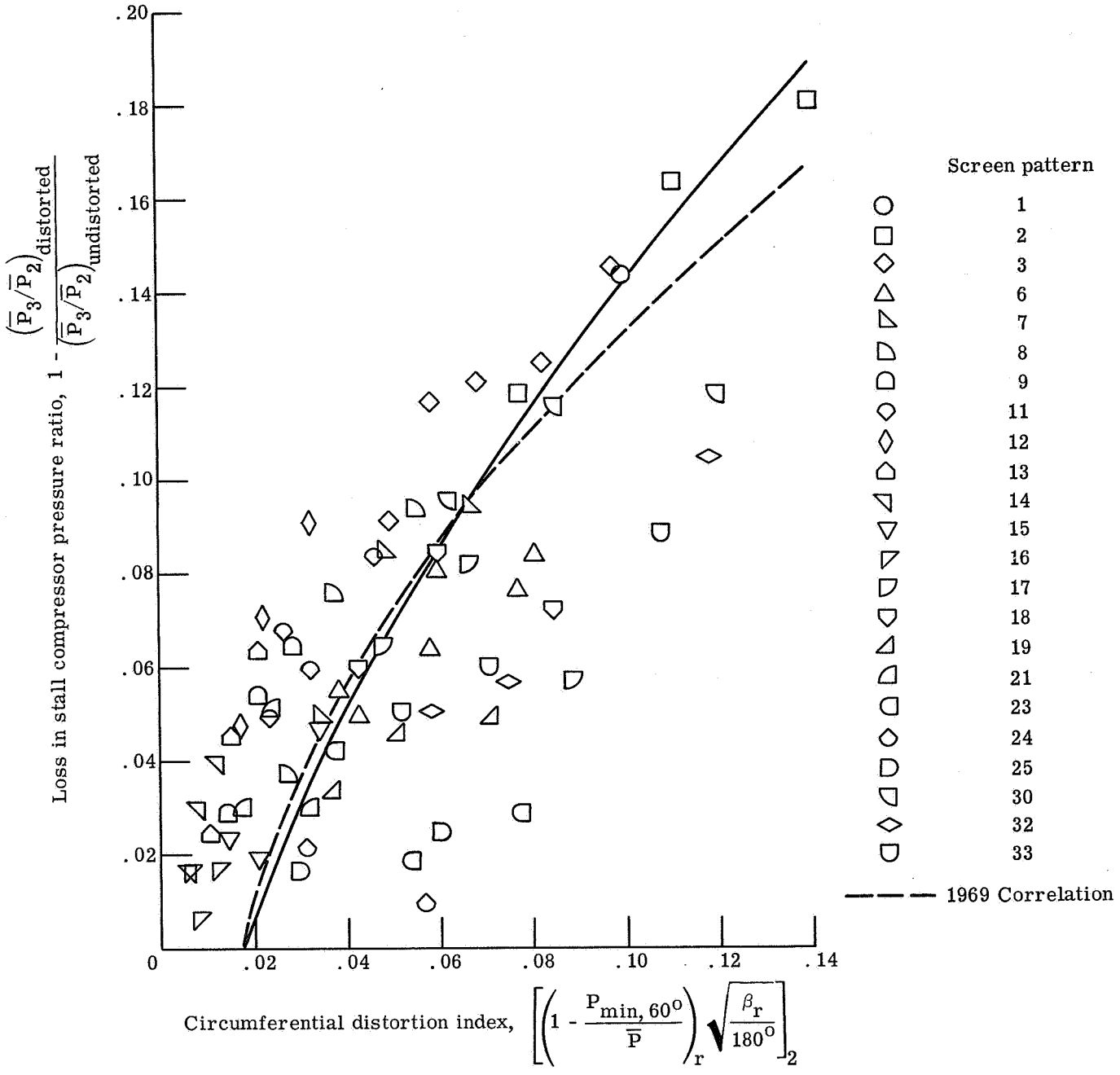

Figure 28. - Comparison of correlations for engines A and B with that for 1969 engine.